Aston University

Some pages of this thesis may have been removed for copyright restrictions.

If you have discovered material in Aston Research Explorer which is unlawful e.g. breaches copyright, (either yours or that of a third party) or any other law, including but not limited to those relating to patent, trademark, confidentiality, data protection, obscenity, defamation, libel, then please read our Takedown policy and contact the service immediately (openaccess@aston.ac.uk)

INTERLAMELLAR MODIFICATION OF SMECTITE CLAYS

STEPHEN PETER BOND

Doctor of Philosophy

The University of Aston in Birmingham

October 1991

The copy of this thesis has been supplied on condition that anyone who consults it is understood to recognize that its copyright rests with the author and that no quotation from the thesis and no information derived from it may be published without the author's consent.

The work described in this thesis was carried out between October 1988 and September 1991 at The University of Aston in Birmingham. It has been carried out independently and has not been submitted for any other degree.

.....

Stephen Peter Bond

.....

Professor W. R. McWhinnie

The University of Aston in Birmingham

INTERLAMELLAR MODIFICATION OF SMECTITE CLAYS

Stephen Peter Bond

A thesis submitted for the degree of Doctor of Philosophy 1991

Clay minerals, both natural and synthetic, have a wide range of applications. Smectite clays are not true insulators, their slight conductivity has been utilized by the paper industry in the development of mildly conducting paper. In particular, the synthetic hectorite clay, laponite, is employed to produce paper which is used in automated drawing offices where electrographic printing is common. The primary objective of this thesis was to modify smectite clays, particularly laponite, to achieve enhanced conductivity. The primary objective was more readily achieved if the subsidiary objective of understanding the mechanism of conductivity was defined.

The cyclic voltammograms of some cobalt complexes were studied in free solution and as clay modified electrodes to investigate the origin of electroactivity in clay modified electrodes. The electroactivity of clay modified electrodes prepared using our method can be attributed to ion pairs sorbed to the surface of the electrode, in excess of the cationic exchange capacity. However, some new observations were made concerning the co-ordination chemistry of the tri-2-pyridylamine complexes used which needed clarification.

The a.c. conductivity of pressed discs of laponite RD was studied over the frequency range 12 Hz - 100 kHz using three electrode systems namely silver-loaded epoxy resin (paste), stainless-steel and aluminium. The a.c. conductivity of laponite consists of two components, reactive (minor) and ionic (major) which can be observed almost independently by utilizing the different electrode systems. When the temperature is increased the conductivity of laponite increases and the activation energy for conductivity can be calculated. Measurement of the conductivity of thin films of laponite RD in two crystal planes shows a degree of anisotropy in the a.c. conductivity.

Powder X-ray diffraction and ^{119}Sn Mössbauer spectroscopy studies have shown that attempts to intercalate some phenyltin compounds into laponite RD under ambient conditions result in the formation of tin(IV) oxide pillars. ^{119}Sn Mössbauer data indicate that the order of effectiveness of conversion to pillars is in the order:

$$Ph_3SnCl > (Ph_3Sn)_2O, Ph_2SnCl_2$$

The organic product of the pillaring process was identified by ^{13}C m.a.s.n.m.r. spectroscopy as trapped in the pillared lattice. This pillaring reaction is much more rapid when carried out in Teflon containers in a simple domestic microwave oven. These pillared clays are novel materials since the pillaring is achieved *via* neutral precursors rather than sacrificial reaction of the exchangeable cation. The pillaring reaction depends on electrophilic attack on the aryltin bond by Brønsted acid sites within the clay.

Two methods of interlamellar modification were identified which lead to enhanced conductivity of laponite, namely ion exchange and tin(IV) oxide pillaring. A monoionic potassium exchanged laponite shows a four fold increase in a.c. conductivity compared to sodium exchanged laponite RD. The increased conductivity is due to the appearence of an ionic component. The conductivity is independent of relative humidity and increases with temperature. Tin(IV) oxide pillared laponite RD samples show a significant increase in conductivity. Samples prepared from Ph_2SnCl_2 show an increase in excess of an order of magnitude. The conductivity of tin(IV) oxide pillared laponite samples is dominated by an ionic component.

KEY WORDS: Laponite, Conductivity, Pillared Clay, Clay modified electrode, ^{119}Sn Mössbauer Spectroscopy.

To Grace

and to

those members of my family who have

provided encouragement and support

throughout the last three years

Acknowledgements

I would like to express my thanks to Professor W. R. McWhinnie for his guidance, invaluable advice, inspiration and encouragement throughout the period of this research. I would also like to thank Dr. M. S. Beevers for many hours of useful discussion and guidance in particular areas of this work.

I would like to express my thanks to the S.E.R.C. and James River Graphics, Chartham Paper Mill, for funding this research, particularly Chris Rundle and Carl Willetts for their interest in the research and their constant help over the last three years. I am particularly grateful for the opportunity to visit their research headquarters at South Hadley, Massachusetts in July 1990, and I would like to thank Keith Webb and Dr. Dene Taylor for their help while at South Hadley.

Many thanks are due to the technical staff within the department who have been of assistance constantly. I would also like to thank technical staff in other departments, in particular Roger Howell and Bassi Singh.

I am grateful to Professor Frank Berry for providing Mössbauer spectra throughout this research and to Dr. David Walton and Carl Hall for their help in obtaining cyclic voltammetry data.

I would like to thank my friends within the department for their encouragement and for making the last three years so enjoyable. Also, I would like to thank those who have helped, in many ways, in the preparation of this manuscript.

Thanks are also due to the members of my family who have provided constant encouragement throughout my time at Aston. Finally, I would like to thank Grace for her constant support over the last three years and her help in preparing this manuscript.

CONTENTS

Title Page 1
Declaration 2
Thesis Summary 3
Dedication 4
Acknowledgements 5
Contents 6
List of Figures 10
List of Tables 12

Chapter One Introduction

1.1 Introduction 15
1.2 Simple Silicate Minerals 15
1.2.1 Island Structure 16
1.2.2 Isolated Group Structures 16
1.2.3 Chain Structures 16
1.2.4 Sheet Structures 17
1.2.5 Framework Structures 18
1.3 Introduction to Clay Minerals 18
1.3.1 The Kandite Group 18
1.3.2 The Illite Group 20
1.3.2.1 Pyrophyllite and Talc 20
1.3.2.2 The Micas 21
1.3.2.3 The Illites 22
1.3.3 The Smectite Group 23
1.3.4 The Vermiculite Group 25
1.3.5 The Chlorite Group 26
1.3.6 Mixed Layer Minerals 26
1.4 Properties of Smectite Clays 28
1.4.1 Hydration and Dehydration 28
1.4.2 Colloidal Properties 30
1.4.3 Intercalation 33
1.4.4 Ion Exchange 35
1.4.5 Pillaring of Smectite Clays 38
1.5 Uses of Smectite Clays 40
1.5.1 The Use of Clays in the Paper Industry 41

1.5.2 The Use of Smectite Clays in Electrographic Papers 42
1.6 Objectives.....43
1.7 Previous Work.....44

Chapter Two Physical Techniques

2.1 Atomic Absorption Spectroscopy.....46
2.2 Cyclic Voltammetry.....46
2.3 Electron Spin Resonance Spectroscopy.....46
2.4 Elemental Analysis.....46
2.5 Diffuse Reflectance UV/Visible Spectroscopy 46
2.6 Fourier Transform Infra Red Spectroscopy 46
2.7 Gas Liquid Chromatography 46
2.8 M.A.S. Nuclear Magnetic Resonance Spectroscopy 47
2.9 Mössbauer Spectroscopy 47
2.10 Powder X-Ray Diffraction.....47
2.11 Scanning Electron Microscopy.....47
2.12 Solution Conductivities 47
2.13 UV/Visible Solution Spectroscopy 47
2.14 Solid Disc Conductivities.....48

Chapter Three Tri-(2-pyridyl)amine Complexes on the Surface of Laponite

3.1 Introduction.....52
3.2 Sample Preparation 53
3.2.1 Ligand Synthesis.....53
3.2.2 Complex Synthesis 54
3.2.3 Methods of Exchange of Complexes onto Laponite 55
3.2.3.1 Ion Exchange Using a Mechanical Shaker.....55
3.2.3.2 Ion Exchange Using a Microwave Oven.....55
3.2.4 Preparation of Clay Modified Electrodes.....55
3.3 Results and Discussion.....56
3.3.1 $Co(tripyam)_2 (ClO_4)_2$ Complexes and Ion Exchanged Clays 56
3.3.2 $Cu(tripyam)_2 (ClO_4)_2$ Complexes and Ion Exchanged Clays 59
3.3.3 $Fe(tripyam)_2 (ClO_4)_2$ Complexes and Ion Exchanged Clays.....59
3.3.4 Cyclic Voltammetry.....60
3.4 Conclusions 64

Chapter Four The Electrical Conductivity of Laponite

4.1 Introduction....67
4.2 Structure and Chemical Composition of Laponite....69
4.3 Resistors and Capacitors in A.C. Fields....69
4.4 Interpretation of the Frequency Dependence of the Electrical Conductivity of Laponite....71
4.5 Variable Temperature Conductivity Measurements....75
4.5.1 Theory....75
4.5.2 Experimental Technique....75
4.5.3 Metal-Sample Electrode Interfaces....77
4.5.4 Variable Temperature Behaviour of Laponite RD....79
4.6 Relative Humidity Dependence of the Electrical Conduction of Laponite....81
4.6.1 Sample Preparation....81
4.6.2 X-Ray Powder Diffraction Results....82
4.6.3 Dependence of Conductivity on Relative Humidity....83
4.7 Charge Carrier Determination....84
4.7.1 Theory....84
4.7.2 Experimental Technique....86
4.7.3 Results and Discussion....87
4.8 Thin Film Conductivity Measurements....90
4.8.1 Experimental....90
4.8.2 Anisotropic Conductivity Measurements....92
4.8.3 Activation Energy Measurements....93
4.9 Conclusions....95
4.10 Further Work....96

Chapter Five The Formation Of Novel Tin(IV) Oxide Pillared Laponite

5.1 Introduction....100
5.2 Chemicals....100
5.3 Intercalation of Phenyltin Compounds....101
5.3.1 Mechanical Shaker At Ambient Temperature....101
5.3.2 Microwave Heating....102
5.4 Analysis of the Intercalated Clays....104
5.4.1 ^{119}Sn Mössbauer Spectroscopy....104

5.4.2 ^{119}Sn Magic Angle Spinning Nuclear Magnetic Resonance Spectroscopy 106
5.4.3 Powder X-Ray Diffraction 107
5.5 Mechanism of Tin(IV) Oxide Pillaring 108
5.6 Conclusions 110
5.7 Further Work 111

Chapter Six The Electrical Conductivity of Modified Laponites

6.1 Introduction 113
6.2 Alkali Metal Exchange 113
6.2.1 Experimental Methods 113
6.2.2 Conductivity of Alkali Metal Exchanged Laponite Samples 114
6.2.3 Temperature Dependence of Potassium Exchanged Laponite RD Conductivity 116
6.2.4 Dependence of Potassium Exchanged Laponite RD Conductivity on Humidity 117
6.2.5 Physical Properties of Potassium Exchanged Laponite RD 117
6.3 Tin(IV) Oxide Pillared Laponite RD 118
6.3.1 Introduction 118
6.3.2 Conductivity of Novel Tin(IV) Oxide Pillared Laponite Samples 119
6.3.3 Temperature Dependence of Tin(IV) Oxide Pillared Laponite RD Conductivity 122
6.3.4 Dependence of the conductivity ofTin(IV) Oxide Pillared Laponite RD on Humidity 123
6.4 Conclusions 124
6.5 Further Work 127

References 128
Appendix One: Chapter Four Raw Data 137
Appendix Two: Chapter Six Raw Data 160

List of Figures

1.1 $(SiO_4)^{4-}$ Tetrahedron....16
1.2 $(Si_2O_7)^{6-}$ Isolated group structure....16
1.3 $(SiO_3^{2-})_n$ Chain structure....17
1.4 $(Si_2O_5^{2-})_n$ Sheet structure....17
1.5 Structure of kaolinite....19
1.6 Structure of pyrophyllite....20
1.7 Structure of talc....21
1.8 Structure of montmorillonite....23
1.9 Structure of hectorite....25
1.10 Structure of Tetron....33
1.11 Schematic representation of a pillared clay....39

2.1 A simplified block diagram of the Genrad 1689 RLC Digibridge measuring circuit....48

3.1 Cyclic voltammogram of $[Co(tripyam)_2]^{2+}$ immobilized on a laponite RD electrode, prepared by dipping the electrode in an acetonitrile solution of the complex....61
3.2 Cyclic voltammogram of a clay modified electrode prepared from laponite RD pre-exchanged with $[Co(bipy)_3]^{3+}$ (electro-inactive)....62

4.1 Chart of typical conductivities....67
4.2 Structure of laponite RD....68
4.3 Digibridge test configuration....69
4.4 Conductivity of different laponite grades....71
4.5 Frequency dependence of the conductivity of laponite RD....72
4.6 Frequency dependence of the capacitance of laponite RD....72
4.7 Components of impedance for laponite RD....73
4.8 Cross section of stainless steel die....76
4.9 Variation of laponite RD conductivity with applied pressure....77
4.10 Conductivity of laponite RD with Al and steel electrodes....78
4.11 Variation of the a.c. conductivity of laponite RD with temperature....79
4.12 Plot of $\log_e \sigma$ against T^{-1}, to calculate activation energy, at 100 kHz....80

4.13 Variation of laponite RD conductivity with increasing relative humidity....84
4.14 The Hall effect....85
4.15 Sample geometry for the Hall effect experiment....86
4.16 Hall effect measuring circuit....87
4.17 Plot of V_H against I_s to calculate R_H and n for laponite RD....88
4.18 Electrode configuration for parallel measurement from above and from the side....91
4.19 Electrode configuration for perpendicular measurements....91
4.20 The anisotropic components of laponite RD conductivity....93
4.21 Proposed measuring circuit to compensate for interface effects...97

5.1 ^{119}Sn Mössbauer spectra recorded at 77 K from (a) crystalline Ph_2SnCl_2 (b) Ph_3SnCl + laponite RD (c) Ph_2SnCl_2 + Laponite RD....105

6.1 Conductivity of alkali metal exchanged laponite samples....114
6.2 Components of impedance of potassium exchanged laponite....115
6.3 Conductivity of pillared clays from different precursors....119
6.4 Conductivity of clays prepared from different weights of Ph_3SnCl....120

List of Tables

1.1 Summary of the properties of clay minerals 27

3.1 UV/Visible spectra results for cobalt complexes 57
3.2 Diffuse reflectance uv/visible results for exchanged clays 58
3.3 Basal spacings of exchanged clays 58
3.4 Cyclic voltammetry data for complexes in solution and as clay modified electrodes 63

4.1 R, Xc and Z for laponite RD for steel electrodes.....78
4.2 R, Xc and Z for laponite RD for aluminium electrodes 78
4.3 Variation of activation energy with frequency.....80
4.4 Saturated solutions used to create constant relative humidity atmospheres at 293 K 82
4.5 Increase in basal spacing with relative humidity 82
4.6 Hall voltages as a function of sample current for laponite RD, 20°C, B = 0.46 T 87
4.7 Comparison of Hall constants.....89
4.8 Summary of results for R_H and n obtained from constant sample current experiments.....89
4.9 Summary of anisotropic conductivity measurements for laponite RD 92
4.10 Anisotropic activation energies for films of laponite RD.....94

5.1 Percentage of phenyltin precursors intercalated using a mechanical shaker.....101
5.2 Uptake of Ph_3SnCl as amount of precursor is increased.....101
5.3 Comparison of shaker and microwave methods for the intercalation of phenyltin compounds 102
5.4 Measurement of HCl release during intercalation 103
5.5 ^{119}Sn Mössbauer parameters of phenyltin compounds and the products of their intercalation with laponite.....104
5.6 Powder XRD data for intercalated laponites.....107
5.7 Dependence of basal spacing of a pillared clay on relative humidity (laponite RD + Ph_2SnCl_2).....107
5.8 Sodium release on pillaring with different amounts of Ph_3SnCl..109

6.1 Properties of alkali metal ions 115
6.2 Variation of activation energy with frequency for potassium exchanged laponite RD.....116
6.3 Conductivity of potassium exchanged laponite RD at 100 kHz...117
6.4 Basal spacing of potassium exchanged laponite RD.....118
6.5 Components of impedance for tin(IV) oxide pillared laponite RD 121
6.6 Variation of activation energy with frequency for tin(IV) oxide pillared laponite RD.....122
6.7 Conductivity of tin(IV) oxide pillared laponite RD at different humidities.....124

Chapter One

INTRODUCTION

1.1 Introduction

Clays are formed by natural geological processes. The constituents of the clay depend on the minerals present at the time of formation and the effects of subsequent weathering and ageing [1]. The term clay mineral is imprecise and can be used to describe a wide range of products. Many systems of classifications exist, orientational to their system of use. A precise definition of clay by the American Ceramic Society states [2] "a clay is a fine-grained rock which when suitably crushed and pulverized becomes plastic when wet, leather hard on drying and on firing is converted to a permanent rock like mass". For our purposes it is convenient to define a clay as a hydrous silicate of aluminium, magnesium or iron.

Clay science, agrillogy (derived from the Greek agrilla-clay and logos-science), has developed onto a wide interdisciplinary science [3] since the first application of X-ray diffraction analysis to clay minerals in the 1920's. By the 1940's the crystallinity and chemical structure of the main groups of clay minerals and related layer silicates had been established, and work in this field became directed more towards the properties and applications of clay minerals [4].

There are now many industrial uses for clay minerals [5]. Large volumes are used as drilling muds, as foundry moulding sand binders, filling agents and as absorbents. Small volumes have miscellaneous uses in paint, catalysis, paper coatings, lubricants and nuclear waste disposal.

1.2 Simple Silicate Minerals [2]

Silicates are the basic building blocks for the majority of the geosphere. The simple silicate structures are based on a tetrahedral arrangement of oxide ions about a central Si(IV) ion (fig. 1.1). The unit is represented chemically as $(SiO_4)^{4-}$. Pauling evaluated the approximate percentage of ionic character in a bond between two atoms by considering the difference in electronegativity between them, dipole moments and bond lengths. It was calculated that a Si—O bond has 50% ionic character. Hence, both ionic and covalent effects must be considered when investigating silicate minerals. The excess charge must be balanced by external sources, such as external cations, or by vertex sharing with adjacent $(SiO_4)^{4-}$ tetrahedra. This leads to five different groups of silicates depending on the number of oxygens of a particular tetrahedron that are linked directly to other neighbouring units.

1.2.1 Island Structures

Island structures consist of discrete $(SiO_4)^{4-}$ tetrahedra. They are only joined *via* external cations so that the overall structure is electronically neutral. These cations may be three, four, six, eight or twelve coordinate with oxygen. These minerals are called orthosilicates, e.g. zircon, $ZrSiO_4$, with eight coordinate zirconium ions.

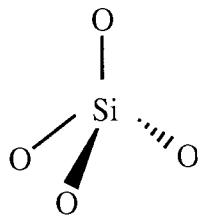

Figure 1.1 $(SiO_4)^{4-}$ Tetrahedron

1.2.2 Isolated Group Structures

Structures formed when two or more $(SiO_4)^{4-}$ units are linked together by sharing one common vertex, introducing a Si—O—Si linkage (siloxane), are known as isolated group structures (fig. 1.2). The basic structural unit is $(Si_2O_7)^{6-}$, e.g. thortveitite, $Sc_2Si_2O_7$.

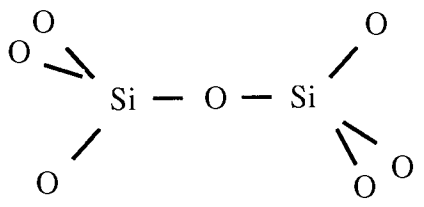

Figure 1.2 $(Si_2O_7)^{6-}$ Isolated group structure

1.2.3 Chain Structures

Chain structures are formed when two oxygen atoms of every $(SiO_4)^{4-}$ unit are vertex shared with other units. The resulting structure is capable of indefinite extension in the form of parallel chains (fig. 1.3). The general formula for these chains is $(SiO_3^{2-})_n$. This single chain structure is exemplified by the pyroxenes. As each chain can be linked to another via an external cation, these structures are capable of extension into three dimensions, e.g. spodumine, $LiAl(SiO_3)_2$.

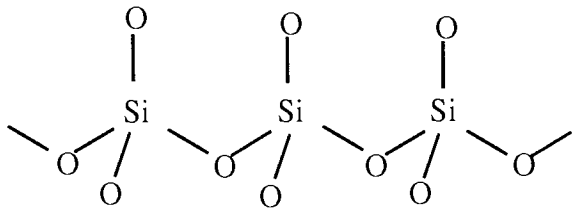

Figure 1.3 $(SiO_3^{2-})_n$ Chain structure

If two identical chains polymerize further by sharing a further oxygen in every alternate tetrahedron, a double chain structure with formula $(Si_4O_{11}^{6-})_n$ is produced. The amphiboles are examples of this, one form of asbestos being a fibrous amphibole. More complex single ring structures are known, such as $(Si_3O_9)^{6-}$, $(Si_4O_{12})^{8-}$, and $(Si_6O_{18})^{12-}$.

1.2.4 Sheet Structures

When three oxygen atoms of each tetrahedral unit are vertex shared with adjacent units, a continuous sheet structure is formed. Only one oxygen ion remains free to complex with external cations. As a consequence, the $(SiO_4)^{4-}$ units form a symmetrical twelve membered ring, viewed as hexagonal from below the layer, surrounded by six similar rings (see fig. 1.4). This sheet structure is capable of indefinite extension in two dimensions with the free oxygen located at right angles to the sheet structure. The composition of the layer can be represented as $(Si_2O_5^{2-})_n$. Layered structures can occur when the free oxygen links with a cation forming a layer above the silicate sheet. External cations can also link two sheets together to form three layer minerals. Clay minerals are an important class of layered silicates and exist as both two and three layer structures. A more detailed investigation of clay mineral structures is presented later in this chapter.

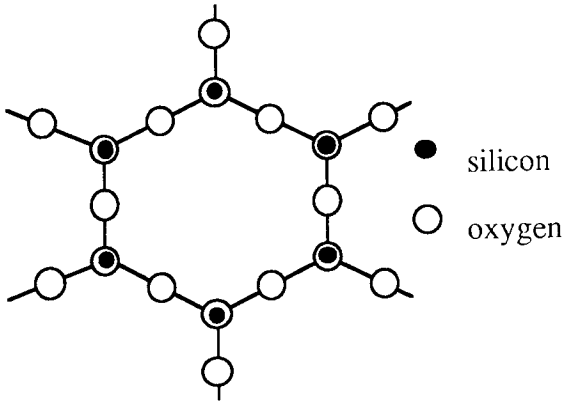

Figure 1.4 $(Si_2O_5^{2-})_n$ Sheet structure

1.2.5 Framework Structures

These structures represent the end of the series with all of the oxygen atoms in the $(SiO_4)^{4-}$ tetrahedra linked directly to another silicon atom. This structure is capable of extension in three dimensions. The formula may be written as $(SiO_2)_n$, examples of this are quartz and cristobalite.

In framework structures aluminium can replace the silicon located in tetrahedral holes. Although they are of similar size (ionic radii, Al = 0.50 Å, Si = 0.41 Å), the replacement of silicon by aluminium leads to a positive charge deficiency that must be remedied by the introduction of other cations. In felspars an alkali or alkaline earth ion balances the electronic charges. Albite, a soda felspar, is $Na(AlSi_3O_8)$. Zeolites are based on the $(AlSiO_2)$ framework structure but the lattice is more open than that of felspars, and cavities and wide channels are present.

1.3 Introduction to Clay Minerals

Clay minerals are hydrous silicate sheet structures and they belong to the phyllosilicate group of minerals [6]. The main building block of the clay minerals is the $(SiO_4)^{4-}$ tetrahedron, where three oxygens of each tetrahedron are linked to other silica units to form a sheet structure. The remaining oxygen atom is perpendicular to the sheet and able to link with cations or groups of cations. The nature of the resultant layers leads to the subdivision of clay minerals into several main groups. The most important groups are; kandites (the kaolinite group); illites (the mica group); smectites (the montmorillonite group); vermiculites; and chlorites. Each group will be investigated in more detail as each has characteristic properties depending on the type of layer structure, chemical composition, the extent of any isomorphous substitution and the swelling properties [1,2,6,7,8].

1.3.1 The Kandite Group

The most important member of this group is kaolinite, commonly known as china clay. It is formed when one silicate sheet condenses with a layer of gibbsite, $Al(OH)_3$, which is also a layer mineral. This forms a 1:1 layer structure, one tetrahedral layer of silicate plus one octahedral layer of gibbsite. Each aluminium is coordinated to two oxygen atoms bonded to silicon atoms, and to four hydroxyl ions. This structure is electronically neutral and the layer can be represented as $Al_2(Si_2O_5)(OH)_4$. The structure is capable of indefinite extension in two directions along the a and b

crystallographic axes. In clay mineralogy the c distance is known as the basal spacing or d_{001}, in the case of kaolinite the basal spacing is approximately 7 Å (see figure 1.5). When the kaolinite layers are separated from each other by water molecules the resulting mineral is known as halloysite, and the basal spacing rises to approximately 10 Å.

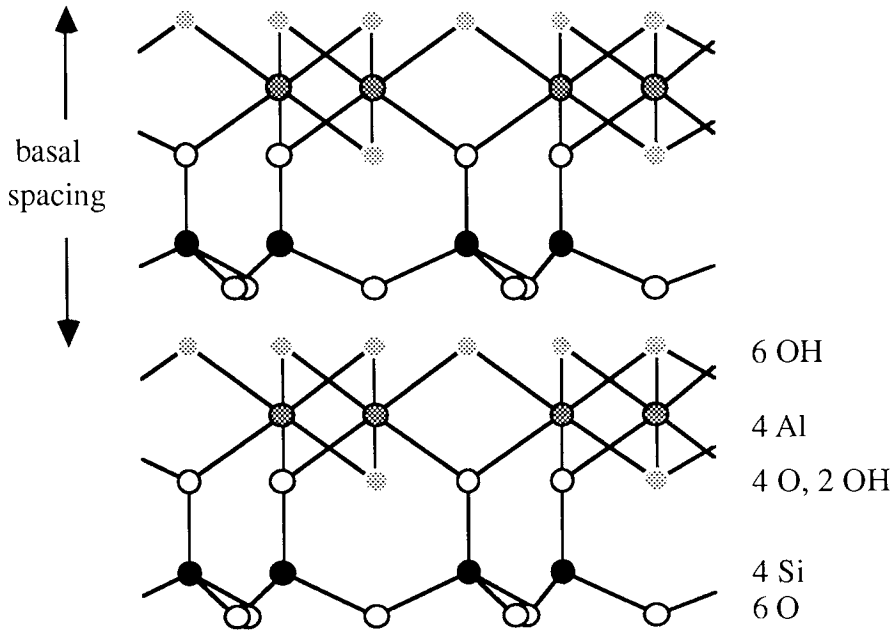

Figure 1.5 The structure of kaolinite

The two aluminium atoms lie directly above each ring of silicon atoms, however there are three possible cation positions, over each ring where an octahedrally coordinated cation could fit. If each of these positions were to be filled by a trivalent cation then the structure would not remain electronically neutral. Aluminium ions fill two thirds of these sites in kaolinite, therefore the structure is called dioctahedral.

In kaolinite isomorphous substitution is almost negligible. Very little Mg^{2+}, Fe^{2+} or Fe^{3+} is found substituted for Al^{3+}, and Al^{3+} substituting for Si^{4+} is also uncommon. This leads to kaolinite having a very low cationic exchange capacity (C.E.C.) in the range 3 to 15 milliequivalents (meq) per 100 g of clay. In kaolinite the C.E.C. is mainly caused by broken bonds around the edge of the crystal, giving rise to unsatisfied charges which must be balanced by exchangeable cations.

Other minerals in this group include the trioctahedral serpentines, e.g., lizardite. This can be represented chemically as $Mg_3Si_2O_5(OH)_4$. Lizardite is formed by the condensation of a layer of silicate sheet with a layer a brucite, $Mg(OH)_2$. The two layers are slightly different sizes, therefore cylindrical rolls are formed with the larger

octahedral (brucite) layer on the outside. Lizardite is a mineral in which all three octahedral sites are occupied by divalent cations. These minerals are termed trioctahedral.

1.3.2 The Illite Group

When a second tetrahedral silicate sheet condenses onto the octahedral layer sandwiching it, a 2:1 layer structure is formed. Illites are characterised by this 2:1 type layer structure. The Illite group can be divided into sub-groups, the most important are discussed here.

1.3.2.1 Pyrophyllite and Talc

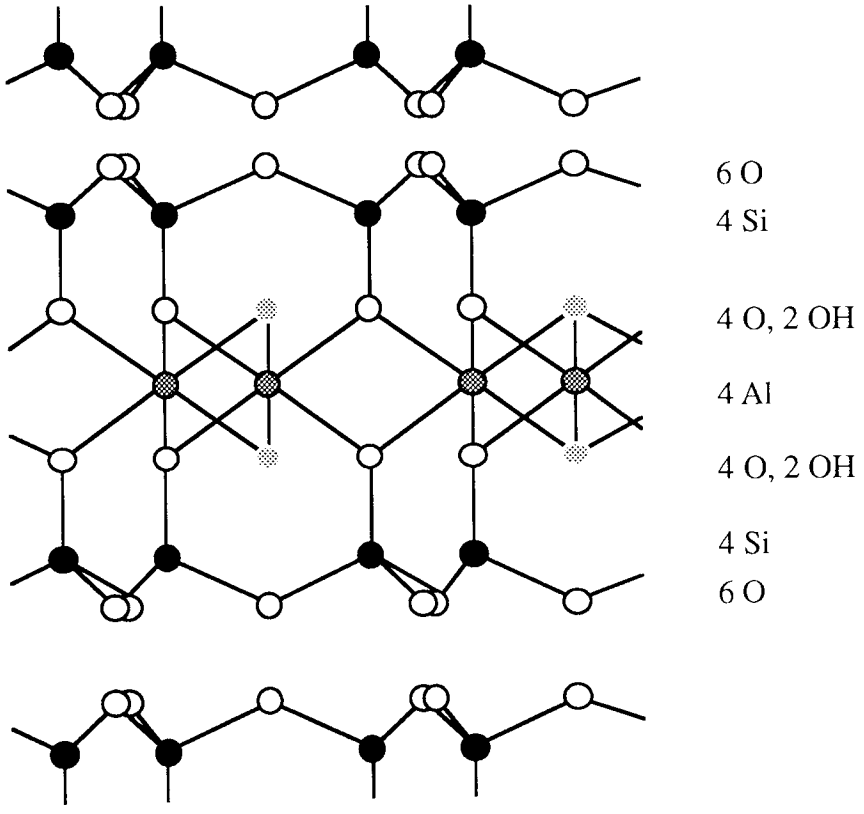

Figure 1.6 The structure of pyrophyllite

There is no substitution in either the tetrahedral or octahedral layers, therefore the sheets are electronically neutral and there are no cations in the interlayer. The layers are only held together by van der Waal's forces, hence the layers slip past each other easily, and the minerals tend to occur as flakes. Pyrophyllite (fig. 1.6) is a dioctahedral structure with the chemical composition $Al_2Si_4O_{10}(OH)_2$, the basal spacing is 9.3 Å. Talc (fig. 1.7) is a trioctahedral structure which can be characterised as $Mg_3Si_4O_{10}(OH)_2$, it has a

basal spacing of 9.6 Å. Structurally, these are the parents of all illite and smectite minerals.

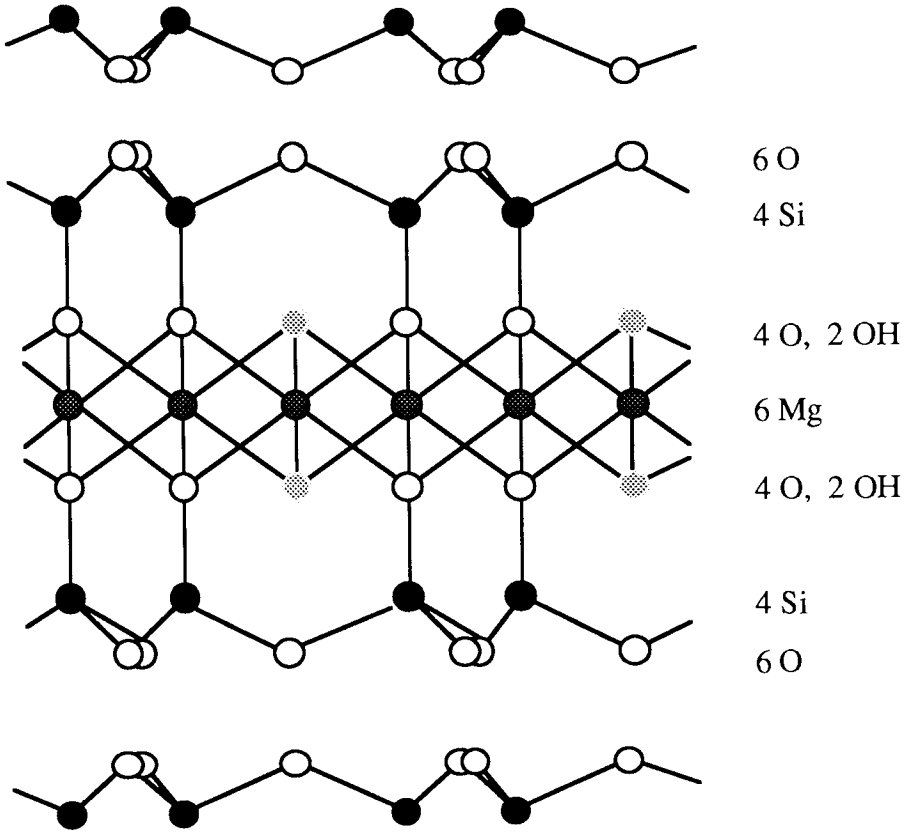

Figure 1.7 The structure of talc

1.3.2.2 The Micas

The structure of micas is based on talc and pyrophyllite. However the layers are not electrically balanced and the presence of cations in the interlayer region is necessary. This leads to a fundamental change in properties. The layers have a large charge deficiency, approximately one per unit, corresponding to the substitution of approximately one in every four silicons by an Al^{3+} ion. The cation introduced into the interlayer to balance the charge deficiency is held very strongly, in fact the bonding is similar to ionic bonding. This introduces a link between successive sheets through these cations. These cations cannot be exchanged or removed without the decomposition of the mineral. The introduction of water into the interlayer does not swell the mineral as the layers are held together. The octahedral layer can contain many different cations, this diversity accounts for the many types of mica.

Muscovite mica is a true dioctahedral mica. It has the chemical composition $KAl_2(AlSi_3)O_{10}(OH)_2$. The potassium ions are symmetrically situated over each hexagonal ring in the outermost sheet of the layers. Thus they are linked to six oxygen atoms in one sheet, and six in the adjacent layer. Therefore the potassium is twelve co-ordinate. The basal spacing of muscovite mica is 9.8 Å.

The biotite micas are true dioctahedral micas with their octahedral layers populated mostly by Mg^{2+} and/or Fe^{2+}. Examples are phlogopite, $KMg_3(AlSi_3)O_{10}(OH)_2$ and biotite $K(MgFe)_3(AlSi_3)O_{10}(OH)_2$. In biotite the proportions of magnesium and iron vary widely.

Although micas have predominantly potassium cations linking the successive sheets, sodium micas are known such as paragonite, $NaAl_2(AlSi_3)O_{10}(OH)_2$. However, as sodium ions are smaller than potassium ions, they do not fit the hexagonal ring of basal oxygens as well, and are not held as strongly as potassium ions. Therefore sodium micas do not form as easily as potassium micas and are more easily decomposed.

Brittle micas are similar in chemical composition to micas. The distinguishing feature is that brittle micas always have calcium or magnesium as the linking cation, and the charge deficiency per unit is higher and still located in the tetrahedral layer. An example of this is margarite. Every alternate tetrahedral silicon is replaced by an aluminium ion and the charge is balanced by calcium ions. The chemical composition is $CaAl_2(Al_2Si_2)O_{10}(OH)_2$.

1.3.2.3 The Illites

Illites are the most common clay minerals in nature, they are often found in marine clays. They often occur interstratified with smectite layers and it is difficult to detect with certainty the presence of less than 10% swelling (smectite) layers. Illites resemble micas in many respects, except that the amount of aluminium for silicon substitution in the tetrahedral layer is much less, one in eight silicons are substituted. As a result there are fewer cations in the interlayer region. Isomorphous substitution of the octahedral aluminium by Mg^{2+}, Fe^{2+} and Fe^{3+} is possible. Sodium and calcium can appear in the interlayer region along with the H_3O^+ ion, which can lead to the presence of more interlayer water than in micas. The basic structural formula for the illites is $K_xAl_2(Si_{4-x}Al_x)O_{10}(OH)_2$, where $0.5 < x < 0.75$. Glauconite is an important member of the illite group, it contains more iron in the octahedral layer than most illites.

1.3.3 The Smectite Group

Smectites are 2:1 layer structures and are similar in chemical composition to micas. The bonds between adjacent layers are considerably weaker, as only dipolar and van der Waal's forces hold the layers together. Smectite structures are based on those of talc and pyrophyllite, deviations from these structures arise from isomorphous substitution of octahedral and tetrahedral cations by cations in a lower oxidation state. This results in a layer charge of 0.2 - 0.6 per structural unit, balanced by mainly sodium or calcium cations in the interlayer. The average extent of this substitution requires about 0.33 monovalent cations (or their equivalent) per structural unit. These ions are generally easily exchangeable, smectites have cationic exchange capacities of 80 - 150 meq per 100 g of clay.

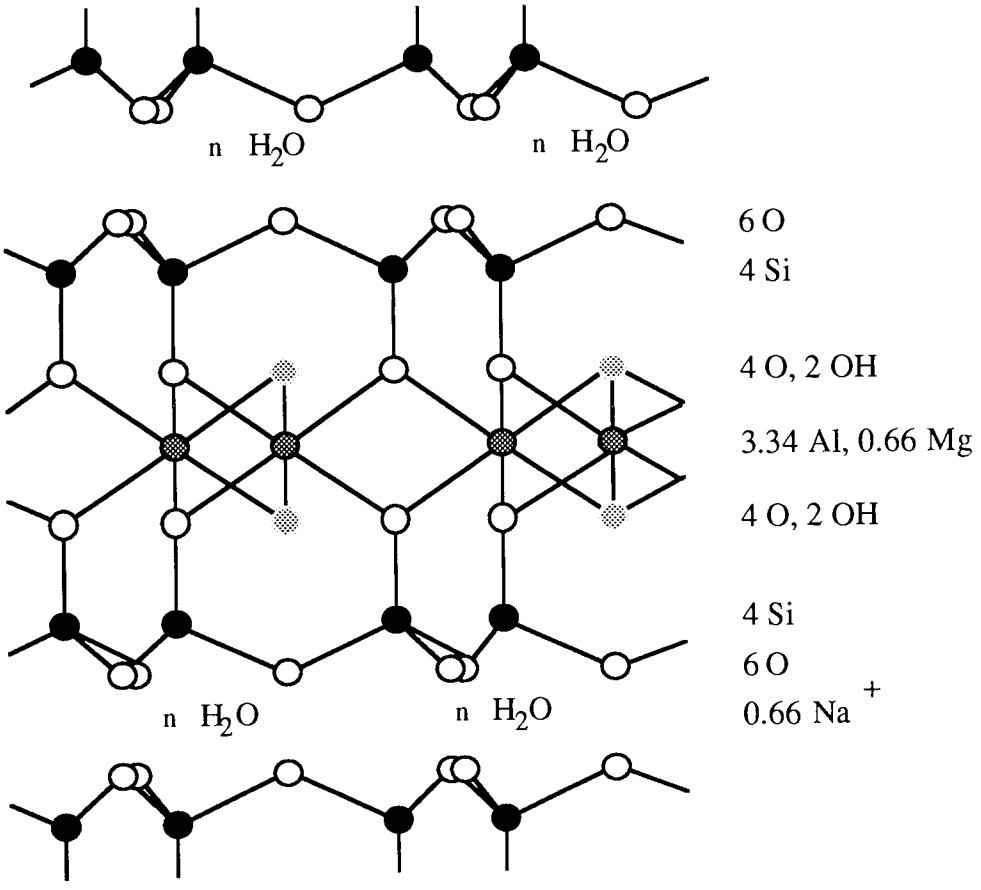

Figure 1.8 Structure of montmorillonite

In most smectites the majority of the substitution occurs in the octahedral layer. As a result interlayer cations are less strongly held and the bonds between layers are weaker. Due to these weaker bonds varying amounts of water can enter between the layers and the stacking of successive layers is random. A dehydrated smectite can have a basal

spacing of 10 Å, while hydrated smectites can have basal spacings up to 20 Å and in dilute aqueous solution the layers may completely disperse. Frequently the basal spacing is around 14 Å. As a result smectites are also known as expanding lattice clays or swelling clays.

In addition to their ability to absorb inorganic cations and water, smectites are capable of taking up organic molecules into the interlamellar region. Large organic cations such as quaternary amines and proteins can replace the exchangeable cations. Mono- and di-molecular layers can be absorbed in this way depending on the size of the organic cation and the cationic exchange capacity of the clay. The absorption of quaternary amines onto smectite clays is used to make hydrophobic drilling muds for the oil industry. These are known as bentones. Organic liquids and solids can also be absorbed and held between the layers, the best known example of this is the absorption of glycerol.

Both dioctahedral and trioctahedral smectite clays are well known. Montmorillonite is a dioctahedral smectite which may be represented as $Na_{0.33}(Al_{1.67}Mg_{0.33})Si_4O_{10}(OH)_2$, although this varies a great deal depending on the source of the mineral (fig. 1.8). The octahedral aluminium can be replaced with iron(III), this is known as nontronite, $Na_{0.33}(Fe_{1.67}Mg_{0.33})Si_4O_{10}(OH)_2$. Ferric cations can replace aluminium in all proportions in the octahedral layer, so there is a complete range of solid solutions between montmorillonite and nontronite. However, nontronite has a range of chemical compositions as aluminium replaces silicon in the tetrahedral layer, the structure varies from the above formulation to $Na_{0.33}Fe_{2.22}(AlSi_3)O_{10}(OH)_2$, a high aluminium or aluminian nontronite. The complete range between the two extremes are known. High aluminium montmorillonites are known as beidellites, the complete range of tetrahedral substitutions between montmorillonite and beidellite, $Na_{0.33}Al_{2.22}(AlSi_3)O_{10}(OH)_2$, is known.

An analogous, complete series is apparent in the trioctahedral smectites. Hectorite (fig. 1.9), $Na_{0.33}(Mg_{2.67}Li_{0.33})Si_4O_{10}(OH)_2$, has only substitution in the octahedral layer, while saponite, $Na_{0.33}Mg_3(Al_{0.33}Si_{3.67})O_{10}(OH)_2$, has only tetrahedral substitution. In hectorite there is often some anionic substitution of F^- for $(OH)^-$.

It is unlikely that dioctahedral and trioctahedral smectites form intermediate structures. In all the above structures the exchangeable cation has been given as sodium. This is not always the case and in nature sodium, calcium and potassium may be exchanged, mixtures are also found, especially of sodium and calcium. The structural formula is not

in any way influenced by the inclusion of different cations but the properties are greatly affected by the cation.

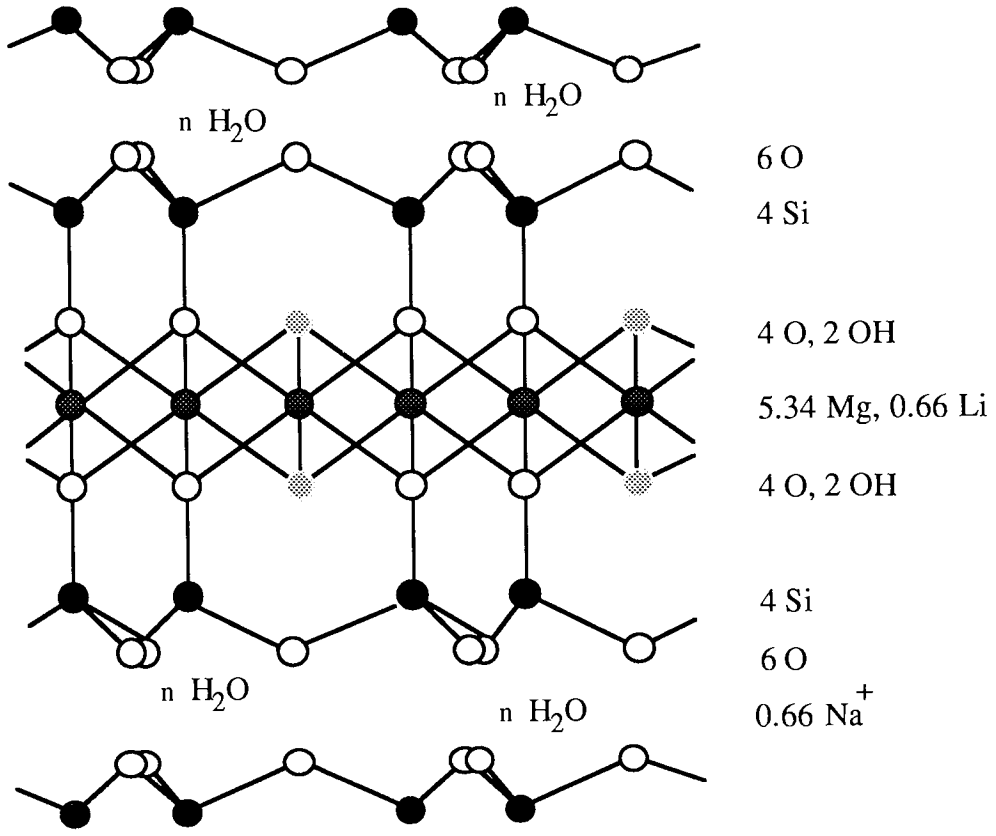

Figure 1.9 The structure of hectorite

Copper, nickel, chromium, vanadium and zinc may occasionally substitute in major amounts into the octahedral layer of smectite clays, forming minerals such as volkhonskoite (Cr), sauconite (Zn) and pimelite (Ni).

1.3.4 The Vermiculite Group

Vermiculites are trioctahedral 2:1 layer type structures. The layers are not electrically neutral, they possess a unit charge of 0.6 - 0.9 and a cationic exchange capacity of 100 - 150 meq per 100 g of clay. This arises mainly from substitution in the tetrahedral layer. The balancing, interlayer cations are commonly calcium or magnesium. The basal spacing of vermiculites is not fixed. Any expansion is limited to about 5 Å, or two layers of water greater than the size of dehydrated vermiculite, 9.3 Å. The hydrated basal spacing is usually 14 Å, depending on the nature of the interlayer cation. Vermiculites can also absorb certain organic molecules, but the absorbed layer is thinner

than in smectite clays. Particle size is larger than smectites and stacking is also less random.

A general structural formula for vermiculites is $(Ca,Mg)_{x/2}(Mg,Fe^{II})_3(Al_xSi_{4-x})O_{10}(OH)_2$.

1.3.5 The Chlorite Group

The chlorite structure consists of 2:1 layers with a further octahedral layer situated in the interlayer region. Thus chlorites can be described as 2:1:1 layer structures. The mineral is therefore composed of two tetrahedral layers and two octahedral layers, in total. The interlamellar layer balances the effects of substitution in the 2:1 layers, it is generally an octahedral magnesium or aluminium hydroxide (brucite or gibbsite like) and forms hydrogen bonds from its hydroxyl groups to sheet oxygens, which when added to the electrostatic attraction forms a strong interaction between the 2:1 layers and the hydroxide sheet. Most of the substitution in the 2:1 layer is in the tetrahedral layer (Al for Si), although substitution in the octahedral layer is not unknown.

Different types of chlorites are known depending on the composition of the octahedral layers. In trioctahedral chlorites both of the layers are trioctahedral, in dioctahedral chlorites both of the layers are dioctahedral. Di, trioctahedral chlorites are dioctahedral in their 2:1 layer and trioctahedral in the interlayer sheet. No natural chlorites are known that are trioctahedral in the 2:1 layer and dioctahedral in the interlayer sheet. The majority of chlorites are trioctahedral, they can be represented as $[(M^{2+},M^{3+})_3(Si_{4-x}Al_x)O_{10}(OH)_2][(M^{2+},M^{3+})_3(OH)_6]$. In the octahedral sheets magnesium and iron(II) are the most common and substantial amounts of manganese and nickel can occur in some chlorites. Natural chlorites are often iron rich minerals. Substitution in the interlamellar sheet is also known .

The cationic exchange capacity of chlorites is low (10 - 40 meq per 100 g of clay) as there are no exchangeable cations. The basal spacing of the chlorites is generally 14 Å, and unlike the smectites and vermiculites it is not variable.

1.3.6 Mixed Layer Minerals

Mixed layer, or interstratified clay minerals are those in which individual crystals are composed of unit cells or unit layers of two or more types of clay mineral. There are three types of mixed layer minerals. The most common of these, and the second most

common of all clay minerals in nature, are randomly stratified minerals. No law governs the alternation of the layers and they have no particular mineral names, they are described in terms and proportions of the types of layers. Some mineral names have been given to the regular layer interstratified minerals. These alternate to a specific law, the simplest being of the form ABABAB. The final type is when zones of random and regularly interstratified clay minerals are found within the same crystal.

The most common mixed layer clay mineral is illite-montmorillonite. Other common mixtures found in mixed layer minerals are combinations of chlorites, illites, smectites and vermiculites.

Mineral Group	Mineral Name	Layer Type	Layer Charge	C. E. C. / meq	d_{001} / Å
kandite	kaolinite	dioctahedral, 1:1	< 0.2	3 - 15	7 Å
	halloysite	trioctahedral, 1:1	> 0.2	5 - 40	10 Å
illite	pyrophyllite	dioctahedral, 2:1	< 0.2	~ 0	9.3 Å
	talc	trioctahedral, 2:1	< 0.2	~ 0	9.6 Å
	muscovite	dioctahedral, 2:1	1	~ 0	9.8 Å
	brittle mica	dioctahedral, 2:1	2	~ 0	
	illite	dioctahedral, 2:1	> 1	10 - 40	10 Å
smectite	montmorillonite	dioctahedral, 2:1	0.25 - 0.6	80 - 150	~14 Å
	hectorite	trioctahedral, 2:1	0.15 - 0.45	75 - 115	~14 Å
vermiculite		trioctahedral, 2:1	0.6 - 0.9	100 - 150	~14 Å
chlorite		2:1:1	variable	10 - 40	~14 Å

Table 1.1 Summary of the properties of clay minerals

1.4 Properties of Smectite Clays

The smectite (swelling) clays exhibit a combination of properties, stemming from their physicochemical structure, which is not displayed by other known minerals. The unique properties displayed by smectite clays are a result of small crystal size, variations of internal chemical structure, large cationic exchange capacity, variation of types of exchangeable cation and surface charge, large and chemically active surface area and the ability to interact with organic and inorganic molecules. The particular properties of smectite clays examined in more detail below are important in the interlamellar modification of smectite clays.

1.4.1 Hydration and Dehydration [6]

The relative weakness of the forces between successive layers of smectite clays leads to the presence of varying amounts of water in the interlayer region [6]. Although this hydration occurs regardless of the type of exchangeable cation present, the degree of hydration depends on the species of ion. The size of the cation and its charge are important, as the principal driving force for hydration is electrostatic attraction between the dipole of the polar water molecule and the charge of the exchangeable cation. Smectite clays with small monovalent cations (Li^+, Na^+) show extensive interlayer expansion at high humidities as the cation becomes hydrated. It is important to note that this hydration is affected more by the nature of the interlayer cation than by the silicate surface. Despite this, in smectite clays some water is associated with the silicate surface. This is called crystalline water and is relatively constant. There is another type of interlayer water found in highly hydrated smectite clays, free water. Free water is not associated with either the interlayer cation or the silicate surface, thus it is very labile.

Early studies of smectite clays showed what appeared to be a continuous increase in basal spacing with increasing water content. However, it is now established that the hydration of the interlamellar surfaces of smectite clays occurs in a series of steps as the clay is subjected to increasing levels of humidity. It has been shown that one, two, three or four layers of water can be sorbed in montmorillonite. This step-wise uptake of water varies depending on the exchangeable cation, however the first layers of water are always arranged in a highly ordered, rigid manner. Monovalent ions tend to reinforce a rigid structure of water layers, this is because the ions dissociate from the layer surface. The greater this degree of dissociation, the less they disrupt the quasicrystalline water layers, thus the ions are, in effect, dissolved in the water structure. In the case of sodium montmorillonite the one and two layer hydration states are most common.

Multivalent cations enhance the rigidity of the first layer but as additional water layers are sorbed the multivalent cations promote disorder and act to make the water more fluid. If calcium is the exchangeable ion the two layer hydrate will be favoured over a large range of humidities.

Lithium and sodium montmorillonites are capable of swelling to give much larger basal spacings than those normally observed. This type of swelling is called osmotic or type two swelling. The large spacings result from a different balance of forces between layers. Electrostatic and van der Waal's forces are balanced by the osmotic pressure of the interlamellar ions. The transition between normal or type one swelling and type two swelling is sharp. When sodium montmorillonite is subjected to increasing water content the basal spacing first increases in steps corresponding to various ordered states until 20 Å is reached. As the water content is further increased the basal spacing jumps to 40 Å, after which it increases steadily. In lithium and sodium montmorillonites individual layers dissociate completely as the water content is increased. With divalent cations unlimited swelling is not observed because these ions provide a bridge between the charged sites on facing silicate surfaces.

When smectite clays are heated varying amounts of water are lost [5]. At low temperatures (100°C - 200°C) the water loss is from the interlayer region, resulting in the "collapsed" structure. The process of dehydration depends on the nature of the exchangeable cation and also, to a lesser extent, on the structure of the smectite. When sodium is the exchangeable ion the low temperature water loss is in a single stage, but when calcium is the predominant cation this water loss often proceeds in two steps. This can be observed using differential thermal analysis.

At higher temperatures (500 - 700°C) there is a further loss of water [5]. This is known as OH lattice water loss or dehydroxylation as the water is mainly from the octahedral metal hydroxide layer of the silicate structure. Variations in dehydroxylation are primarily related to crystalline structure, strength of metal hydroxide bonds and chemical composition, as dehydroxylation involves the breakdown of the silicate structure.

The rehydration characteristics of dehydrated smectite clays are less well understood. However, when smectite clays are heated to temperatures not exceeding 200°C most will rehydrate completely in the presence of liquid water. This gives rise to changes in the swelling and colloidal properties of the clay. Industrially it has been shown that it is

unwise to remove the last traces of interlayer water, because of the possibility of a change in properties.

In the presence of liquid water smectite clays will rehydrate to some degree even after heating to 500°C - 700°C. The degree of rehydration depends mainly on the degree of structural change that has occurred due to the loss of lattice OH. On further heating the clay structure is completely lost and is replaced by a variety of other silicates. This structural change can be thoroughly investigated using different spectroscopic methods to follow the lattice cations from the breakdown of the clay structure to the formation of new silicates.

1.4.2 Colloidal Properties

In dry solids the smectite clay structure is an ensemble of independent elementary particles [9]. Each particle results from the stacking of many layers, with some orientational (turbostatic) and translational disorder around the normal to the stack. These individual crystals may be as large as two micrometers (2 μm) and as small as 0.2 μm, with an average size [5] of about 0.5 μm. This small size can be used to help explain the colloidal properties of smectite clays. The smectite clay - water system covers three states:- an opalescent suspension, a thixotropic gel and a stiff paste which resembles the highly hydrated solid [10].

When the concentration of clay in water is less than approximately 2% a colloidal suspension is formed. The electrical potential causes the particles, and groups of particles to repel each other. As the crystals are so small they may remain suspended indefinitely. Different exchangeable ions affect the state of aggregation [11]. Small angle neutron scattering of clay suspensions shows pairs of potassium montmorillonite platelets separated by a double layer of interlayer water. Caesium montmorillonite suspensions show three platelets again interleaved with a double layer of water. A recent study of n.m.r. relaxation times of dilute aqueous clay suspensions showed a higher degree of formation of tactoids [10]. A tactoid may be visualized as the result of the interleaving and piling up of smectite clays forming a stack, containing up to ten layers per tactoid, separated from each other by a few layers of interlayer water, and totally separated from other tactoids in the suspension. However a recent small angle X-ray study [12] concludes that in dilute suspensions, most of the particles are individual layers, separated by over 100 Å.

On further concentration the clay develops a rigid structure throughout the bulk. The ability to form a thixotropic gel is unique to smectite clays, particularly those with a high cationic exchange capacity. The viscosity exhibited by smectite clays is mainly due to the small crystal size, the large surface area and high dispersability [13]. Electrical forces between the particles are a secondary factor, however they are important when considering the resulting gel structure.

Van Olphen stated [13] that in concentrated clay suspensions a three dimensional house of cards structure is formed that extends throughout the available volume forming a solid gel. In concentrated clay suspensions delamination of clay particles occurs and the exchangeable cations diffuse into the bulk, resulting in an ion atmosphere around the particles. Three different modes of particle association can occur:- face to face, edge to face and edge to edge. The electrical interaction energy for the three types of association is governed by different combinations of electrical interactions at the platelet surfaces. Also, the van der Waal's interaction would be different for the three types of association, since a different geometry must be considered for the approaching plates and their ion atmospheres in each case. Hence the net potential curves of interaction are different for each of the three types of mutual approach. Consequently, the three types of association will not necessarily occur simultaneously or to the same extent.

The voluminous house of cards structure contains mainly face to edge interactions. If face to face interactions occur simultaneously the number of units building the house of cards structure is reduced, lowering the number of links in the structure, thus decreasing the viscosity. Face to face association merely leads to thicker and larger particles.

Recent evidence from electron microscopy [14] suggests that the structure of the gel is dominated by face to face associations. This study suggested a network of lenticular (doubly convex) pores, the walls of which are connected to each other by flexible face to face associations of layers. A recent n.m.r. study [10] and a small angle X-ray study [12] also suggested that the main feature of the gel is face to face association. However there are serious (apparent) discrepancies in their conclusions [15]. Fripiat et al. studied spin-lattice relaxation times (T_1) of water molecules in the bulk of the system and on the external surface of tactoids. These relaxation times are drastically different from each other. Knowing that the two populations of water molecules are in rapid exchange, it is possible to calculate the external surface area of clay aggregates over a wide concentration range. Fripiat suggested a high degree of tactoid formation even at very low clay concentrations, and that the size of the tactoid does not change significantly as

the clay concentration increases. This suggests a micellization process in which any increase in clay concentration merely leads to an increase in the number of independent tactoids, all identical to each other and the formation of a gel results from this increase in tactoids.

The small angle X-ray study of Pons et al.[12] suggested that as gelation begins "soft" stacks of layers are formed with large internal separation distances, of around 35 Å. The number of layers per stack begins at approximately eight and rises to around twenty as the clay concentration in the gel rises. This is accompanied by a further transition in the gel structure."Hard" stacks are formed, with internal separation distances of 31 Å, separated further by more "soft" stacks in a disordered interstratified arrangement. On further concentration (or drying) the system thickens as "hard" stacks are formed from the "soft" stacks. Van Damme et al. [9] have used a fractal aggregation model in an exploratory attempt to resolve these discrepancies and fully describe the structure of the gel. For some particle dimensions a diffusion limited aggregation model is consistent with experimental observations, leading van Damme to suggest the formation of "fingers" connecting parts of the aggregate and particle entanglement in the aggregate. Entanglement is confirmed by electron microscopy.

The addition of electrolyte to the gel leads to dramatic changes in viscosity [13]. In the presence of a few milliequivalents of electrolyte (eg. NaCl) edge to face attractions diminish and face to face repulsions are promoted. This leads to a lowering of viscosity as the gel structure breaks down. As the electrolyte concentration is increased edge to edge association and edge to face association by van der Waal's attraction contribute to an increase in viscosity. At high electrolyte concentrations the viscosity decreases as larger particles are formed.

The viscosity of concentrated clay suspensions can be controlled by the addition of a peptizing compound [13]. When a small quantity of peptizer is added to a pure smectite clay gel the viscosity decreases sharply. Upon further addition of peptizer the viscosity remains low, in contrast to the action of an electrolyte. Only at high concentrations of peptizer does the viscosity begin to rise. Thus peptizers are economically attractive. An example of a commercial peptizer is tetrasodium pyrophosphate (TSPP or Tetron), an anionic peptizer.

The peptizing agents are attracted to the positive edge sites of the clay particle. Peptization causes the reversal of the positive edge charge. Only a small quantity of peptizer is required to cause the breakdown of the gel structure and therefore lower the

viscosity of the suspension. If the peptizer was adsorbed onto the face of the clay platelet the uptake required to have the same effect would be much higher, and this would require an increase in the basal spacing of the clay, which is not observed.

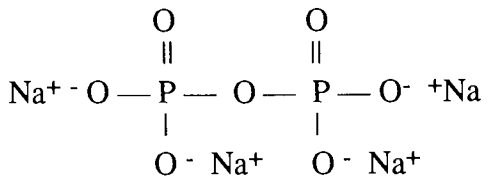

Figure 1.10 The structure of Tetron

The addition of electrolyte to a peptized system would lead to a reduction of the effectiveness of the peptizer, as the positive ions are attracted to the anionic peptizer, reducing its activity. This is known as ion antagonism.

Peptization can also be achieved by reversal of the face charge of the clay platelet. Immobile organic cations, particularly long chain quaternary ammonium ions, can be easily ion exchanged onto the clay, neutralizing the negative face charge. This method is less attractive economically as it requires approximately equal weights of peptizer and clay.

1.4.3 Intercalation

Intercalation refers to the insertion of atoms, ions or neutral molecules into the interlayer region of clays or other layer structures [16] such as graphite, TaS_2 or MoS_2. Intercalation is the reversible insertion of guest species into a lamellar host structure with the maintenance of the structural features of the host. The host and guest may experience some perturbation in their geometric, chemical, optical or electrical properties. This can vary from the subtle to the extreme depending on the reaction. The expanding layers of smectite clays are particularly conducive to the formation of intercalation complexes. There is abundant scope for tailoring the intercalate to produce the desired change in the properties of the clay.

Replacement of interlayer water with neutral organic liquids, such as benzene, pyridine and the aliphatic alcohols can be achieved by simply reacting dried smectites directly with the organic liquids [17]. If the interactions are strong the cations are completely solvated by the organic liquid and there are organic molecules between cations and the oxygen atoms of the silicate layer. If the interactions are weak the cation will reside at

the silicate surface, and only some of the cation coordination sites are occupied by organic molecules. The ease of intercalation of organic liquids enables the intercalation of ethylene glycol and glycerol to be used in the identification of smectite clays and measurement of their surface area.

Intercalated aliphatic compounds with polar groups can be divided into two groups [6], α-complexes, where the chain of the molecule is parallel to the layer of the clay, and β-complexes where the chain stands either perpendicular or at a steep angle to the layer. It follows that α-complexes give relatively small interlayer spacings that remain constant in a series when only the chain length increases, β-complexes can lead to very large increases in basal spacings.

The types of organic complex formed can also be classified according to the bonding mechanism [18], which in turn depends on the properties of the organic molecule, the water content of the system, the nature of the exchangeable cation and the unique properties of the clay mineral structure. Ion exchange reactions are possible with charged organic compounds, these will be considered in the following section. The exchangeable cations determine the surface acidity and therefore the possibility of protonation of the organic compound. However, even in a homoionic clay the surface acidity will vary with hydration level, becoming more acidic as hydration decreases. When protonation of the organic molecule does not occur, the cation may act as an electron acceptor, interacting with electron donating functional groups of organic compounds. The hydration of the clay may be a factor, if the cation retains its primary hydration shell the functional groups of the organic compound may interact with the cation forming a water bridge by hydrogen bonding. When organic cations occupy the exchange sites, other organic compounds may interact with them by hydrogen bonding to form an organic-organic complex on the clay surface. The clay surface makes a contribution to the intercalation of organic molecules through hydrogen bonding between its oxygens or hydroxyl groups and the functional group of the organic molecule. This contribution is highest when the exchangeable cations have a low solvation energy. In addition the charge density of the clay will sterically affect the position and orientation of organic molecules associated with the exchange sites either as cations or indirectly through ion-dipole interactions.

Van der Waal's forces between molecules decrease rapidly with distance between the interacting species. They only become significant in clay-organic complexes, particularly for organic compounds with a high molecular weight. Therefore the

principal van der Waal's interaction is between the intercalated organic molecules rather than between the organic molecule and the clay surface.

If the clay interlayer contains transition metal ions, complexes may be formed by the donation of π-electrons from the transition metal ion to an organic compound. This complexation has been observed between benzene, xylene, toluene and chlorobenzene and copper(II) exchanged montmorillonite, under dry conditions. It is possible to form covalent bonds between the silicate surface and organic groups by reacting a Si—OH group on the silicate surface with an acid anhydride or thionyl chloride and an organolithium reagent.

1.4.4 Ion Exchange

Smectite clays contain cations held outside the silicate lattice structure [1], mainly in the interlayer region. While these ions have no effect on the structure of the silicate lattice they have a great influence on the properties of the clay. These ions can be replaced with other cations, usually by a treatment with ions in aqueous solution. This exchange reaction is stoichiometric. The property of ion exchange is known as the cationic exchange capacity (C.E.C.) and is measured in terms of milliequivalents (meq) per 100 g of clay, this is measured at pH 7. A range of cationic exchange capacities are quoted for different clay minerals as there is no single value that is characteristic of a given group of minerals. The most common exchangeable cations are Ca^{2+}, Mg^{2+}, H^+, K^+, NH_4^+ and Na^+.

There are three causes of cationic exchange in smectite clays [1]. In smectite clays around 80% of the C.E.C. is caused by lattice substitution. The substitution of magnesium for trivalent aluminium in the octahedral layer of montmorillonite results in a positive charge deficiency, this is balanced by the introduction of cations into the interlayer region of the clay. A charge deficiency can also be caused by the substitution of aluminium for tetravalent silicon in the tetrahedral layer of the silicate structure. Cations resulting from lattice substitution are mainly found at the basal surface, balancing the charge within the platelet.

Broken bonds around the edges of the platelet give rise to unsatisfied charges which are balanced by exchangeable cations. As broken bonds appear at crystal edges when the particle size decreases, the number of broken bonds, and exchangeable cations, increases. Broken bonds account for approximately 20% of the C.E.C. in smectite clays. In the kandite group this is the major cause of exchangeable ions. In smectite

structures there is a small number of exposed hydroxyl groups around the broken edges of the crystal. The hydrogen of these hydroxyl groups may be replaced by a cation which would become exchangeable.

Depending on the cause of exchange capacity, the cations can be at the basal surface or at the edge of the platelet. This gives rise to different bonding energies for cations in different positions. Cations on the edges of the platelet can be replaced more readily than cations in the interlayer region and cations balancing tetrahedral lattice substitution are held more strongly to the lattice than cations balancing octahedral substitution as they are closer to the site of the charge deficiency. In a hydrated smectite clay the cations at the crystal edges are held directly in contact with or very close to the clay surface. The cations located in the interlayer region are held midway between successive basal surfaces. As the concentration of water increases the exchangeable cations are separated from the clay surfaces by increasing layers of water molecules. Thus the most rapid ion exchange reactions take place in dilute aqueous solutions.

There are many factors that determine the rate of cationic exchange, and they may differ for different groups of minerals. In montmorillonites the replacing power of common cations is $Li^+ < Na^+ < K^+ < Ca^{2+} < Mg^{2+} < Al^{3+}$. It can be seen from this that divalent ions will replace monovalent ions more readily than monovalent ions will replace divalent ions. In ions of the same valency, replacing power increases as the unhydrated radius of the ion increases. Increased concentration of the replacing ion causes greater ion exchange by that ion. This is to be expected as cationic exchange is a stoichiometric reaction and the laws of mass action will hold. The ease of replacement of an ion depends not only on the nature of the replacing ion but on the ions filling the remaining exchange sites. As the amount of exchangeable calcium ions on the clay is reduced, the remaining calcium ions become more difficult to remove. In contrast, sodium ions become easier to replace as the degree of saturation of sodium ions is reduced. Magnesium and potassium are not affected by the degree of saturation to the same extent as calcium and sodium.

Any advantages of heating an ion exchange reaction are outweighed by a decrease in cationic exchange capacity on heating. Even moderate heating (<130°C) causes the fixation of the resident cations making them irreplaceable. At low pH ion exchange is slow as hydrogen ions can compete with the metal ion for the exchange sites. At high pH changes in the solution chemistry of the metal ion become the dominant factor in determining the rate of ion exchange.

The anion used in the ion exchange experiment can affect ion exchange, but the effect is different for different cations and different minerals. The exchange reaction of copper onto a sodium montmorillonite [19] depends on the nature of the anion: NO_3^-, ClO_4^- > Cl^- > SO_4^{2-}. For exchanged transition metals the effect of organic ligands must be considered. Two groups of organic ligands can be easily identified. Acidic ligands (e.g. the carboxylic acids) facilitate desorbtion of clay bound metal ions due to the presence of acidic protons. Amine ligands (e.g. ammonia, 2,2'- bipyridyl, 1,2-diaminoethane) enhance the affinity of the metal ion for the interlayer region, due to complexation. Transition metal complexes can be formed on the clay by allowing a transition metal ion exchanged clay to contact with a solution of the appropriate ligand. Smectite clays exchanged with transition metals can be used to remove amine pollutants from aqueous solutions by complex formation in the interlayer of the clay [20].

Large transition metal complexes can be exchanged into smectite clays [21,22]. It has been shown that the stability constants of copper, cobalt, nickel and zinc complexes of polyamines such as ethylenediamine and diethylenetriamine are three orders of magnitude higher when the complex is exchanged onto montmorillonite, than in aqueous solution [23]. There are two mechanisms for the uptake of transition complexes by smectite clays, ion exchange and the intercalation of excess beyond the cation exchange capacity [24]. The extent of the intercalation reaction, beyond the cationic exchange capacity, is dependent on the nature of the counter anion: SO_4^{2-}, Br^- > ClO_4^- > Cl^-. Ion exchanged metal complexes can exhibit catalytic activity when immobilized in the clay interlayer. A $[Co(bipyridyl)_3]^{3+}$ complex on hectorite has been shown to efficiently catalyze the reduction of nitrobenzene to aniline, both chemically, in the presence of $NaBH_4$ and electrochemically on a platinum electrode [25].

Organic cations can easily replace exchangeable metal ions [4]. The affinity of alkylammonium cations for the clay is linearly related to the molecular weight, with the exception of small methylammonium and large quaternary ammonium ions. Thus, the more the length of the chain increases the greater the affinity for the clay. Within a group of primary, secondary and tertiary amines the ease of ion exchange is R_3NH^+ > $R_2NH_2^+$ > RNH_3^+. This is explained in terms of the shape and size of the ion. In common with inorganic ion exchange, sodium cations are more easily replaced than calcium ions by organic cations. Certain properties such as pH, hydrogen bonding, ion-dipole interactions and van der Waal's forces influence the ease of exchange and ease of replaceability of organic cations. Also the interaction of the organic cation with water must be considered when investigating the relationship between organic and inorganic cations in the interlayer region.

In addition, organic compounds may become cationic after intercalation [18], through protonation and then undergo ion exchange. The sources of the protons are (i) exchangeable protons occupying exchange sites, (ii) water associated with metal cations at the exchange sites, particularly the more electro-negative ions such as Al^{3+}, or (iii) proton transfer from another cationic species at the clay surface. The most common proton acceptors are nitrogen containing compounds, such as ammonia, amines and pyridine.

In partially exchanged systems organic and inorganic cations are not distributed uniformly and a segregation of the two kinds of ions takes place, as an incoming organic ion will replace a metal ion in a layer containing some exchanged organic cations before replacing a metal ion in a layer with no exchanged organocation. This is because mixtures of cations in any one interlayer makes the formation of a geometrically regular water layer difficult. In montmorillonite interstratified layers occur in which each layer contains mainly one type of cation, a situation which is thermodynamically favoured.

1.4.5 Pillaring of Smectite Clays

Smectite clays have been studied as catalysts for acid calalyzed reactions (alkylations, redox reactions, additions to alkenes) [26]. It is believed that under reaction conditions the clay remains expanded with the catalytic process taking place in the interlayer region. To achieve optimum conditions the reaction temperature must be raised, often to 250°C. At these elevated temperatures any catalytic activity is precluded by dehydration of the clay and collapse of the interlayer region destroying potential calalytic activity. The problems imposed by interlayer collapse have largely been removed by the introduction by ion exchange of thermally robust molecular pillars to prop the silicate layers apart in the absence of a swelling solvent at high temperatures.

The concept of pillaring was first demonstrated using tetraalkylammonium ions to introduce interlayer porosity into montmorillonite [27,28]. However these pillars thermally decompose above 250°C. Large transition metal complexes can be ion exchanged into the clay giving enhanced catalytic activity but these begin to thermally decompose below 450°C [29]. Pillared smectite clays that are thermally stable above 500°C are now well known, these are based on polynuclear hydroxymetal cations [26]. Many pillared clays have been produced using polycationic species of aluminium, chromium, iron, magnesium, nickel, niobium, silicon, tin and zirconium. Using these polycationic

species it is possible to produce pillared clays with pore sizes varying from 2 Å to above 25 Å (figure 1.11), which is a greater range than that provided by the zeolites (2 Å to 8 Å). Thus by varying the size of the pillar and/or the spacing between pillars it is possible to adjust the catalyst to suit a certain application. This has renewed interest in pillared clays as catalysts particularly in hydrocarbon cracking at 500°C where pillared clays show catalytic activity comparable with present industrial catalysts such as zeolites.

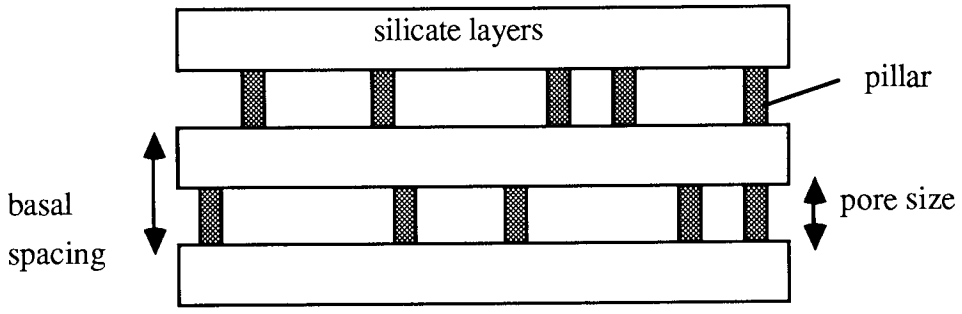

Figure 1.11 Schematic representation of a pillared clay

Aluminium [30] and zirconium [31] produce pillared clays thermally stable above 500°C, with surface areas of 200 - 500 m^2g^{-1} and interlayer (gallery) spacings (pore size) of 6 - 10 Å. A recent solid state n.m.r. study indicates that the dominant species in aluminium pillared clays is an Al_{13} oligomer based on the known cation $Al_{13}O_4(OH)_{28}^{3+}$. At elevated temperatures this species undergoes dehydroxylation to form metal oxide clusters. This interlayer dehydroxylation can be written:

$$Al_{13}O_4(OH)_{28+n}^{(3-n)+} \longrightarrow 6.5\ Al_2O_3 + (3-n)H^+ + 12.5\ H_2O$$

where the aluminium oxide is in the form of small clusters. The formation of oxide pillars is thought to account for the thermal stability of these pillared clays. The precise nature of the pillars depends on the method used to prepare the pillaring solution, the OH/M ratio and the age of the solution. Electrolytic hydrolysis of an $AlCl_3$ solution with an OH/Al ratio of 2.4 produces a solution that contains effectively only Al_{13} as judged by ^{27}Al n.m.r. [32].

The solution chemistry of zirconium is also complex [30], but it is known that the species present in solid zirconium chloride is $[(Zr(OH)_2.4H_2O)_4]^{8+}$. The four zirconium ions are located at the corners of a slightly distorted square linked together by OH bridges. When dissolved in water the solution becomes acidic due to hydrolysis. Eventually a tetramer with the formula $[Zr_4(OH)_{14}(H_2O)_{10}]^{2+}$ is formed [33], with two zirconium

atoms having a single positive charge and the other two being neutral. On ageing the solution, larger species are found due to the polymerization of tetramers. The largest basal spacing for a zirconium pillared clay, 22 Å, is formed when the solution is aged at 100°C for 24 hours before being added to the clay and the resulting slurry is aged at room temperature for a further 30 minutes before drying at 60°C.

Chromium pillared clays exhibit exceptionally large basal spacings (up to 28 Å) and unique properties as dehydrogenation catalysts at temperatures up to 550°C [34]. For optimum pillar size a solution of $Cr(NO_3)_3.9H_2O$ and Na_2CO_3 is aged at 95°C for 36 hours before addition of the clay and for 1.5 hours at room temperature after the hot addition of the clay. The elevated ageing temperature is required as the kinetics of formation of polyoxochromium species is slow. A recent EXAFS study [35] of the chromium pillar suggests that the pillaring species is $[Cr_4(OH)_2(H_2O)]^{10+}$ and on heating to 250°C a mixed valence material based on $Cr^{III}_2Cr^{IV}_3O_{12}$ is formed on the clay.

The number of metals that produce oligomeric species in solution is limited, therefore the hydration and oxidation of metal cluster cations has been considered for the formation of pillars in smectite clays. The trinuclear acetate iron(III) ion, $[Fe_3(OCOCH_3)_7OH]^+$ has been used to produce iron oxide pillared clays [36]. Other metal cluster cations such as $Ta_6Cl_{12}^{2+}$ and $Nb_6Cl_{12}^{2+}$ have also been used to produce oxide pillars [37].

1.5 Uses of Smectite Clays

The uses of smectite clays can be divided into two groups; high volume uses and low volume uses [5]. Over the past two decades the major uses of smectite clays have been in foundry moulding sands, oil well drilling and iron ore pelletizing. Other large volume uses are animal feed pelletization, filtering, decolourizing and clarifying liquids, absorbents and civil engineering (waterproofing, mortar). Small volume uses include paints, radioactive waste disposal, lubricants, catalysts, inks, soaps, seed coatings, paper coatings and pottery.

Several million tonnes of smectite clays are used annually in the metallurgical industry for preparing moulding sands. Sand, clay and water are mixed together to make the sand plastic and cohesive so that it can be moulded around a pattern. After the pattern is removed the smectite clay must give the sand mould sufficient strength to maintain the shape of the cavity before, during and after the pouring of the hot metal. The

preparation of drilling muds requires over two millions tonnes of smectite clay per year. Smectite clays are used to thicken the drilling muds used to lubricate drill heads and transport mined material from the drill bit to the surface. Only sodium and calcium exchanged smectite clays are suitable for this application. Further improvements to the performance of the muds may be achieved by the introduction of organic and inorganic additives to the clay, particularly organic cations.

Only sodium exchanged smectite clays are suitable for iron ore pelletization as they are the only smectites to provide the required pellet strength and good binding properties. Low grade iron ore is ground finely during its separation and then pelletized with a smectite clay before drying and packaging. Animal feeds use both sodium and calcium smectite clays as binders in the pelletization process.

For centuries smectite clays have been used to clarify wine because the negative layer charge of the clay coagulates the positively charged particles that form colloidal impurities in wine. Smectite clays are now used to clarify water, beer, vinegar and fruit juices, and they are used in the treatment of animal and mineral oils. Acid treated smectites are used to filter and decolourize vegetable oils. Acid exchanged clays are used for pet litter and for absorbing oil and grease from floors. High swelling smectite clays are used as waterproofings and groutings in civil engineering. Also they are used to increase the plasticity of mortar and to make concrete pliable as well as impermeable.

There are many miscellaneous small volume and speciality uses of smectite clays. Industry is constantly investigating further speciality uses of smectite clays. This research aims to further the use of smectite clays in the paper industry.

1.5.1 The Use of Clays in the Paper Industry

Clays have been used in the paper industry for many years. Kaolinite has been used as a filler and a surface coating [38]. As a filler, because of its white colour, kaolinite provides increased opacity to the paper. When kaolinite is added as a surface coating the appearance of the paper is improved and a smooth receptive surface is provided for printing. Gloss, brightness, opacity and smoothness are all increased with increasing kaolinite coat weight and with decreasing clay particle size. Smectite clays can also be used as surface coatings for speciality papers [39]. The small crystal size and good film forming properties are distinct advantages.

1.5.2 The Use of Smectite Clays in Electrographic Papers

Electrographic printing requires a dielectric paper which consists of a base paper with a conductive surface coating on both sides and a dielectric film of high resistivity on one side [40]. Typically the dielectric coating is a highly resistive polymer such as polyvinyl butyral, polystyrene or polyvinyl acetate. Smectite clays can be used to provide the conductivity required in electrographic papers.

Electrographic printing is a non impact printing method that is particularly well suited for large format text and graphic printing. It is often used in automated drawing offices and computer aided design (CAD). In the electrographic printing process the paper passes between the writing nib and a backing electrode. The dielectric coated side of the paper faces the writing electrode and the conductive side faces the backing electrode. The voltage gradient between the electrodes on imaging is up to 600 V and the air gap is only a few micrometers. The high voltage gradient causes ionization of the air in the gap and ions migrate to the surface of the dielectric coating. As charge accumulates on this surface, ions of the same charge flow through the conductive paper into the external circuit. A charge opposite to the surface charge is formed on the back side of the dielectric layer to create a strong electric field through the dielectric layer in the shape of the writing electrode. This leaves the paper with a negative charge on the dielectric coated surface of the paper. The printer applies a programmed voltage to densely spaced writing electrodes (nibs) embedded in a stationary writing head. On digital command the nibs create a latent image on the paper as it passes over the writing head [40].

The latent electrographic images are exposed to a liquid toner producing a permanent image. The toner is a non polar liquid containing submicrometer sized positively charged particles. In modern printers the toner is applied with a toner fountain, a vacuum drier removes excess toner leaving only electrostatically attracted toner which becomes fixed during the drying process.

Manufacturers of electrographic paper include James River Graphics Chartham Paper Mill, the sponsors of this research. James River is the second largest paper manufacturer in the world and is a major integrated producer of pulp, paper and converted products as well as coated and multilayer film products. Chartham has been an active paper mill since 1738 and was acquired by James River in 1988. Chartham now manufactures speciality, high quality opaque and translucent papers, including conductivized base paper. Conductivized base paper is dielectric coated by James River in the U.S.A..

Base paper can be conductivized by the addition of a 1 gm^{-2} per side surface coating of a white smectite clay. The clay is added from aqueous solution during the manufacture of the paper. Before the final drying process the paper is passed through the size bath where the paper is completely immersed in the clay solution. The viscosity of the solution in the size bath is carefully controlled as this determines the coat weight applied to the paper. If the viscosity falls, the coat weight falls and the conductivity will fall below the required specification. If the viscosity rises, the solution will begin to form a gel, preventing the formation of a uniform surface coating.

1.6 Objectives

At present there is a demand for conductive paper that can be manufactured cheaply and efficiently, for electrographic printing. The smectite clays show promise as conductive coatings for electrographic coatings, particularly the synthetic hectorite, laponite [41]. However, as laponite is a synthetic clay it costs ten times as much to use as natural smectites. In the production of electrographic paper the laponite accounts for approximately 11% of the final cost (pulp accounts for 25%). The small crystal size of laponite presents a problem during the application of the coating. As the individual laponite crystals are small, a thixotropic gel is readily formed from an aqueous suspension. This can lead to problems in maintaining a uniform coat weight (and conductivity) throughout a reel of paper, leading to a potential waste problem.

If the conductivity of laponite was increased by an order of magnitude, and this increase was passed on to the conductivity of the paper, the coat weight of laponite applied to the paper could be greatly reduced. This would allow the use of a more dilute suspension of laponite in the size bath, reducing the potential for gelation. This would lead to reduced costs and greater efficiency. Another way to reduce costs would be to replace laponite with a natural smectite clay. This would be possible if the conductivity of natural smectite clays could also be increased by an order of magnitude.

Electrographic papers show a humidity dependence in their conductivity. At high relative humidity excess charge is deposited on the paper. This leads to charge bleeding away from the exact point where it was applied resulting in blurring. Also excess toner is applied to the paper which can cause smearing. At high humidities debris builds up on the electrode leading to poor printing quality. At low relative humidities the conductivity of the paper is low. This leads to low charge deposition and low plot

density. The recommended operating relative humidity range at 21°C is 38 - 58% [42]. However this can be difficult to maintain as relative humidity is temperature dependent.

The conductivity of smectite clays is not well understood. If the mechanism of conductivity was known it could be possible to produce increases in the conductivity of the smectite clay with some certainty. Also, it could be possible to decrease the humidity dependence of the conductivity. Paper with greatly enhanced conductivity is also required by new printing technology.

1.7 Previous Work

Attempts to increase the conductivity of laponite and montmorillonite have been previously reported [43,44]. In both cases tetrathiafulvalene (TTF) was intercalated into clays exchanged with transition metals in addition to the sodium form of the clays. Evidence from ^{57}Fe Mössbauer spectroscopy and e.s.r. shows a small amount of charge transfer from TTF to structural iron(III) in montmorillonite, forming $TTF^{0.7+}$ and structural iron(II). This is a similar mechanism to that proposed for the formation of benzidine cations on montmorillonite. With laponite the formation of $TTF^{0.7+}$ can be observed in the presence of a redox active cation such as Cu(II). If the laponite is in the sodium form there is no evidence for TTF radical cation formation (there is no structural iron in laponite). However the conductivity of the resulting clay is increased by almost an order of magnitude. The conductivity of sodium montmorillonite intercalated with TTF is similarly enhanced. Clays ion exchanged with $[TTF]_3(BF_4)_2$ show no increase in conductivity.

Disc conductivities were measured over the voltage range 4 - 20 V. Direct current (d.c.) measurements are not ideal for the investigation of clays as polarization of the clay dipoles will easily occur. During the production of electrographic paper the d.c. conductivity is routinely monitored. In an electrographic printer the writing head is switched on and off rapidly to produce the required image, this produces large voltages that are then quickly removed by the back electrode. Therefore the potential performance of papers for electrographic printing could be more suitably measured using an alternating current (a.c.) method. The conductivity of clay discs should be measured over a range of a.c. frequencies, and results compared at a frequency mimicking the operation of an electrographic printer.

Chapter Two

PHYSICAL TECHNIQUES

2.1 Atomic Absorption Spectroscopy

Atomic absorption measurements were carried out on a Perkin Elmer 360 instrument. NaCl BDH atomic absorption standard was used for sodium analysis.

2.2 Cyclic Voltammetry

Cyclic voltammetry was carried out at Coventry Polytechnic on Princeton Research 273 and 362 scanning potentiostats linked to a Rikadenki X-Y recorder. All potentials are cited relative to a saturated calomel electrode (SCE). In all cases the supporting electrolyte was 0.1 M tertabutylammonium perchlorate in dry acetonitrile, degassed with dry nitrogen prior to scanning.

2.3 Electron Spin Resonance Spectroscopy

Some e.s.r. spectra were measured using a Jeol PE-1 X band instrument. Variable temperature measurements were provided by Dr. K. D. Sales of Queen Mary and Westfield College.

2.4 Elemental Analysis

Carbon, hydrogen and nitrogen analysis was carried out in duplicate by Elemental Microanalysis of Oakhampton, Devon.

2.5 Diffuse Reflectance UV/Visible Spectroscopy

Diffuse reflectance uv/vis spectroscopy was carried out on a Pye Unicam SP800 instrument, MgO was used as a reference.

2.6 Fourier Transform Infra Red Spectroscopy

Infra-red analysis was carried out using a Perkin Elmer 1710 FT-IR. Either KBr discs or nujol mulls with caesium chloride windows were employed for analysis.

2.7 Gas Liquid Chromatography

A Pye Unicam GCD chromatograph was used for Gas Liquid Chromatographic analysis.

2.8 M.A.S. Nuclear Magnetic Resonance Spectroscopy

Solid samples were analysed on a Brucker AC300 instrument with a solid state probe. Samples were spun at the magic angle at approximately 5 kHz. Solid state ^{13}C spectra were measured at a frequency of 75.469 MHz, solid state ^{119}Sn spectra were measured at a frequency of 106.918 MHz.

2.9 Mössbauer Spectroscopy

Mössbauer spectra were provided by Dr. F. J. Berry, School of Chemistry, Birmingham University. ^{119}Sn Mössbauer spectra were recorded at 77K with a microprocessor controlled Mössbauer spectrometer using a calcium stannate ($Ca^{119m}SnO_3$) source. The drive velocity was calibrated with a natural iron foil absorber. All spectra were computer fitted.

2.10 Powder X-Ray Diffraction

X-ray powder diffraction patterns were recorded with a Phillips X-ray diffractometer using cobalt K_α radiation.

2.11 Scanning Electron Microscopy

In the early stages of this work s.e.m. was utilized to provide elemental compositions of modified clay samples. The analysis was carried out on Cambridge Instruments Company, Sterioscan S90B. A linked systems analyzer was used for X-ray energy analysis.

2.12 Solution Conductivities

Solution conductivities were obtained from 1×10^{-3} M solutions of compound using a Mullard bridge in configuration with a bright platinum electrode.

2.13 UV/Visible Solution Spectroscopy

UV/Visible solution spectra were obtained from a Pye Unicam SP1800 spectrometer using 1 cm quartz cells.

2.14 Solid Disc Conductivities

In order to measure the conductivity of a clay sample, 0.25 g of the sample was pressed into a solid disc using a conventional hydraulic press, normally reserved for pressing KBr discs for infra red analysis. Pressing at 5 tonnes for 3 minutes created a disc 13 mm in diameter and approximately 1 mm thick. Disc thickness was measured using a dial micrometer. Discs were stored at 52% relative humidity in a desiccator containing a saturated aqueous solution of magnesium nitrate [45]. Freshly stripped enammelled copper wires (0.7 mm thick) were attached to the disc surface using silver loaded epoxy resin (paste), obtained from R.S. components. Care was taken to completely cover the disc surfaces with resin while avoiding the edges of the disc. Samples were stored for one week prior to measurement. All samples were measured at least in duplicate.

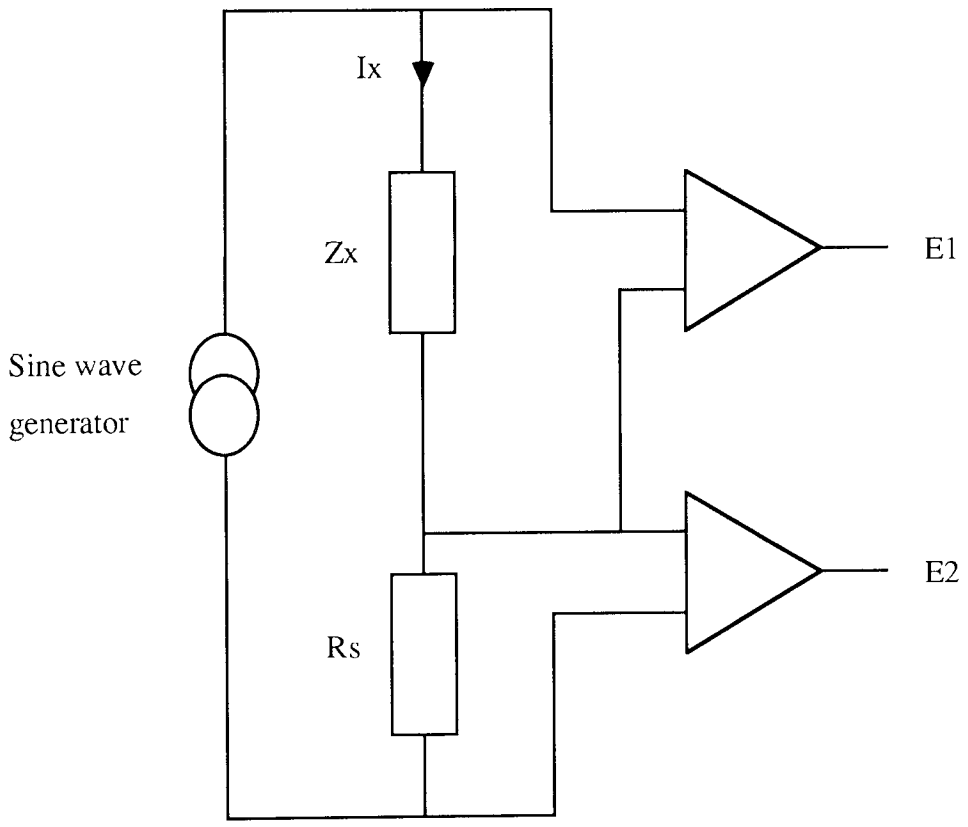

Figure 2.1 A simplified block diagram of the Genrad 1689 RLC Digibridge measurement circuit.

The resistivity of the silver loaded epoxy resin and connecting wire was measured and found to be several orders of magnitude lower than that of the clay samples.

All measurements were taken on a Genrad 1689 Precision RLC Digibridge, a microprocessor controlled, automatic, a.c. impedance meter. In the Digibridge a microprocessor calculates impedance characteristics of the sample under test from a series of voltage measurements. These measurements are made across a standard resistor, R_S, carrying the same current as the sample under test, Z_X. Each set of voltage measurements is made in rapid sequence with a phase sensitive detector (which uses four reference signals 90° apart, which have the same frequency as the test signal), therefore these measurements subtract out any fixed offset errors, and the value of the common current cancels out of the calculations.

The measuring technique of the Digibridge requires no calibration of the instrument after the initial manufacturer's calibration. Also there is no reactance standard required. The only precision components in this instrument are four standard resistors and a quartz-crystal stabilized oscillator. The microprocessor can remove any stray capacitance and conductance from the test connections if a simple open circuit and short circuit zeroing procedure is followed on power up. The instrument autoranges to find the correct measuring range.

A sine wave generator drives current, Ix, through the sample under test, Z_X, and a standard resistor, R_S, in series. Two differential amplifiers with the same gain, K, produce voltages E1 and E2.

$$E1 = KZ_X I_X \qquad \text{equation 2.1}$$

$$E2 = KR_S I_X \qquad \text{equation 2.2}$$

therefore

$$\frac{E1}{E2} = \frac{Z_X}{R_S} \qquad \text{equation 2.3}$$

and

$$Z_X = R_S\,[E1/E2] \qquad \text{equation 2.4}$$

Z_X is the impedance of the sample under test. From this and information stored in the microprocessor it is possible to calculate the capacitance and resistance (and other properties) of the sample under test. The resistance and capacitance can be displayed simultaneously by the Digibridge.

The resistance and capacitance of clay discs were recorded over a range of frequencies from 100 kHz to 11.7 Hz. Resistance values were converted to resistivity, ρ, (and conductivity, σ) using the equation [45]:-

$$\text{resistivity} = \frac{1}{\text{conductivity}} = \frac{Ra}{l} \qquad \text{equation 2.5}$$

where R is the measured resistance of the sample in ohms, a is the cross sectional area of the disc in mm^2 and l is the thickness of the disc in mm. The units of volume resistivity are Ω mm. Therefore the units of conductivity are $\Omega^{-1}mm^{-1}$.

Chapter Three

TRI-2-PYRIDYLAMINE COMPLEXES ON THE SURFACE OF LAPONITE

3.1 Introduction

The ion exchange of large co-ordination complexes into smectite clays (see section 1.4.4) is well known [21,22] and this exchange can in some cases increase the stability of the complex to dissociation [23]. Also, in addition to ion exchange, complexes can be sorbed in excess of the cationic exchange capacity [24]. Large complex ions have been used to pillar smectite clays, however they are not as effective as polycationic pillars as they decompose below 450°C [29]. It has been demonstrated [25] that $[Co(bipyridyl)_3]^{3+}$ ions exchanged onto hectorite may be reduced chemically (using $NaBH_4$) or electrochemically to the Co(I) complex. The $[Co(bipyridyl)_3]^{3+}$ complex on hectorite can effectively catalyze the reduction of nitrobenzene to aniline, both chemically, in the presence of $NaBH_4$, and electrochemically on a platinum electrode. The clay supported catalyst offers the twin advantage of ease of separation and reusability.

The exchange of $[Co(bipyridyl)_3]^{2+}$ onto a clay colloid has also been reported [48] and recently a quantitative examination of a $[Co(bipyridyl)_3]^{2+}$ clay system was reported [49]. The electrochemically produced Co(I) species was an effective catalyst for the dehalogenation of 4,4'-dibromodiphenyl and of chloroalkanes in organized assemblies (in the presence of cetyl trimethylammonium bromide). The electrode surface provided an environment featuring high local concentrations of reactants, causing enhancement of the second order catalytic process.

The ligand tri-2-pyridylamine, tripyam, co-ordinates either as a bidentate or as a vicinal (tripodo-) terdentate base [50]. In the *bis*-terdentate complex, $[Co(tripyam)_2](ClO_4)_2$, which exhibits spin cross over behaviour [51], the room temperature structure [52] (pseudo- "high spin") shows Co—N bond lengths in the range 2.100(2) to 2.152(2) Å and N—Co—N angles between 84.86(7) and 86.09(8)°. By contrast, the low spin Fe(II) complex deviates only trivially from true octahedral symmetry [53]. The behaviour of the corresponding copper(II) system, $Cu(tripyam)_2(ClO_4)_2$ is more complex [50] with interchangeable bi- and terdentate isomers [50,54].

Smectite clays ion exchanged with large co-ordination complexes can be cast as films on the surfaces of platinum electrodes for electrochemical investigation, these electrodes are known as clay modified electrodes [55]. Cyclic voltammetry has been used in recent years to investigate clay modified electrodes [56]. Ghosh and Bard [55] added finely divided platinum and polyvinyl alcohol (PVA) to the clay in order to produce more robust electrodes. They speculate that the role of the platinum is not to generate electroactivity but to provide strength within the film. Also, they suggested that the role

of the PVA is to enhance electrical communication between the particles, by swelling the clay and enhancing edge to edge interactions, giving the film better binding qualities and a stronger voltammetric response.

Clay modified electrode systems have been extensively studied by Bard and his co-workers [55,57-60]. They suggested that the electroactivity of the bound species was dependent on the swelling and spacing between the layers of the clay. Charge mobility within the clay layers was thought to occur via an electron hopping mechanism. It was also concluded that there was a physical movement of electroactive species through the clay interlayer region, so that intercalated species could eventually appear at the surface of the electrode. A recent investigation of electroactivity by Pinnavaia [61] demonstrated that cations bound electrostatically to any exchange site on a smectite clay, up to the cation exchange capacity, are rigorously electro-inactive. The electroactivity of clay modified electrodes was attributed to cations which are bound to the surface in excess of the clay cation capacity, by an ion pair mechanism.

The initial objective of this study was to investigate the electrochemical response of clay (laponite) modified electrodes doped with complexes of tri-(2-pyridyl)amine. However, some new observations were made concerning the co-ordination chemistry of the complexes which needed clarification before these objectives could be addressed.

3.2 Sample Preparations

3.2.1 Ligand Synthesis

Tri-(2-pyridyl)amine, a yellow crystalline solid, was prepared by a literature method [62]; found: C, 72.6; H, 4.93; N, 22.6%; $C_{15}H_{12}N_4$ requires: C, 72.6; H, 4.87; N, 22.6%. M.p. 129°C (lit [62], 130°C).

6-Methyl-2-pyridyldi-(2-pyridyl)amine, a dark oil, was synthesized by a literature method [63]; found C, 73.3; H, 5.51; N, 21.4%; $C_{16}H_{14}N_4$ requires: C, 73.3; H, 5.34; N, 21.4%.

4-Methyl-2-pyridyldi-(2-pyridyl)amine, a semi-crystalline solid was prepared by a literature method [63]; found: C, 73.2; H, 5.40; N, 21.4%.

3.2.2 Complex Synthesis

Metal salts were commercial specimens and were used as obtained.

Bis(tri-2-pyridylamine)cobalt(II) diperchlorate was by prepared by a literature method[50], found: C, 47.4; H, 3.04; N, 14.8%. $C_{30}H_{24}N_8CoCl_2O_8$ requires: C, 47.7; H, 3.20; N, 14.9%.

Bis[6-methyl-2-pyridyl-di-(2-pyridyl)amine]cobalt(II) diperchlorate monohydrate was prepared [64] using ethanol rather than triethylorthoformate [65] as a solvent. This preparation yields the monohydrate [64] rather than the anhydrous product [65].

Bis(tri-2-pyridylamine)iron(II) diperchlorate monohydrate was prepared [64] by the reaction of $Fe(ClO_4)_2.6H_2O$ (10.35 g) in triethylorthoformate (10 ml) with tri-2-pyridylamine (0.7 g) in ethanol (10 ml) with the passage of dinitrogen. A red-orange solid precipitated immediately and was separated and washed with ethanol. Found: C, 46.9; H, 3.22; N, 14.6%. $C_{30}H_{28}FeN_8O_9$ requires C, 46.9; H, 3.38; N, 14.6%. The previously reported complex was anhydrous [50] but the Mössbauer parameters [64] are identical to those previously reported [66]. However, the Mössbauer spectrum shows a resonance (5% of total intensity) for a high spin iron(II) complex [64]. This is likely to be the *tris*-bidentate (tri-2-pyridylamine)iron(II) species. In support of this, if the above synthesis is repeated without the passage of dinitrogen a pale green complex is found, $Fe(tripyam)_3(ClO_4)_2.3H_2O$ with bidentate ligands, found C, 52.0; H, 4.06; N, 16.0%. $C_{45}H_{42}Cl_2FeN_{12}O_{11}$ requires C, 51.2; H, 4.00; N, 15.9%.

Blue $[Cu(tripyam)_2](ClO_4)_2$ and yellowish-green $[Cu(tripyam)_2(ClO_4)_2]$ were prepared as previously reported [50]. The blue isomer was prepared from a cold ethanolic solution and the yellowish-green isomer was prepared by boiling the solution.

Reactions were carried out between 4- and 6-methyl-di-(2-pyridyl)amines and copper(II) perchlorate. Although a literature method [54] was followed, the products isolated here were hydroxo-bridged dimers of the type $[CuL(OH)]_2(ClO_4)_2$, found (4-methyl-): C, 43.3; H, 3.12; N, 12.2%. $C_{32}H_{30}Cl_2Cu_2N_8O_{10}$ requires C, 43.4; H, 3.40; N, 12.6%. Found (6-methyl-): C, 42.2; H, 3.22; N, 11.9%. $C_{32}H_{32}Cl_2Cu_2N_8O_{11}$ (the monohydrate) requires: C, 41.7; H, 3.69; N, 12.1%. Solution conductivity measurements in acetonitrile confirm that the complexes were 2:1 electrolytes based on the dimeric formula, thus $[Cu_2L_2(OH)_2](ClO_4)_2$, Λ_M (10^{-3}) = 278 Ω^{-1} $mol^{-1}dm^{-1}$, compared with $[CoL_2]$ $(ClO_4)_2$, $\Lambda_M(10^{-3})$ = 280 $\Omega^{-1}mol^{-1}$ dm^3.

3.2.3 Methods of Exchange of Complexes onto Laponite

Laponite, a synthetic hectorite clay, was supplied in the sodium form. Laponite RD was the chosen grade of laponite as it the purest of the forms available to us. Two methods of ion exchange were used.

3.2.3.1 Ion Exchange Using A Mechanical Flask Shaker

Laponite RD was added to 100 ml of de-ionized water and treated with 0.75 g of tri-2-pyridylamine complex dissolved in 150 ml of de-ionized water. The mixture was sealed in a 500 ml conical flask and attached to a mechanical flask shaker for one week. The clay was then removed, separated and air dried.

3.2.3.2 Ion Exchange Using A Microwave Heating Method

The use of microwave heating in chemistry laboratories is known to produce great enhancements in the rates of organic [67] and organometallic [68] reactions. Also remarkable heating of inorganic substrates [69] can occur. It was recently demonstrated that the process of ion exchange onto clay may be greatly accelerated [70]. Lithium exchanged laponite can be produced in 5 mins. in a microwave oven [70] compared to several weeks using a method based on the classic method of Posner and Quirk [71]. A further advantage of microwave heating is that the rapidity of the process may reveal chemistry which could be missed during the passage of time required by conventional exchange methods [70]. These observations will be confirmed here.

1 g of laponite RD and 0.12 g of tri-2-pyridylamine complex were added to absolute ethanol (10 ml). The mixture was tightly sealed in a Teflon reaction vessel. The vessel was subjected to five one minute bursts of microwave energy in a Sharp Carousel 650 W microwave oven. On cooling, the vessel was opened in a fume cupboard and the clay was separated, washed with ethanol and then air dried.

3.2.4 Preparation of Clay Modified Electrodes

Clay modified electrodes were prepared from laponite RD, polyvinyl alcohol (PVA) and platinum. PVA and platinum are required to produce robust clay modified electrodes. The method is based on that developed by Bard and his co-workers [55,57,58]. Laponite RD (10 g) was sonicated in de-ionized water (100 ml) for 30 mins. The resultant gel was centrifuged at 4000 rpm in a Clandon T62 centrifuge for 3 hours to remove larger

particles. Platinum dichloride (0.05 g) and PVA (0.66 g) were added to a 40/60 ethanol/de-ionized water mixture (50 ml) and refluxed to form a homogeneous mixture (approx 30 mins.) to which 5 g of the clay gel was added. The reflux was continued for a further 1 hour. A 1 x 1 cm platinum plate electrode (cleaned ultrasonically) was treated on one side with a few drops of the clay/PVA/Pt mixture, to completely cover the surface. The electrode was allowed to air dry slowly overnight in an enclosed space, to prevent cracking of the drying film. The reverse side was treated similarly.

The electrode was then dipped in a 0.1M acetonitrile solution of the desired complex for 1 hour, washed in a stream of de-ionized water and allowed to air dry. To examine possible differences between the electrochemical response of clay modified electrodes dipped into solutions of redox active cations and those prepared from clay specimens previously ion exchanged with these complexes, two electrodes were prepared with clays that had initially been exchanged with $[Co(tripyam)_2]^{2+}$ (prepared using the shaker method, above) and with $[Co(bipyridyl)_3]^{3+}$ (prepared using the shaker method, above, complex prepared by a literature method [72]).

3.3 Results and Discussion

3.3.1 $Co(tripyam)_2(ClO_4)_2$ Complexes and Ion Exchanged Clay

The spin crossover ($^4T \leftrightarrow {}^2E$) behaviour of $[Co(tripyam)_2](ClO_4)_2$ has been well documented [51, 65]. It has been suggested previously [73] that some low spin isomer was trapped in the initially prepared specimen. However, subsequent variable temperature measurements [51, 65] showed Curie-Weiss behaviour to 200 K, a transformation to the low spin form occurred between 190 and 143 K [65].

A freshly prepared sample of $[Co(tripyam)_2](ClO_4)_2$ was immediately subjected to e.s.r. analysis. A weak anisotropic signal was seen at room temperature centred on g = 2, but after one month the signal became broad and isotropic. After three months the complex was e.s.r. silent at room temperature, however, on cooling to 190K a broad resonance was seen to arise (full width at half maximum, fwhm, = 493 Hz). As cooling continued, the intensity of the signal increased and the line width narrowed. The maximum intensity was reached at 145 K. At 105 K, g = 2.1285 and fwhm = 239 Hz. It appears that some low spin isomer is "frozen" into the freshly prepared solid but, on passage of time, a true room temperature equilibrium favouring the ^4T state is reached.

complex	uv/vis maximum
$[Co(tripyam)_2](ClO_4)_2$ crystals	460 nm
$[Co(tripyam)_2](ClO_4)_2$ acetonitrile solution	400 nm
$[Co(tripyam)_2](ClO_4)_2$ aqueous solution	500 nm
$[Co(pyridine)_4(H_2O)_2]^{2+}$ aqueous solution	502 nm

Table 3.1 UV/Visible spectra results for cobalt complexes

Attempts to exchange $[Co(tripyam)_2](ClO_4)_2$ onto laponite RD using the two methods described above (section 3.2.3) produced two different clays. Using the shaker method, a pink clay was produced. The reflectance spectrum (see table 3.2) was distinct from that of the orange parent complex (see table 3.1). As the difficulty of oxidizing this Co(II) complex has been previously reported [65], a change from terdentate to bidentate ligands is more likely. To confirm this, an aqueous solution of $[Co(tripyam)_2](ClO_4)_2$ was placed on the flask shaker for one week, resulting in a pink solution. Comparison of the visible spectrum for this solution with that of $[Co(pyridine)_4(H_2O)_2]^{2+}$ and the diffuse reflectance spectrum of the pink clay (table 3.2) leaves little doubt that the exchanged cation is the diaquo (*bis*-bidentate) ion, $[Co(tripyam)_2(H_2O)_2]^{2+}$. If this solution was concentrated and allowed to crystalize an orange solid was obtained which was found to be $[Co(tripyam)_2](ClO_4)_2.3H_2O$ (terdentate ligands).

When laponite is treated with ethanolic $[Co(tripyam)_2](ClO_4)_2$ in a microwave oven for 5 mins. an orange clay is produced. The diffuse reflectance spectrum is consistent with the presence of the *bis*-terdentate ion, $[Co(tripyam)_2]^{2+}$. On standing for 12 months this material undergoes an aquation reaction on its surface to give the pink *bis*-bidentate ion, $[Co(tripyam)_2(H_2O)_2]^{2+}$. This suggests that the surface of the clay has a greater affinity for the *bis*-bidentate diaquo form.

It appears that the microwave preparation has greatly accelerated the exchange reaction, but not the aquation reaction, thus allowing the preparation of a clay complex not previously obtainable.

Exchanged Complex	Colour	uv/vis maximum
$[Co(tripyam)_2](ClO_4)_2$—laponite RD (shaker method)	pink	≈ 500 nm
$[Co(tripyam)_2](ClO_4)_2$—laponite RD (microwave method)	orange	≈ 440 nm (v.br.)
$[Cu(tripyam)_2](ClO_4)_2$—laponite RD	green	≈ 420 nm (sh.)
$[Cu(tripyam)_2(ClO_4)_2]$—laponite RD	green	≈ 420 nm (sh.)
$[Fe(tripyam)_2](ClO_4)_2$—laponite RD	red/orange	≈ 420 nm (sh.) ≈ 500 nm (sh.)

Table 3.2 Diffuse reflectance uv/visible results for exchanged clays

Exchanged Complex	basal spacing ± 0.1Å
$[Co(tripyam)_2](ClO_4)_2$—laponite RD (shaker method)	15.1 Å
$[Co(tripyam)_2](ClO_4)_2$—laponite RD (microwave method)	15.3 Å
$[Cu(tripyam)_2](ClO_4)_2$—laponite RD	15.3 Å
$[Cu(tripyam)_2(ClO_4)_2]$—laponite RD	15.3 Å
$[Fe(tripyam)_2](ClO_4)_2$—laponite RD	15.1 Å

Table 3.3 Basal spacings of exchanged clays

3.3.2 $Cu(tripyam)_2(ClO_4)_2$ Complexes and Ion Exchanged Clays

The two isomeric copper(II) perchlorate complexes of tri-2-pyridylamine were prepared and ion exchanged onto laponite. Both the blue (terdentate) isomer and the green (bidentate) isomer give green aqueous solutions and green ion exchanged clays. The solutions contain $[Cu(tripyam)_2(H_2O)_2]^{2+}$ and it is therefore the diaquo ion that exchanges onto the clay. This is consistent with the view expressed above that the surface of the clay has a greater affinity for the *bis*-bidentate ion. The basal spacings are similar to those obtained for the cobalt exchanged clays (see table 3.3).

When either of the copper complex exchanged laponites are heated to 100°C a colour change occurs (green → blue). This change is both completely and indefinitely reversible. The colour change is due to the ligands of the complex changing from bidentate to terdentate. The temperature at which this transition occurred was altered by using copper complexes with substituted ligands. Complexes of the type $[Cu\ L(OH)_2]^{2+}$ were prepared and exchanged onto laponite (L = 4- and 6-methyl-di-(2-pyridyl)amine). A reversible colour change (green → blue) occurred at 145°C for the 4-methyl-ligand complex and an irreversible change (green/brown → orange/brown) at 215°C was obtained for the 6-methyl-ligand complex.

This illustrates that thermochroic clays can be prepared by the exchange of coloured metal complexes with ligands of variable denticity and the transition temperature can be tuned, depending on the complex used. The transition is not instantaneous, but the materials are robust and in two cases the transition is totally reversible, therefore the materials could expect to have a long useful lifetime. A use for these materials has not yet been found but their robustness and durability suggests that they could find an application as warnings of excess temperature.

3.3.3 $Fe(tripyam)_2(ClO_4)_2$ Complexes and Ion Exchanged Clays

In the case of both $[Cu(tripyam)_2](ClO_4)_2$ and $[Co(tripyam)_2](ClO_4)_2$ only the *bis*-bidentate form of the complex can be ion exchanged using the shaker method. Accordingly, the low spin $[Fe(tripyam)_2](ClO_4)_2$ complex was prepared (*bis*-terdentate). The contamination by the *tris*-bidentate $[Fe(tripyam)_3](ClO_4)_3$ complex is detailed above (section 3.2.2). Ion exchange resulted in a red-orange clay suggesting that the *bis*-terdentate form was unchanged by ion exchange. However, the basal spacing for this clay was similar to those observed for $[M(tripyam)_2(H_2O)_2]$ complexes. It is possible that in the terdentate co-ordinated ligand complexes the

terdentate ligands can "fit" into the pseudo hexagonal rings of the silicate layers, therefore not producing the increase in basal spacing expected.

It can be seen that when a *bis*-terdentate $M(tripyam)_2$ complex has truly octahedral symmetry, as the iron(II) complex has [53], it can ion exchange onto laponite as the *bis*-terdentate ion. This is in contrast to the cobalt and copper complexes which deviate from true octahedral symmetry and become *bis*-bidentate on exchange.

3.3.4 Cyclic Voltammetry

In comparison to $[Co(bipyridyl)_3]^{2+}$, the corresponding tri-2-pyridylamine complex, $[Co(tripyam)_2]^{2+}$, is resistant to oxidation. In fact, the synthesis of a (tri-2-pyridylamine)cobalt(III) complex has not yet been achieved. By contrast the preparation of cobalt(III) complexes of substituted tri-2-pyridylamines is relatively easy [65].

The electrochemical behaviour of these Co(II) complexes was studied, both as free solutions and as clay modified electrodes, using cyclic voltammetry. The solvent for all of the electrochemistry was dry acetonitrile and the supporting electrolyte was 0.1 M tertiarybutylammonium perchlorate (TBAP). The acetonitrile solutions of the complexes were carefully monitored by uv/visible spectroscopy over time to ensure that no time dependent change of the species would occur during the electrochemical study.

The acetonitrile solution of $[Co(tripyam)_2]^{2+}$ was orange in colour, characteristic of the *bis*-terdentate complex, also found in the solid. Therefore, by preparing a clay modified electrode and dipping it in an acetonitrile solution of the complex (as described above), it was possible to study the electrochemical behaviour of the *bis*-terdentate complex. It is not possible to study the corresponding *bis*-bidentate complex by this method as it exists in water and water is not a suitable solvent for this electrochemical experiment. In order to study the *bis*-bidentate complex, a clay modified electrode was prepared using previously exchanged and rigorously washed (pink) clay.

Clay modified electrodes were also prepared from bis-(6-methyl-2-pyridyldi-(2-pyridyl)amine)cobalt(II) by dipping a clay modified electrode in an acetonitrile solution of $[Co(6\text{-}mpdpa)_2](ClO_4)_2$ and of tris-(2,2'-bipyridyl)cobalt(III) by dipping and by using a pre-exchanged clay.

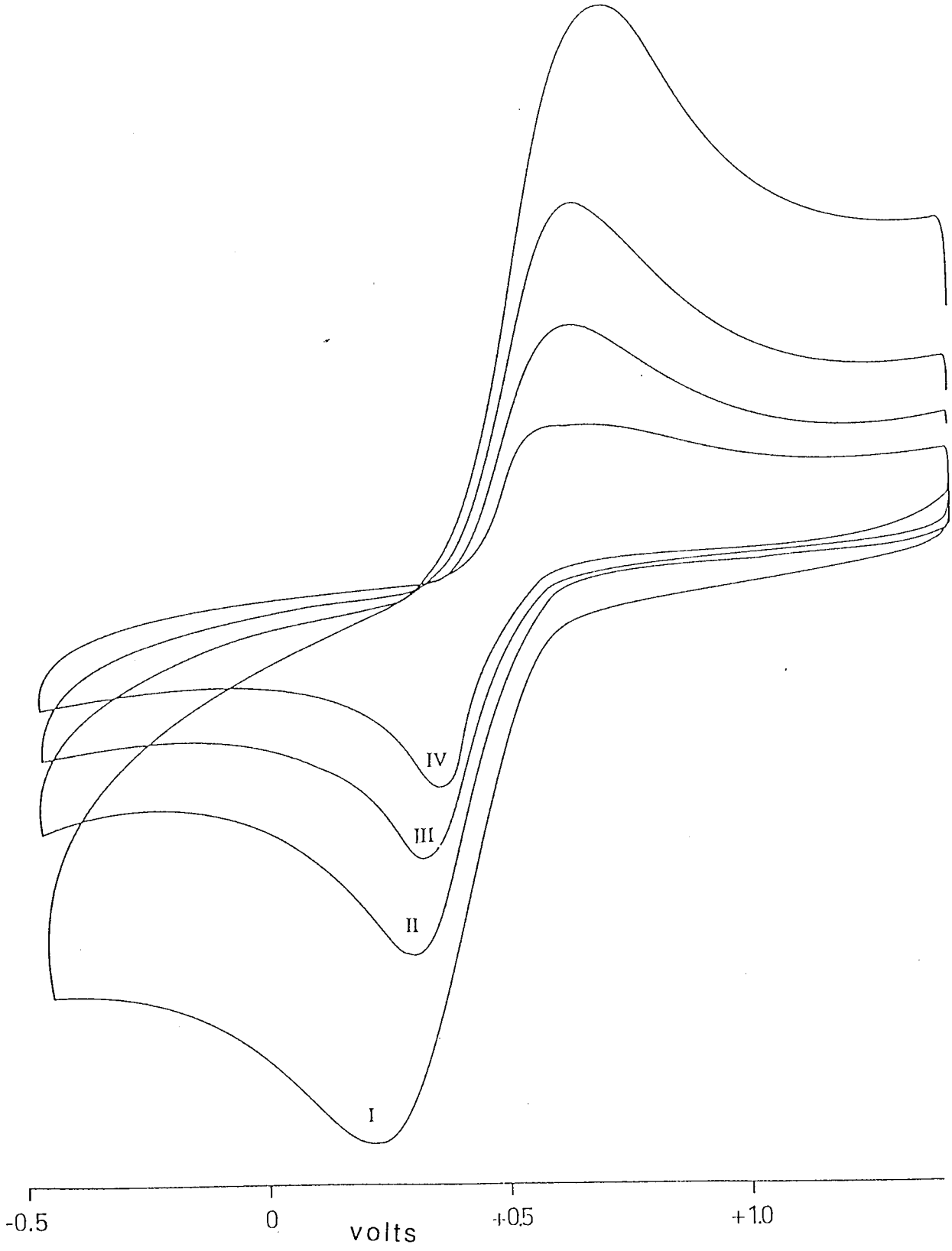

Figure 3.1 Cyclic voltammogram of $[Co(tripyam)_2]^{2+}$ immobilized on a laponite RD electrode, prepared by dipping the electrode in an acetonitrile solution of the complex. (I - 500 mVs^{-1}, II - 200 mVs^{-1}, III - 100 mVs^{-1}, IV - 50 mVs^{-1})

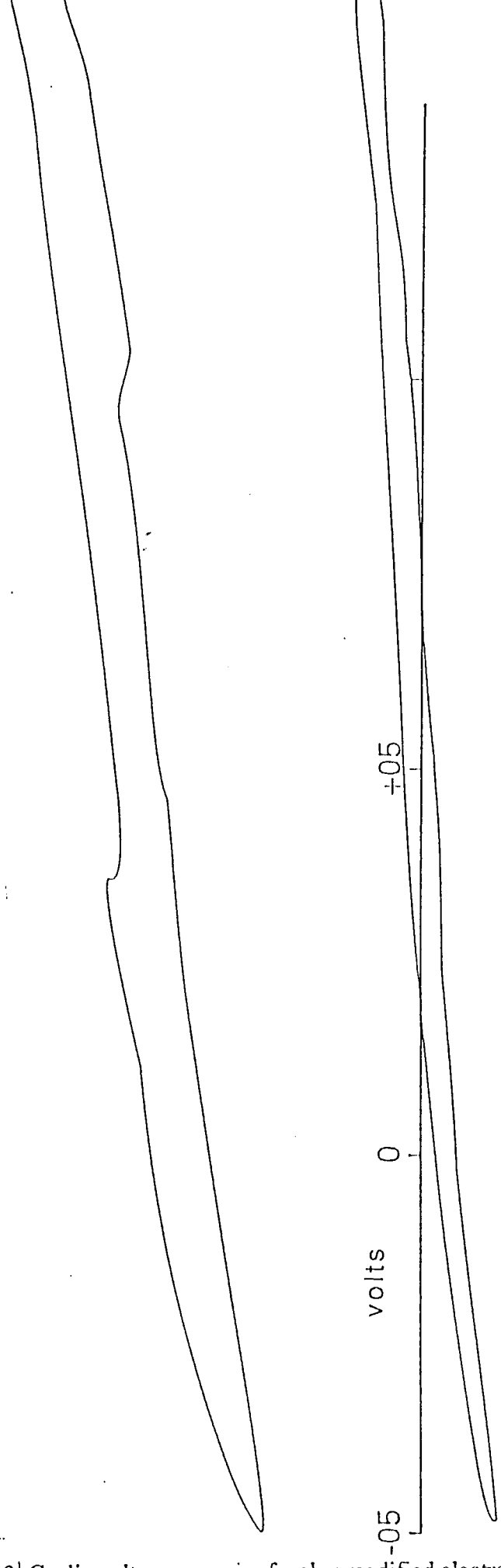

Figure 3.2' Cyclic voltammogram of a clay modified electrode prepared from laponite RD pre-exchanged with $[Co(bipy)_3]^{3+}$ (electro-inactive)

The cyclic voltammograms obtained from the free solutions were typical of complexes in solution and the $E_{1/2}$ values are shown in table 3.4. The $Co^{2+/3+}$ redox process was investigated and the data confirms that the ease of oxidation is in the order:

$$[Co(bipy)_3]^{2+} > [Co(6\text{-}mpdpa)_2]^{2+} > [Co(tripyam)_2]^{2+}.$$

This is quantitative confirmation of the difficulty in synthesizing $[Co(tripyam)_2]^{3+}$. The greater basicity expected for the 2-pyridyl-group bearing the 6-methyl ligand should lead to greater σ-bond strength compared to that for the co-ordinated unsubstituted 2-pyridyl-groups (substituted tripyam complexes of cobalt(III) are easily formed [65]). However, the difference in bond strength may be more significant for the more positive Co(III) than for Co(II). Hence the thermodynamic drive to form a bond between Co(III) and the unsubstituted ligand may not be great enough.

Complex	$E_{1/2}$/ Volts ± 0.1V
$[Co(tripyam)_2](ClO_4)_2$	
free solution	0.50 V
dipped electrode	0.49 V
$[Co(6\text{-}mpdpa)_2](ClO_4)_2$	
free solution	0.39 V
dipped electrode	unsatisfactory
$[Co(bipyridyl)_3](ClO_4)_3$	
free solution	0.21 V
dipped electrode	0.21 V
$[Cu(tripyam)_2(ClO_4)_2]$	
free solution	0.21 V
dipped electrode	unsatisfactory

Table 3.4 Cyclic voltammetry data for complexes in solution and as clay modified electrodes

The dipped clay modified electrodes prepared from $[Co(tripyam)_2]^{2+}$ and $[Co(bipy)_3]^{3+}$ gave good quality cyclic voltammograms. The $E_{1/2}$ values gave good agreement with the results obtained from solution measurements. This suggests that the complexes have not undergone any major changes when they were sorbed onto the clay. Despite several

preparations, the cyclic voltammograms obtained from a clay modified electrode dipped in an acetonitrile solution of $[Co(6\text{-mpdpa})_2]^{2+}$ were unsatisfactory.

The clay modified electrodes made by the pre-exchange of the cobalt complexes $[Co(tripyam)_2(H_2O)_2]^{2+}$ (pink) and $[Co(bipy)_3]^{3+}$ were both rigorously electro-inactive (as was an untreated clay modified electrode). This confirms the observation of Pinnavaia [61], that cations bound electrostatically to any exchange site on a smectite clay, up to the cation exchange capacity, are always electro-inactive. The electroactivity of our clay modified electrodes can be attributed to cations which are surface bound at edge sites of the clay crystal, in excess of the clay cation exchange capacity, by an ion pair mechanism. This is in contrast to the work of Bard [56,57] who suggested that all exchanged cations could become electroactive and the influence of exchanged cations in the interlayer could be seen at the electrode surface.

Clay modified electrodes, prepared by dipping an electrode in an acetonitrile solution of $[Cu(tripyam)_2](ClO_4)_2$, were of unsatisfactory quality. The free complex gave a poor spectra with an $E_{1/2}$ value of approximately 0.21 V.

3.4 Conclusions

Electron spin resonance studies of a freshly prepared sample of $[Co(tripyam)_2](ClO_4)_2$ confirm the presence of some low spin isomer (^2E ground state) frozen into the solid, which reverts to the ^4T form over a period of approximately three months.

Ion exchange of orange $[Co(tripyam)_2](ClO_4)_2$ onto laponite from aqueous solution, using the shaker, produced a pink clay. The exchanged species was found to be $[Co(tripyam)_2(H_2O)_2]^{2+}$, which has bidentate ligands. Orange $[Co(tripyam)_2](ClO_4)_2$ (terdentate ligands) can be exchanged unchanged using a novel microwave method which accelerates the ion exchange reaction, but not the aquation reaction. However, after approximately one year the complex aquates to $[Co(tripyam)_2(H_2O)_2]^{2+}$, and the clay appears pink.

Copper tri-2-pyridylamine complexes are also exchanged onto laponite as the *bis*-bidentate species $[Cu(tripyam)_2(H_2O)_2]^{2+}$. This clay is thermochroic, undergoing a reversible change from green to blue at 100°C. This is consistent with a change from bidentate to terdentate ligands. The temperature of the colour change can be increased by employing the complexes of substituted tri-2-pyridylamine ligands.

Low spin $[Fe(tripyam)_2]^{2+}$ (terdentate ligands) is stable on laponite, although the clay surface has greater affinity for the *bis*-bidentate complex species.

Cyclic voltammetric studies of acetonitrile solutions of Co(II) species show an order of ease of oxidation:

$$[Co(bipy)_3]^{2+} > [Co(6\text{-}mpdpa)_2]^{2+} > [Co(tripyam)_2]^{2+}.$$

Clay modified electrodes dipped in acetonitrile solutions of $[Co(bipy)_3]^{3+}$ or $[Co(tripyam)_2]^{2+}$ give very similar $E_{1/2}$ values to those obtained for the free complexes, suggesting that the species are essentially unchanged on sorbtion.

The electro-inactivity of electrodes prepared from clays pre-exchanged with cobalt complexes confirms the observation of Pinnavaia [61], that electrostatically bound species are rigorously electro-inactive. A recent review [74] confirms that the electroactivity of clay modified electrodes will depend on the situation of electroactive cations and the method of film preparation. Using our method of film preparation, the electroactivity is dependent on ions sorbed onto the clay surface from dipping the electrode in a solution of the electroactive complex. The electroactive ions are sorbed in a quantity in excess of the cation exchange capacity of the clay, by an ion pair mechanism, and they are located at the edge sites of the clay crystals.

Chapter Four

INVESTIGATION OF THE ELECTRICAL CONDUCTIVITY OF LAPONITE

4.1 Introduction

Two studies have shown that smectite clays are electrical conductors [43,44]. While no experimental evidence for the mechanism of conduction has been presented, both groups of workers suggest that the mechanism of conductivity may be ionic. One of the clays investigated in these studies was the synthetic smectite clay, laponite, which is added to electrographic papers at Chartham Paper Mill. Only d.c. conductivity data for the clays have been presented, no information about the dielectric properties of the clays was included. More information about the clay can be obtained from resistance and capacitance measurements over a range of alternating current (a.c.) frequencies than from simple direct current (d.c.) measurements.

Electrical conductivity of materials is a property which spans a wide range. Eighteen orders of magnitude separate a good insulator from a semiconductor and superconductors (at low temperatures) may be twenty five orders of magnitude more conductive than a semiconductor (see fig. 4.1).

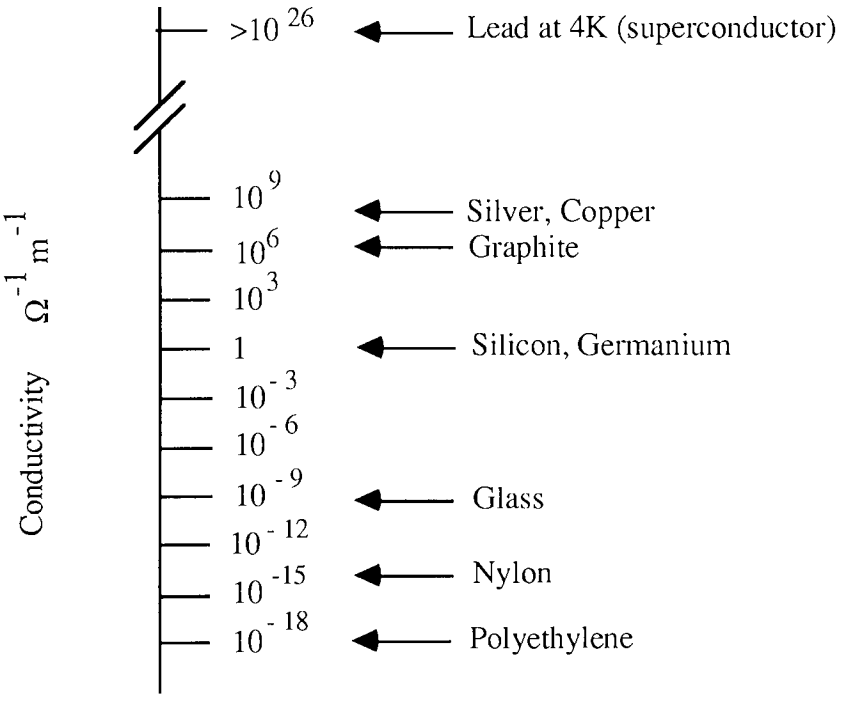

Figure 4.1 Chart of typical conductivities [46]

Semiconductors can lie in the conductivity range 10^{-5} to 10^{3} Ω^{-1} m^{-1} , however the boundaries between conductors, semiconductors and insulators are blurred and arbitrary and a certain amount of overlap can occur. The distinction between insulators, semiconductors and conductors is the mechanism of conduction, not the magnitude.

AND SERVICES

Electrical conductivity can arise from the movement of electrons, ions or holes. The basic equation for conductivity [75] is:-

$$\text{Conductivity, } \sigma = q\,n\,\mu \;\; \Omega^{-1}\,m^{-1} \qquad \text{equation 4.1}$$

where q is the charge of an electron (and of a monovalent cation), n is the number of charge carriers per cubic meter and μ is the drift velocity (mobility) of the charge carrier. There may be contributions to the conductivity from different types of carriers, notably electrons and holes or cation and anion pairs. Theories of conductivity aim to show how n and μ are determined by molecular structure and how they depend on such factors as temperature and applied magnetic field.

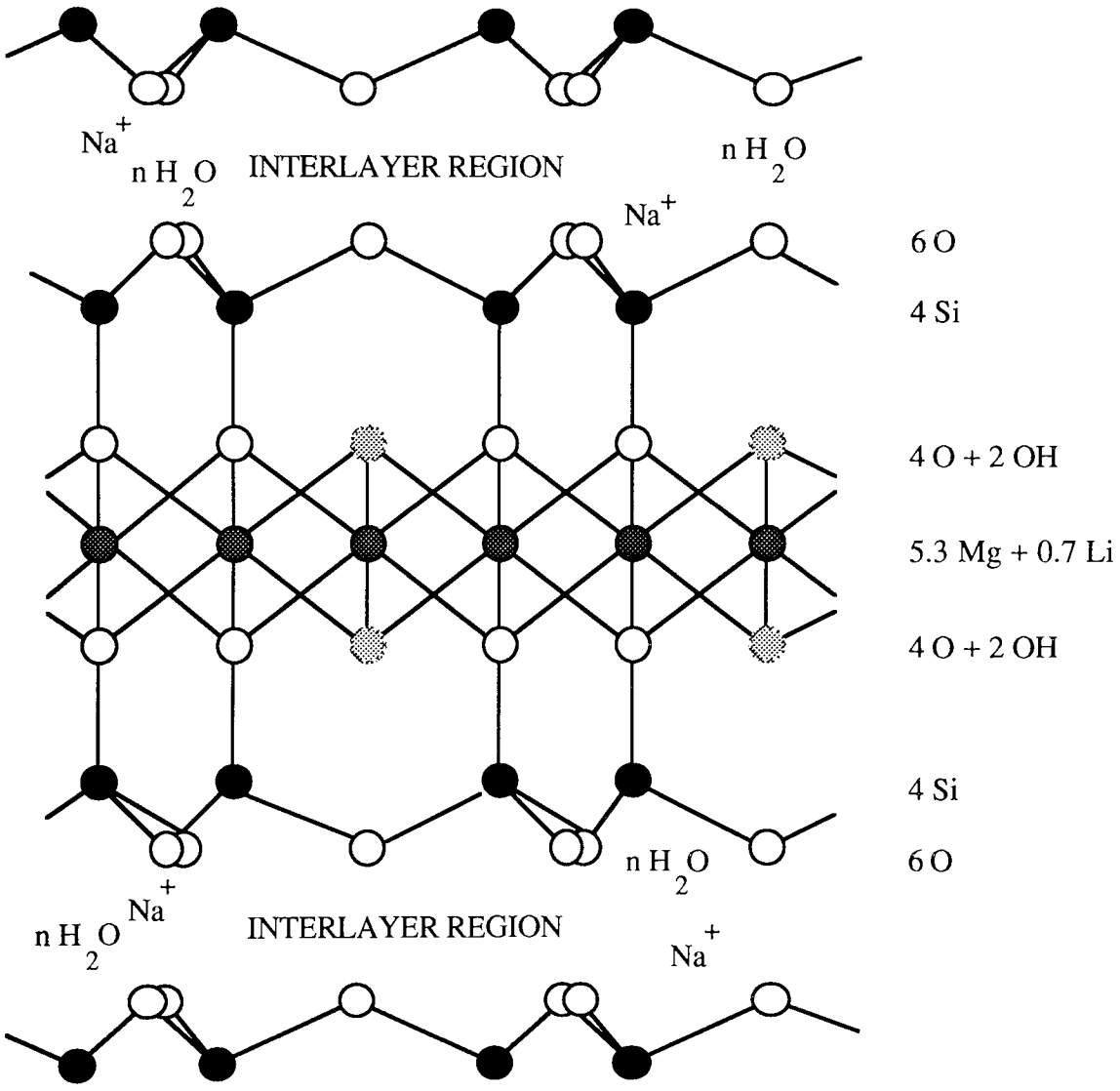

Figure 4.2 Structure of laponite RD

4.2 Structure and Chemical Composition of Laponite

Laponite is a synthetic smectite clay, its natural analogue being hectorite. Laponite is supplied by Laporte Industries Ltd. in several forms, including RD, RDS, B and S. In all of these forms the interlayer ion is sodium. Laponite RD is the purest of these four forms, its idealized formula [76] is $\{Si_8(Mg_{5.3}Li_{0.7})\ O_{20}\ (OH)_4\}Na^+_{0.7}$. Laponite RDS is laponite RD with Tetron (tetrasodium pyrophosphate, see fig 1.10) added as a viscosity improver. Laponite B contains 2.3% fluorine as some of the octahedral hydroxyl ions are replaced by fluorine ions. This can be represented as $\{Si_8(Mg_{5.3}Li_{0.7})\ O_{20}\ (OH, F)_4\}Na^+_{0.7}$. Laponite S is laponite B with added Tetron. Laponite S is used in paper making at Chartham Paper Mill. Figure 4.2 shows the chemical structure of laponite. While laponite is a trade name, mineral names begin with lower case letters, therefore the lower case will be used here.

4.3 Resistors and Capacitors in A.C. Fields

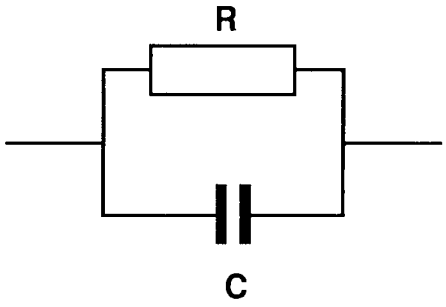

Figure 4.3 Digibridge test configuration

The sample under test was considered by the Digibridge to behave as if it were an ideal resistor and an ideal capacitor in parallel (fig. 4.3). When an ideal resistor is subjected to an alternating current it obeys Ohm's Law, and its resistance is independent of the frequency. An ideal capacitor does not allow the passage of direct current, but it does allow the passage of a.c. current. The space between the two plates of a capacitor can be considered as an insulator as there are no free electrons available for conduction. However, when an alternating electric field is applied, a displacement current flows in response to changes in the potential difference. This a.c. current is often regarded as an imaginary component and is described as:-

$$I_c = j2\pi fC \qquad \text{equation 4.2}$$

where f is the a.c. frequency, C is the capacitance and $j = \sqrt{-1}$. The presence of the factor j indicates that there is a difference in phase angle of 90° between the sinusoidal

current and the voltage and by convention the current leads the voltage by 90°. As the capacitor can allow the passage of a.c. current, it should be considered as contributing to the total impedance of the parallel circuit. This capacitive impedance is known as reactance (or capacitive reactance), X_C, and is given by equation 4.3.

$$X_C = \frac{1}{2\pi fC} \qquad \text{equation 4.3}$$

The total resistance of the parallel circuit is known as the impedance, Z. The impedance contains a real and an imaginary component and can be represented in the complex plane by [47]:-

$$Z' = \frac{R_p}{1 + j\omega R_p C_p} \qquad \text{equation 4.4}$$

Where R_p is the parallel component of resistance, C_p is the parallel component of capacitance, X_p is the parallel reactance and $\omega = 2\pi f$. Scalar values of the total impedance, Z, can be obtained by multiplying Z' by its complex conjugate, Z*,

$$Z^* = \frac{R_p}{1 - j\omega R_p C_p} \qquad \text{equation 4.5}$$

to give

$$Z'Z^* = \frac{R_p^2}{1 + \omega^2 R_p^2 C_p^2} \qquad \text{equation 4.6}$$

As

$$X_p = \frac{1}{\omega C_p} \qquad \text{equation 4.7}$$

equation 4.7 can be substituted into equation 4.6 to give

$$Z'Z^* = \frac{R_p^2}{1 + R_p^2/X_p^2} \qquad \text{equation 4.8}$$

dividing the numerator and denominator of equation 4.8 by R_p^2 gives

$$Z'Z^* = \frac{1}{1/R_p^2 + 1/X_p^2} \qquad \text{equation 4.9}$$

Defining

$$Z^2 = Z'Z^* \qquad \text{equation 4.10}$$

It follows that

$$(1/Z)^2 = (1/X_C)^2 + (1/R)^2 \qquad \text{equation 4.11}$$

which can be rearranged to give

$$Z = \frac{1}{\sqrt{(1/X_C)^2 + (1/R)^2}} \qquad \text{equation 4.12}$$

4.4 Interpretation of the Frequency Dependence of the Electrical Conductivity of Laponite

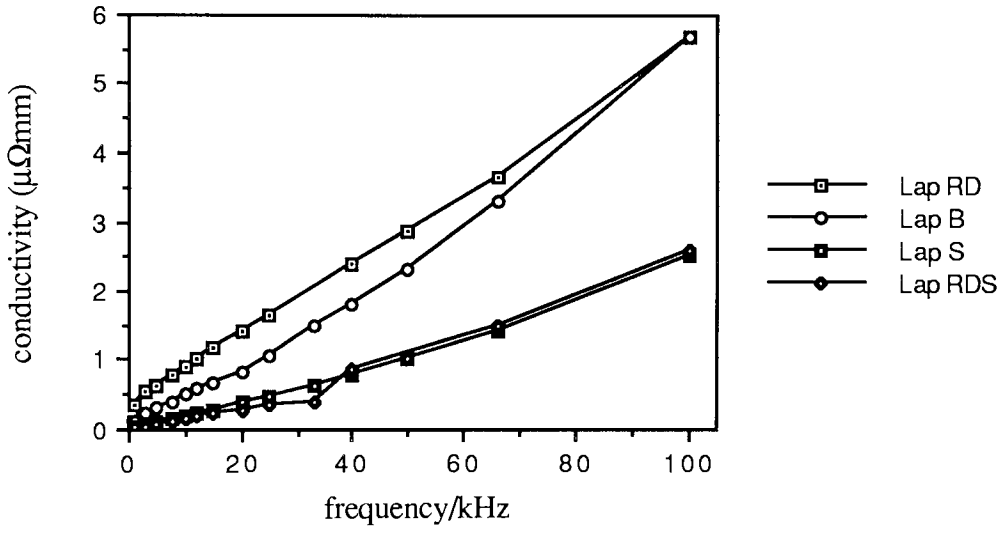

Figure 4.4 Conductivity of different laponite grades

The resistance and capacitance of pressed discs of the above four forms of laponite were measured over a range of a.c. frequencies, as described previously (section 2.14). As similar behaviour is shown by each form (see fig. 4.4), mechanistic discussion will be limited to laponite RD, as this contains no substituted fluorine or added Tetron. Figure 4.5 shows the frequency dependence of the a.c. conductivity of laponite RD.

The a.c. conductivity of laponite contains a significant reactive component, as the calculated reactance is much lower than the calculated resistance, and only electronic oscillations contribute to conduction across a capacitor (displacement current). The a.c. current associated with the reactive component is the displacement current due to the electronic polarization of the electrons of constituent atoms. If the conductivity has

electronic and ionic components they can be thought of as existing in parallel [75]. If the resistance to one component is small, it effectively shorts out the rest of the "circuit".

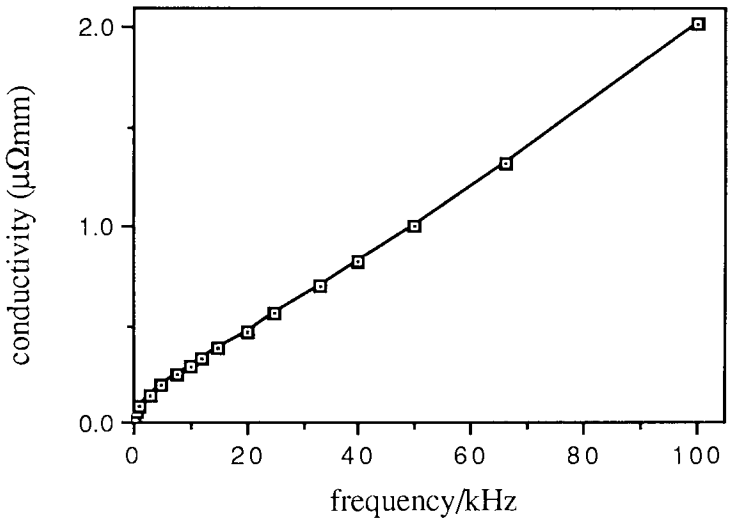

Figure 4.5 Frequency dependence of the conductivity of laponite RD (silver-paste electrodes)

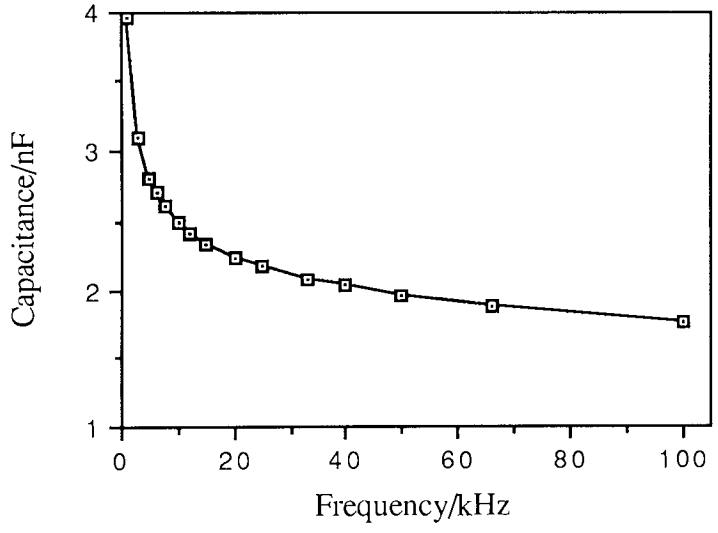

Figure 4.6 Frequency dependence of the capacitance of laponite RD

From the graph of conductivity against frequency, fig 4.5, it can be seen that there is only a slight deviation from a straight line. This suggests that the sample is exhibiting predominantly reactive capacitance, with the deviation being attributed to a parallel resistance. This is confirmed by plotting the reciprocals of Z, X_c and R against frequency. It can be seen from fig 4.7 that the reactive capacitance accounts for the

majority of the impedance of the sample. By plotting capacitance against frequency, it can be seen that the capacitance of the sample is approaching a limiting value at high frequency (see fig. 4.6). If the capacitance measured at 100 kHz is regarded as a limiting, high frequency capacitance it can be said that this represents an "electronic component" of the impedance. If this value is substituted into the impedance calculations, the reactive component can be calculated for any measured frequency and expressed graphically, see figure 4.7. It can be seen that for laponite RD this reactive (electronic) component appears to dominate the total impedance. However, it is important to appreciate that this interpretation assumes a non-conductive sample (under d.c. conditions) and very low resistance, non-capacitive electrode to sample contacts.

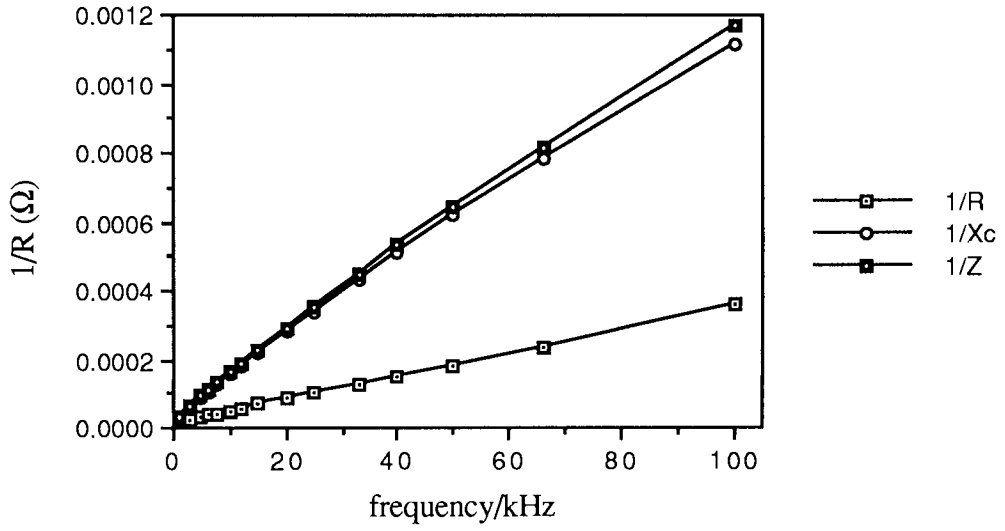

Figure 4.7 Components of impedance for laponite RD

The a.c. frequency dependence of ionic conductivity in solution has been extensively studied [77,78,79]. When an electric field is applied to ions in solution, the ions are caused to move, along with their ion atmosphere. The ion atmosphere takes longer to adjust to the oscillating field than the ion, therefore the ion and its atmosphere become unsymmetrical. This slows down any motion of the ion. This effect on the speed of ion is called the asymmetry (or relaxation) effect.

In dilute solutions, below frequencies of 100 kHz the conductivity is independent of frequency [79]. At these frequencies the oscillations of the electric field are sufficiently slow to allow the distortion of the ion atmosphere by the applied electric field to relax, as the relaxation time of the ion atmosphere is short compared to the rate of oscillation of the field.

At frequencies above 100 kHz the conductivity increases with increasing frequency, as the retarding forces due to the asymmetry effect disappear as the frequency increases. The greater the concentration of the solution and the charge of the ions, the higher the frequency at which this rise in conductivity becomes apparent. If the frequency is increased sufficiently, the conductivity reaches a limiting value. This is when the alternations in the field occur too rapidly for any distortion in the ion atmosphere to take place. The limiting value of conductivity represents the complete absence of the asymmetry effect. This phenomenon is known as the dispersion of conductance.

These arguments can be applied approximately to the a.c. conductivity of laponite, as any ions present are understood to be in a solution-like environment in the interlayer region. There appears to be no significant ionic conductivity in laponite RD under these measuring conditions. However, some evidence for an ionic component to the conductivity is provided by the polarization observed at low frequencies.

For low frequency a.c. fields the impedance rises sharply. This increase is caused by a high impedance layer on the electrode surface [46]. This is accompanied by a large increase in the capacitance (fig. 4.6). This may be caused by imperfect contact between the electrode and the sample. At low a.c. frequencies there is sufficient time for the conduction of the bulk sample to transfer all of the applied field across the electrode surface, and the result is an enormous increase in the measured capacitance [46]. Polarization is also occurring at the sample electrode interface, leading to the formation of an electrical double layer at the interface where electrical charge (ions) build up without being discharged. The presence of this polarization suggests that the a.c. conductivity does contain an ionic component, but that it is not large enough to be seen under these conditions. If the a.c. conductivity was purely electronic, there would be no polarization at electrode surfaces either at low frequencies, or under d.c. conditions.

The presence of electrode polarization is usually complex, and since little is usually known about it, the problem of extracting meaningful results from low frequency measurements is rendered impractical.

4.5 Variable Temperature Conductivity Measurements

4.5.1 Theory

The temperature dependence of a.c. conductivity for different materials can be understood by considering the temperature dependence of the terms q, n and μ. It is usual to consider q to be a constant and independent of temperature. The mobility, μ, behaves similar in most materials in that usually it decreases slightly with increasing temperature due to collisions and lattice vibrations. In metallic conductors n is large and essentially unchanged with temperature. Therefore, as temperature increases, μ decreases and the conductivity decreases. For semiconductors, n usually increases greatly with temperature. The effect of this increase in n on the conductivity more than outweighs the decrease in μ. Hence the conductivity increases with temperature. If the conduction arises from ions, as the temperature rises more ions may be released from a free ion - ion pair equilibrium ($AB \leftrightarrow A^+ + B^-$), increasing the number of charge carriers and often increasing the conductivity. Some insulators undergo such a great increase in n that at high temperatures they become semiconducting. Conversely, some semiconductors become more like insulators at low temperatures.

The temperature dependence of conductivity, σ, is given by the Arrhenius equation

$$\sigma = A\exp^{-E/RT} \qquad \text{equation 4.13}$$

where E is the activation energy for conductivity, R is the gas constant and T the absolute temperature. The pre-exponential factor, A, contains several constants including the vibrational frequency of the charge carriers and the entropy of activation. The pre-exponential factor is almost independent of temperature. A graph of $\log_e \sigma$ against T^{-1} should give a straight line of slope - E/R, from which the activation energy can be calculated [75].

4.5.2 Experimental Technique

As laponite contains variable amounts of interlamellar water, care must be taken with variable temperature conductivity measurements in order to minimize the loss of water from the sample. The normal method of measuring conductivity using discs of clay with silver-paste electrodes is impractical, as water would be lost as the temperature increased. Therfore, some type of sealed system is desirable. A second problem is the maintenance of a constant temperature environment in which the temperature can be

raised and then stabilized at a new constant temperature. To overcome these problems a different measurement system was devised.

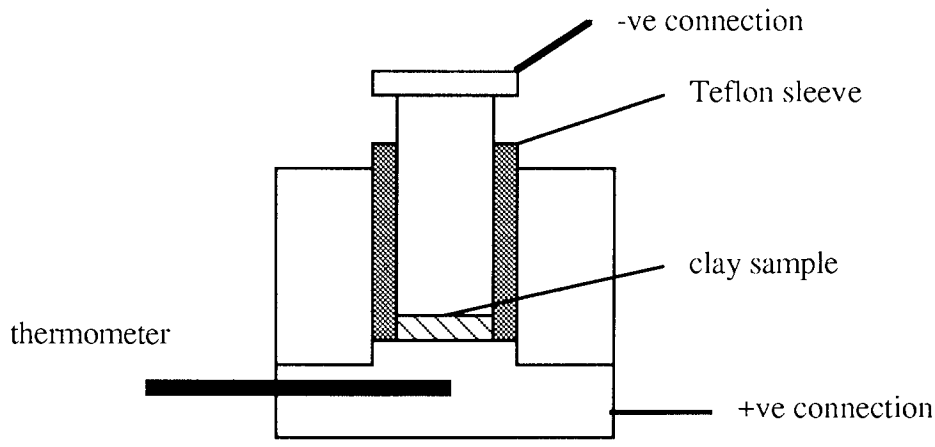

Figure 4.8. Cross section of stainless-steel die

The equipment used was based on a stainless-steel die for pressing solid discs similar to the type used for pressing KBr discs for infra-red analysis (see fig 4.8). This die produces 17 mm diameter discs. The plunger was insulated from the die by a Teflon (polytetrafluoroethylene) sleeve. The clay used in these experiments was allowed to equilibrate at 52% relative humidity for two weeks before use. A disc was pressed in the die using 1 g of clay and 5 tonnes pressure for three minutes. A pressure of 0.5 tonnes was maintained throughout the remainder of the experiment to ensure intimate contact between the electrodes and the sample. One electrode was the raised bottom of the die, the other was the base of the plunger. The electrodes were in contact with the faces of the discs and the edge of the disc was only in contact with the Teflon sleeve. Electrical contacts were made to the plunger and the barrel of the die.

The whole die was wrapped in a strip heating element attached to a Variac transformer. The latter delivers a pre-set electrical current to the strip which heats the die. The temperature of the die is monitored by two thermometers, one held between the strip and the die and the other located in a hole in the die. This second thermometer measures the temperature of the die close to its centre. When the two thermometers read the same temperature there is no temperature gradient within the die and conductivity measurements are made using the Digibridge. Resistivity and conductivity were calculated for a number of selected frequencies at several different temperatures. Temperatures were not allowed to exceed approximately 70 °C to minimize water loss from the sample.

4.5.3 Metal-Sample Electrode Interfaces

The results obtained in these experiments using stainless-steel electrodes cannot be compared directly with data obtained using silver-paste electrodes as the sample-electrode interface will be different and this will affect the total a.c. conductivity. Also, these measurements are taken with 0.5 tonnes pressure applied to the sample. Figure 4.9 shows that the a.c. conductivity of the sample can be increased by increasing the applied pressure. This suggests that the applied pressure increases either the electrode-particle contact or the particle-particle contact (or both), thereby increasing the total a.c. conductivity.

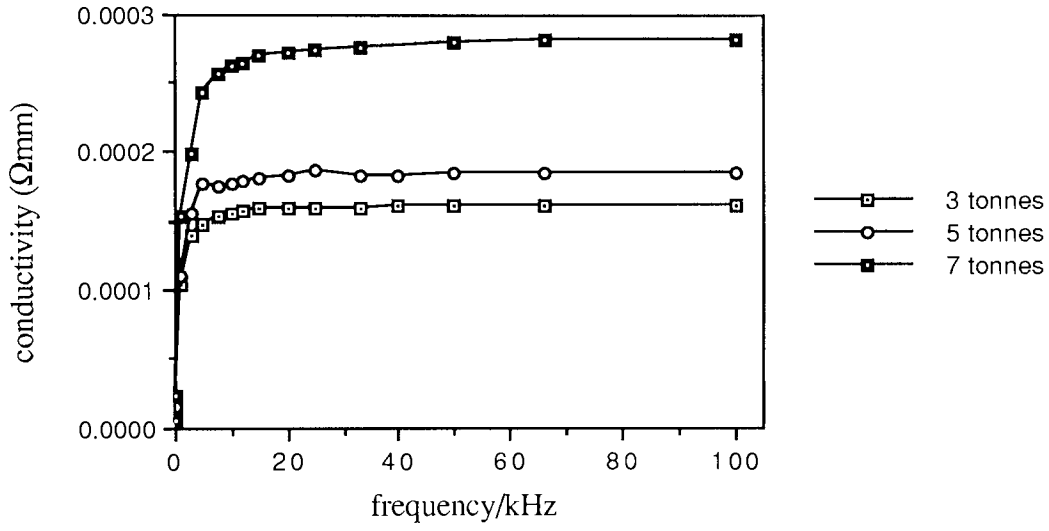

Figure 4.9 Variation of laponite RD conductivity with applied pressure

There are two points to note about figure 4.9. Firstly, the shape of the curve is different to that obtained for laponite RD using silver-paste electrodes (fig. 4.5). Secondly, the a.c. conductivity is higher by approximately two orders of magnitude. The conductivity has little frequency dependence between 100 kHz and approximately 10 kHz. This observation suggests that there is a greater degree of ionic conductivity. The slight slope on the line in this region may be attributed to the electronic component of a.c. conductivity shown in figure 4.5.

Further experiments were carried out with other electrode materials. It can be seen from table 4.1 that when the base and plunger of the stainless-steel die (fig. 4.8) were utilized as the electrodes, the capacitive reactance was orders of magnitude higher than the resistance. The shape of the conductivity against frequency graph (fig 4.10) suggests that ionic conductivity is dominant in this system. The same conclusions can be drawn

when the electrode material is a thin layer of aluminium sputtered onto the surface of a clay disc, see figure 4.10. The aluminium sputtered electrodes appear to be providing a less resistive electrode-sample interface than the silver-paste and this accounts for the increased magnitude of conductivity.

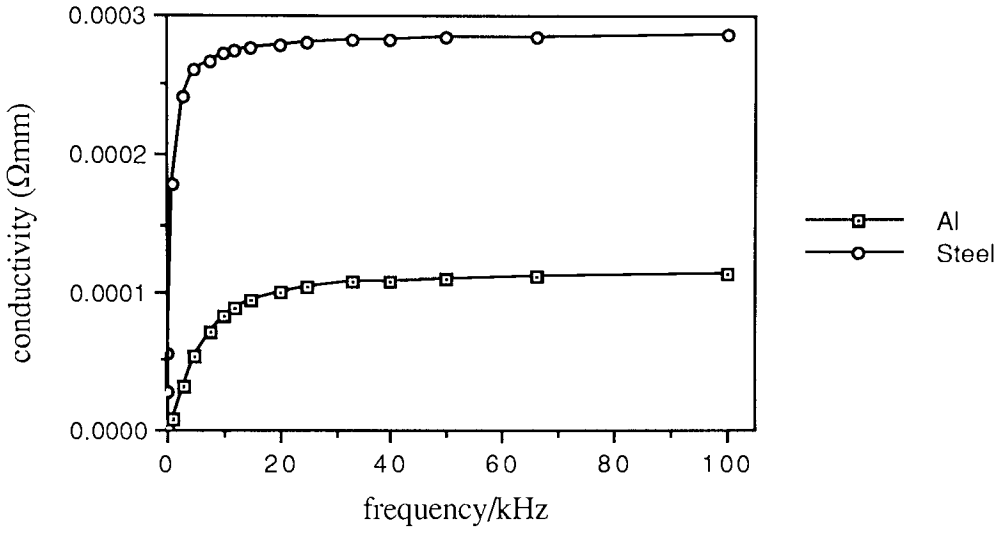

Figure 4.10 Conductivity of laponite RD with Al and steel electrodes

Frequency/kHz	Resistance/Ω	Reactance/Ω	Impedance/Ω
100	28.80	331530	28.80
40	30.26	209387	30.26
20	32.33	150127	32.33
10	36.02	113667	36.02
5	42.48	98841	42.28

Table 4.1 R, X_c and Z for laponite RD for steel electrodes

Frequency/kHz	Resistance/Ω	Reactance/Ω	Impedance/Ω
100	51.53	795671	51.53
40	52.90	361669	52.90
20	57.73	204018	57.73
10	70.56	136479	70.56
5	109.60	119202	109.60

Table 4.2 R, Xc and Z for laponite RD for aluminium electrodes

From figure 4.5 it can be seen that when silver-paste is used as the electrode material, there is no apparent ionic conductivity. However, when stainless-steel (under slight pressure) or aluminium electrodes are used, significant ionic conductivity is observed, and the overall a.c. conductivity is approximately two orders of magnitude greater than that measured using silver-paste electrodes (see fig. 4.10). This is supported by the calculations in tables 4.1 and 4.2. The tables show that in contrast to figure 4.7 the reactive capacitance (reactance, X_C) is not the dominant factor in determining the a.c. conductivity of the sample. The resistance is several orders of magnitude lower than the reactance, indicating that ionic conductivity is dominant in these cases.

When silver-paste electrodes are used the conductivity is significantly lower than that measured using either stainless-steel or aluminium electrodes. The silver paste-clay interface (grain boundary) could be providing a high ohmic resistance. In addition, the silver-paste may be preventing the discharge of ions and thereby causing polarization at the electrodes. The latter phenomena would produce an increase in the total resistivity of the sample.

4.5.4 Variable Temperature Behaviour of Laponite RD

As the temperature is raised the conductivity of laponite RD increases, see figure 4.11. However, the increase is not linear, it is increasing at an increasing rate as the temperature rises. As the sample is cooled the conductivity of the sample decreases with no significant hysteresis. Stainless-steel electrodes were utilized in this experiment.

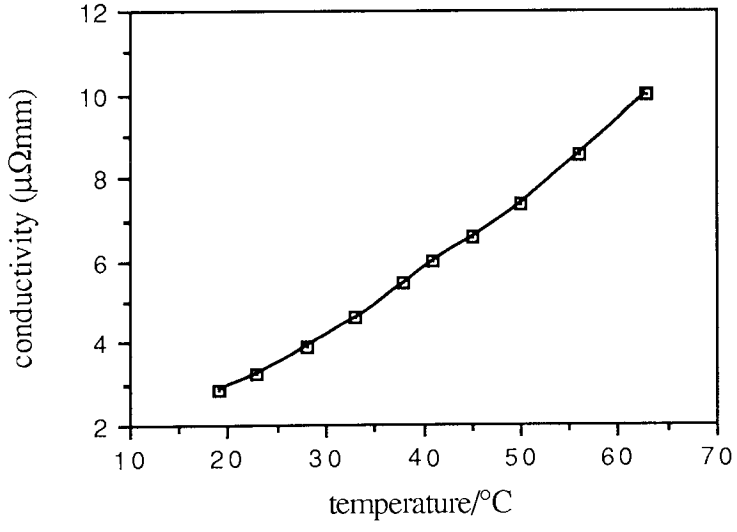

Figure 4.11 Variation of the a.c. conductivity of laponite RD with temperature

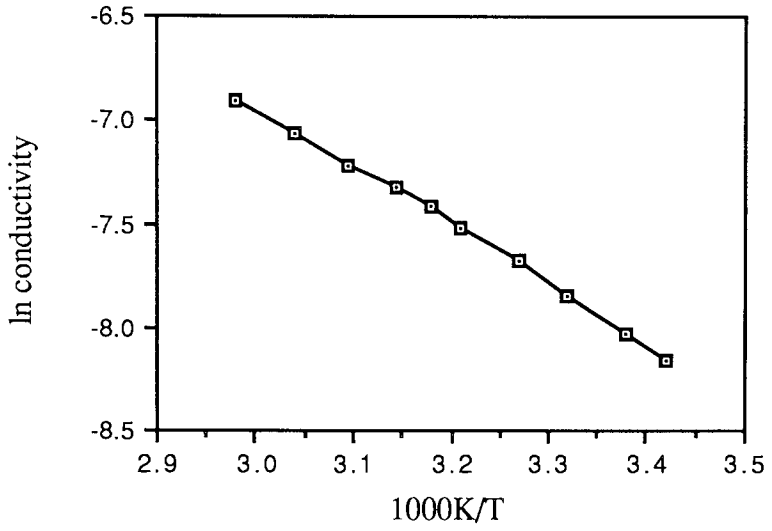

Figure 4.12 Plot of $\log_e \sigma$ against T^{-1}, to calculate activation energy, at 100 kHz

A plot of $\log_e \sigma$ against T^{-1} does not show a straight line at any measured a.c. frequencies. At frequencies above 5 kHz a slight curve is obtained, its shape being similar for all higher measured frequencies. It is not profitable to analyse too deeply the data obtained below 5 kHz as the a.c. conductivity will be dominated by polarization at the electrodes. As the plot is non-linear this suggests that there are at least two energy barriers impeding the diffusion of the ions through the lattice.

Frequency/kHz	Activation Energy/kJmol^{-1} ± 2 kJmol^{-1}	
	High T	Low T
100	+23	+27
40	+23	+27
20	+22	+26
10	+20	+26
5	+18	+24

Table 4.3 Variation of activation energy with frequency

The non linear nature of the plot complicates the calculation of activation energies for conductivity. The shape of the plot suggests that as the temperature increases (T^{-1} decreases) the activation energy decreases, as the gradient of the plot is lower. An approximate activation energy can be calculated at high temperature (High T) and low temperature (Low T) by taking tangents to the corresponding portions of the curve. The

activation energies for a.c. conductivity, at high (50-70°C) and low (20-35°C) temperatures, are summarized at different a.c. frequencies in table 4.3.

Table 4.3 shows that as the temperature rises the measured activation energy is lower. This is consistent with the conductivity increasing with temperature. The lower activation energy indicates that charge carriers are free to overcome a greater range of energy barriers. At higher temperatures the system will be more disorganized and more structurally relaxed because of higher thermal energy in the system. Therefore, the free volume available to the charge carriers (probably ions with this electrode system) will be higher, allowing the charge carriers a higher degree of mobility, enabling them to increase the conductivity of the system.

At lower temperatures the activation energy shows little dependence on frequency (within experimental error), reflecting the observation that the conductivity of laponite shows little frequency dependent variation between 100 kHz and approximately 5 kHz (fig. 4.10).

4.6 Relative Humidity Dependence of the Electrical Conduction of Laponite

4.6.1 Sample Preparation

Smectite clays contain varying amounts of interlamellar water depending on the relative humidity of their environment [6]. Atmospheres of known relative humidity can be created at room temperature in enclosed spaces using saturated solutions of desiccating and deliquescent metal salts [45,80].

Saturated salt solutions were selected to provide a range of humidities. Relative humidity is temperature dependent, as it is the percentage of the theoretical maximum of moisture in the atmosphere and this maximum decreases with temperature. Therefore, a given amount of atmospheric moisture will provide an increasing relative humidity as the temperature drops. Therefore, care must be taken when discussing relative humidity.

Samples of laponite RD were placed in small desiccators containing a beaker of saturated metal salt solution (table 4.4) and allowed to equilibrate at room temperature for two weeks. After pressing discs for conductivity experiments the discs were

returned to the controlled environment for a further week. Samples for X-ray powder diffraction (XRD) were submitted in sealed air-tight containers.

Salt Solution	Relative Humidity
$LiCl.xH_2O$	15%
$CaCl_2.6H_2O$	32%
$Mg(NO_3)_2.6H_2O$	52%
NH_4Cl	79%
$Na_2SO_4.10H_2O$	93%

Table 4.4 Saturated solutions used to create constant relative humidity atmospheres at 293K

4.6.2 X-Ray Powder Diffraction Results

Relative Humidity	Basal Spacing ± 0.1 Å
15%	13.3 Å
32%	13.5 Å
52%	13.5 Å
79%	15.8 Å
93%	18.6 Å

Table 4.5 Increase in basal spacing with relative humidity

The basal spacing of a clay, d_{001}, reveals the dimensions of the clay in the c-axis, this includes the interlayer region. It can be seen from table 4.5 that as the relative humidity of the atmosphere increases, the basal spacing of the clay increases. These results are in agreement with previous work on other smectite clays [6]. The increase in basal spacing is consistent with the step-wise hydration of the interlayer sodium ions It has been shown previously that the sorbtion of one, two and four layers of water is possible.

Also, at high relative humidity the amount of free water (see section 1.4.1) in the interlayer should be increased, increasing the basal spacing.

4.6.3 Dependence of Conductivity on Relative Humidity

The relative humidity dependence of the capacitance and resistance of pressed discs were measured over a range of a.c. frequencies, using silver-paste electrodes. As the relative humidity increased the a.c. conductivity increased, and this increase was much more pronounced at 79% and 93% relative humidity. The increase in a.c. conductivity is accompanied by an increase in basal spacing (table 4.5), which is due to the increase in the water content in the interlayer region [6]. This increased water content will affect ionic conductivity in the interlayer region as there is a strong correlation between ionic conductivity and dielectric constant, ε, as expressed in equation 4.14:-

$$\log \sigma = A\varepsilon + B \qquad \text{equation 4.14}$$

where A and B are constants [46]. Therefore, the increase in water content can greatly increase the ionic conductivity as water has a high dielectric constant and water can promote the dissociation of ion pairs.

As the relative humidity is increased the a.c. conductivity increases and a plot of conductivity against frequency (fig. 4.13) shows a deviation from the straight line previously obtained in figure 4.5. When the reactance of this system is calculated it shows an increase in the magnitude of the capacitive component of the a.c. conductivity and the appearance of a significant ionic component to the a.c. conductivity. The change in shape of the graph of conductivity against frequency also suggests increasing ionic conductivity as the shape of the line, particularly in the high humidity cases, is tending towards that shown in figure 4.10 which shows ionic conductivity.

As the relative humidity increases, both the interlayer ions and the silicate sheet become more hydrated. This will increase the separation of the interlayer cations from the silicate sheet. At high relative humidities the interlayer cations will not be held as strongly by the silicate sheet and as a result these ions will have an increased mobility.

It has been demonstrated above that, using silver-paste electrodes, the a.c. conductivity of the laponite-electrode combination contains a capacitive component, but as the relative humidity increases an ionic component becomes more dominant. Also, as the relative humidity increases, the increase in basal spacing indicates that the exchangeable cations in the interlayer region are becoming more hydrated. The same will be true for

exchangeable cations situated at the edges of the clay crystal, and these hydrated cations may be able to provide a source of charge carriers between crystals by increasing interparticle contact.

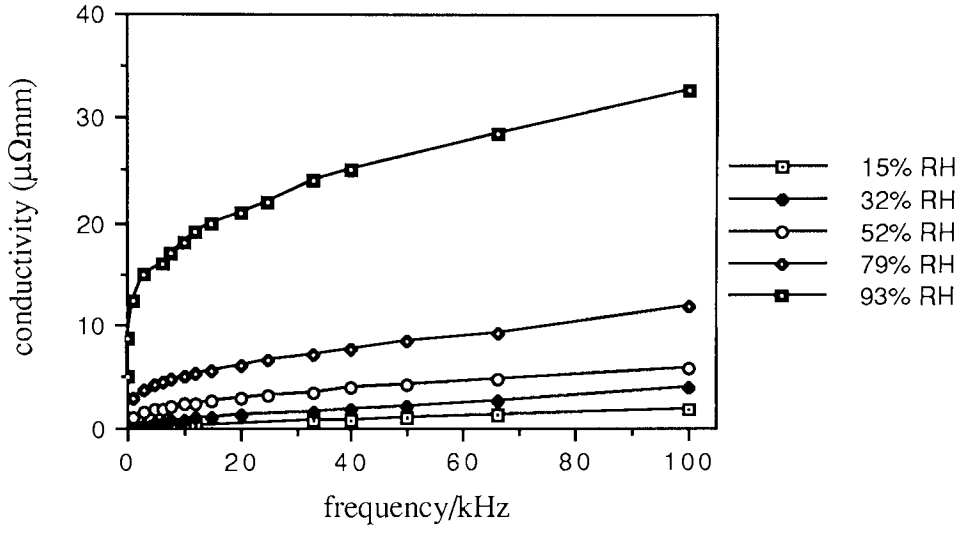

Figure 4.13 Variation of laponite RD conductivity with increasing relative humidity

The naturally occurring mineral talc is structurally related to hectorite (see section 1.3), the natural analogue of laponite. Talc has no substitution in the octahedral or tetrahedral layers, therefore it has no exchangeable ions in the interlayer region, and little or no interlayer water. The a.c. conductivity of talc was measured using silver-paste electrodes, and found to be two orders of magnitude lower than that of laponite RD. This suggests that the a.c. conductivity of laponite is a function of the occupancy of the interlayer region. This is confirmed, with respect to interlayer water, by the above measurements at different relative humidities.

4.7 Charge Carrier Determination

4.7.1 Theory

Electrical conductivity can arise from the movement of ions, holes or electrons, or a combination of carriers. Also, there may be contributions from different types of carriers. To identify the sign of the dominant charge carrier the Hall effect is utilized [81]. Hall discovered that when a conductor, or semi-conductor, which is carrying a d.c. current, I_x, is placed in a magnetic field, B_z, at a right angle to the direction of current flow, an electric field is set up in a direction perpendicular to both the magnetic field and the current flow. The potential difference of the electric field is known as the Hall

voltage, V_H, and can be measured for the majority of conductors and semi-conductors. If the current density is i, then the Hall coefficient R_H is defined by

$$V_H = R_H \, i \, B \qquad \text{equation 4.15}$$

The relative directions of current, magnetic field and induced (Hall) voltage for negative charge carriers (electrons) are shown in figure 4.14 (A). If the carriers are electrons in figure 4.14 (B) and the conducting strip has edges parallel to the x and y directions, when the magnetic field is applied in the z direction the Hall voltage shown is produced.

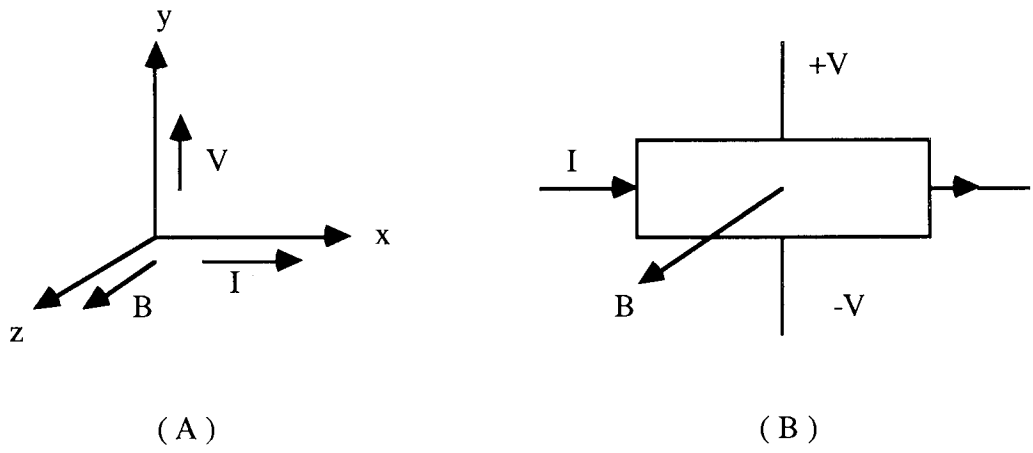

Figure 4.14 The Hall effect [81]

The Hall coefficient, calculated from equation 4.15, is inversely proportional to the number of charge carriers, n. Therefore n can be calculated [81].

$$R_H = 1/ne \qquad \text{equation 4.16}$$

As $\sigma = ne\mu$ (equation 4.1), the mobility of the charge carriers, μ, can also be calculated from Hall effect data, along with conductivity data. If the temperature, T, and mobility are known, the electron diffusion coefficient, D, can be calculated using Boltzmann's constant, k, and the charge of an electron, e.

$$D = \frac{\mu kT}{e} \qquad \text{equation 4.17}$$

4.7.2 Experimental Technique

For the measurement of the Hall effect 1 mm thick discs of laponite RD were stored at 52% relative humidity for two weeks, then four 1.2 mm diameter aluminium spots were sputtered onto the surface under high vacuum. The discs were then stored for a further two weeks at 52% relative humidity. A steel mask was used to ensure the even spacing of the spots, as shown below (fig 4.15), diagonally the spots were 6 mm apart . In the Hall effect experiment the spots used to measure V_H must be aligned accurately opposite each other. If there is some misalignment of electrodes V_H will include a potential drop component as well as the induced Hall voltage [82].

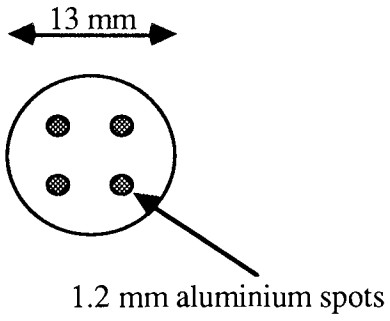

Figure 4.15 Sample geometry for the Hall effect experiment

Thin copper wire was attached to the aluminium spots with silver loaded epoxy resin and used to connect the disc into the Hall effect circuit, figure 4.16. The disc was placed in the poles of an electromagnet and the poles adjusted so as to be 3 mm apart. With a precise knowledge of the pole separation and the magnitude of the current flow through the electromagnet it is possible to obtain the magnetic field strength, B, from a calibration curve. The direction of the current flow through the magnet coils should be noted.

The magnitude of the Hall voltage was measured as a function of sample current (at constant magnetic field strength) and as a function of magnetic field strength (at constant sample current). As a reference the experiment was repeated with a standard silver sample.

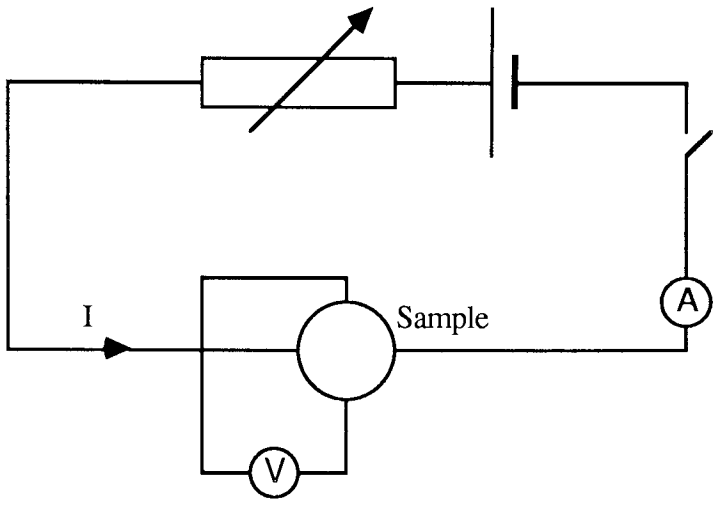

Figure 4.16 Hall effect measuring circuit

4.7.3 Results and Discussion

If equation 4.15 is modified, replacing current density, i, with I/d, the sample current divided by the sample thickness and rearranged, R_H can calculated.

$$R_H = \frac{dV_H}{IB} \qquad \text{equation 4.18}$$

If the gradient of the plot of V_H against I, the sample thickness and the applied magnetic field are known, R_H can be calculated.

sample current/μA	Hall voltage/V
0	-0.6
10	-0.7
20	-0.9
30	-1.3
40	-1.4

Table 4.6 Hall voltages as a function of sample current for laponite RD, 20°C, B = 0.46 T

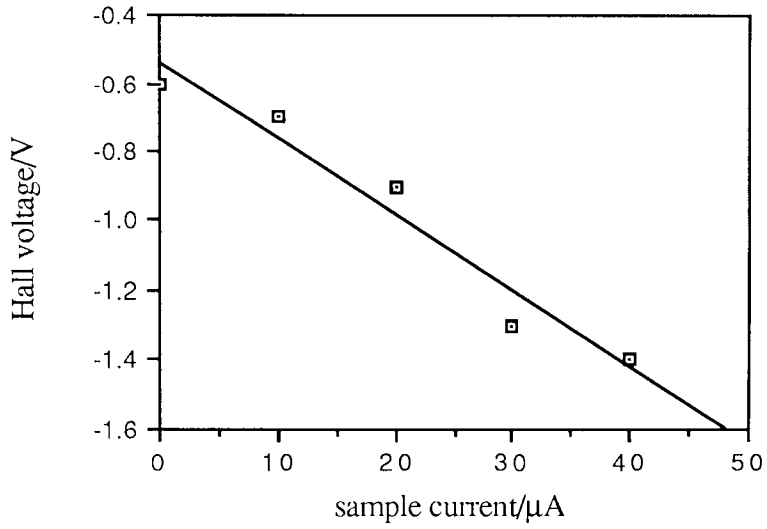

Figure 4.17 Plot of V_H against I_s to calculate R_H and n for laponite RD

Figure 4.17 is the graphical representation of the results in table 4.6. The gradient of the plot is - 22,000. From this R_H can be calculated to be - 46.8 ΩmT^{-1}. From equation 4.16, the charge carrier concentration, n, can calculated to be 1.33 x 10^{17} m^3. From these results the Hall coefficient of laponite is negative, suggesting that the dominant charge carrier has a negative charge. This observation is confirmed when the same experimental configuration is applied to a sample of silver and the Hall coefficient is also calculated to be negative. It is known [81] that the charge carriers in silver are electrons.

From equation 4.1 the charge carrier mobility can be calculated. As no ionic conductivity was detected in the Hall effect experiment a value for the conductivity was chosen that showed predominantly reactive and little ionic conductivity (σ = 2 x 10^{-3} $\Omega^{-1}m^{-1}$, from figure 4.5). Using the value for charge carrier concentration obtained above, the mobility is calculated to be 0.094 $m^2V^{-1}s^{-1}$. From equation 4.18 the electron diffusion coefficient can be calculated to be 2.4 x 10^{-4} ms^{-1}.

Table 4.7 shows that the number of charge carriers, n, in laponite is higher than in silicon [83] but lower than in well known semiconducting minerals such as cassiterite, a mineral form of SnO_2 [84]. The mobility, μ, is also intermediate between silver and silicon. The Hall coefficient, R_H, is higher than silver or cassiterite but below that of silicon. A metallic conductor, silver for example, has a much higher number of charge carriers than the semiconducting materials, and a correspondingly lower Hall coefficient [85].

	R_H / ΩmT^{-1}	n / m^3	μ / $m^2V^{-1}s^{-1}$
laponite RD	- 46.8	1.33×10^{17}	0.094
cassiterite	- 0.016	4.0×10^{20}	0.0015
silver	$- 8.1 \times 10^{-11}$	7.7×10^{28}	0.005
silicon	- 100	6.2×10^{16}	0.40

Table 4.7 Comparison of Hall constants

Similar information can be obtained from experiments using a constant sample current and varying the magnetic field strength, B. The results from experiments at constant sample currents of 10, 20 and 30 μA are summarized in table 4.8. As these experiments use direct current electricity, polarization can occur at the electrode sample interface during the experiment. This is a particular problem when a constant current is required. A constant sample current of above 30 μA cannot be maintained for sufficient time without the occurrence of localized heating at the current input connection on the sample. Therefore, the constant magnetic field strength (varying sample current) experiment is preferable to the constant sample current (varying magnetic field strength) experiment. However, it can be seen from table 4.8 that these results largely confirm the results obtained from table 4.6.

sample current/μA	Hall constant, $R_H/\Omega mT^{-1}$	carrier concentration,n/m^3
10	-93.5	6.68×10^{16}
20	-197.9	3.17×10^{16}
30	-246.7	2.53×10^{16}

Table 4.8 Summary of results for R_H and n obtained from constant sample current experiments

As the sample current is increased, table 4.8 shows that the carrier concentration is decreasing. This confirms that some polarization is occurring, reducing the conductivity of the sample and reducing the charge carrier concentration. There is a corresponding rise in the Hall coefficient as this is dependent on the carrier concentration (equation 4.16).

The Hall voltage measurements were difficult to obtain due to the low magnitude of conductivity of the sample. High sample currents could not be used due to localized heating at the contact points. The observed Hall voltages were small, and tended to decline with time because of polarization at the contacts. Therefore, measurements were taken quickly, before the sample began to polarize. This practice, however, leads to a high degree of experimental error. However, from the results gathered, there can be no doubt that the sign of the dominant charge carrier, under these conditions, is negative.

4.8 Thin Film Conductivity Measurements

4.8.1 Experimental

Smectite clays can be cast into thin films from an aqueous suspension. Laponite can form a transparent film when a suspension or a gel is allowed to air dry on a flat surface. As this drying process is slow, the clay particles can orientate themselves parallel to the surface as they dry, forming a well ordered solid. This is confirmed by X-ray powder diffraction, the basal spacing peak of the ordered solid is over an order of magnitude greater than the basal spacing peak of the powdered sample.

Using a well ordered clay sample it is possible to investigate the conductivity of the clay in two crystal directions. Casting a film onto a glass slide will allow the measurement of the conductivity parallel to the glass slide and perpendicular to it. The parallel measurement can be considered to be measuring the conductivity parallel to the interlayer region, or along the interlayer. The perpendicular measurement is through the crystal in a direction perpendicular to the plane of the interlayer region.

In both cases glass slides were painted with silver loaded paint (obtained from RS Components), the silver loaded paint forming the electrical contacts. Lengths of freshly stripped, thin, enamelled copper wire were attached with silver loaded epoxy resin and used to connect the sample to the Digibridge.

Figure 4.18 shows the electrode configuration for the parallel measurements. A 2 mm gap was left in the silver loaded paint (the slide is 26 mm wide), and a clay film was cast so as to cover the full width of the slide. The average thickness of the clay film was calculated from dial micrometer measurements over the full width of the film. The clay film provides the only path for the passage of electrical current between the contacts.

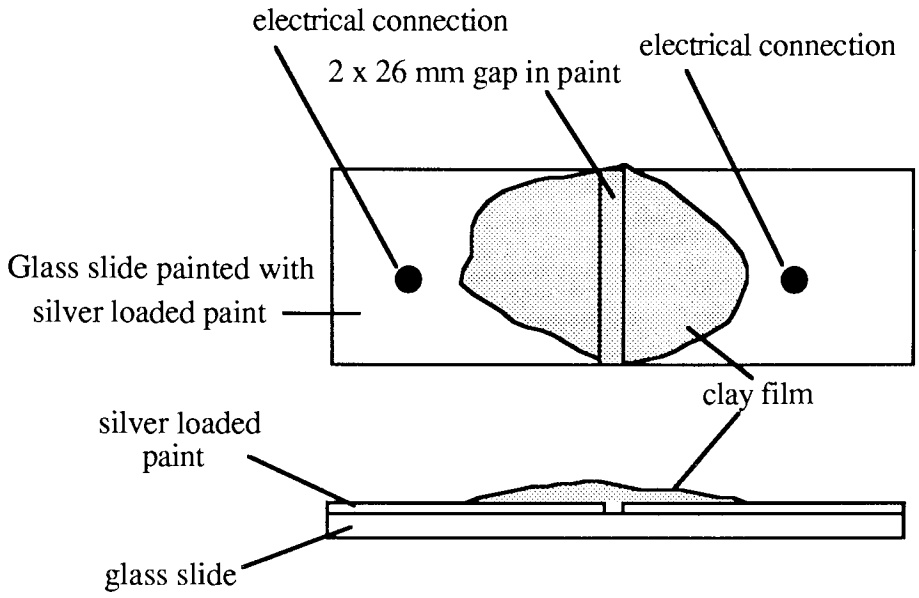

Figure 4.18 Electrode configuration for parallel measurement from above and from the side

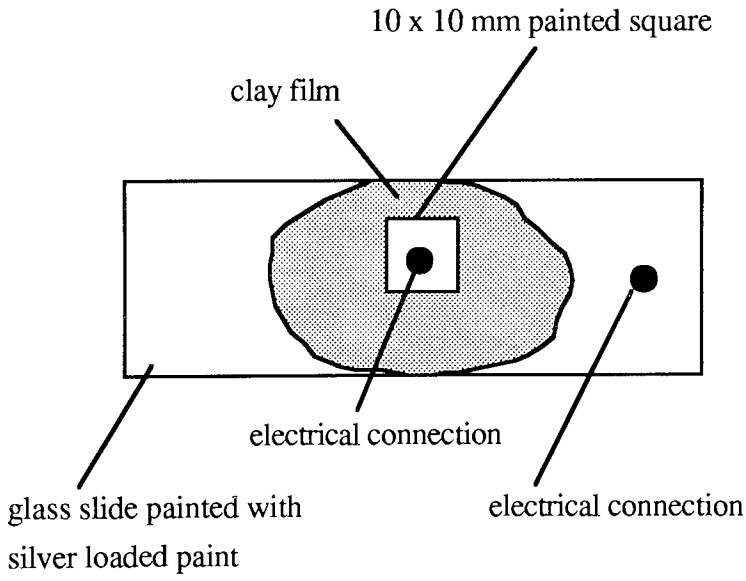

Figure 4.19 Electrode configuration for perpendicular measurements

Figure 4.19 shows the electrode configuration for the perpendicular measurements, the slide was painted fully, dried and the clay cast onto the paint. When the film was dry its thickness was calculated and a 10 x 10 mm square was painted onto the film with silver loaded paint. The paint was allowed to dry, then the electrical contact was attached.

Conductivity data obtained from the anisotropic measurements cannot be related to pressed powder measurements as the water content of the films is much higher than that of the powder, and the water content of films cannot be measured accurately in a none destructive manner. Films of laponite can be produced with water contents up to 70%. To ensure repeatability batches of films were prepared together and stored at 52% relative humidity before use. Care must be taken to avoid drying the films excessively as cracks will form in the films making accurate electrical determinations impossible.

4.8.2 Anisotropic Conductivity Measurements

From a comparison of parallel and perpendicular measurements (table 4.9), it can be seen that there is a degree of anisotropy in the a.c. conductivity of laponite RD. The magnitude of conductivity is approximately two orders higher in the parallel direction relative to the perpendicular direction. This is not entirely unexpected when considering the sheet structure of laponite. These results seem to confirm the observations made above (section 4.7.3, relative humidity dependence of conductivity, conductivity of talc), that the a.c. conductivity arises from within the interlayer region. A similar degree of anisotropy has been reported for graphite [86], which is also a sheet structure. Higher anisotropic ratios have been reported for graphite, but this is explained by probable failure to make electrical contact with all of the layers [87].

frequency/kHz	conductivity/$\Omega^{-1}mm^{-1}$ parallel	conductivity/$\Omega^{-1}mm^{-1}$ perpendicular
100	2.7×10^{-4}	2.5×10^{-6}
50	2.4×10^{-4}	1.8×10^{-6}
10	1.87×10^{-4}	1.06×10^{-6}
5	1.4×10^{-4}	0.9×10^{-6}

Table 4.9 Summary of anisotropic conductivity measurements for laponite RD

Figure 4.20 shows the frequency variation of the anisotropic components of a.c. conductivity. This shows the difference in magnitude between the parallel and the perpendicular components of a.c. conductivity and the shape of the curves. The shape of the curve obtained for the parallel a.c. conductivity can be best compared with that presented in figure 4.13, which shows the increase in a.c. conductivity of laponite with increasing relative humidity. The curve resembles, in shape, the curve obtained at 93%

relative humidity in figure 4.13. This is not unexpected as the water content of the films used here is high and the water content in the interlayer region at 93% relative humidity will be high. Therefore, as the clay crystals are well ordered and highly hydrated, the opportunity for interparticle contact is higher.

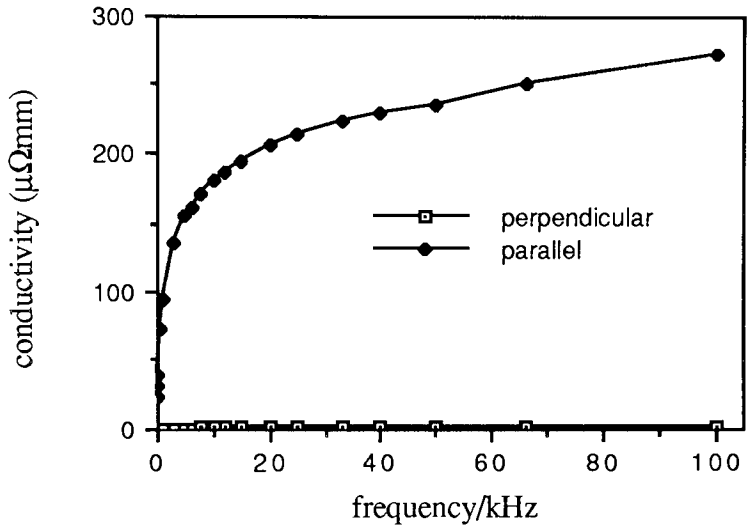

Figure 4.20 The anisotropic components of laponite RD conductivity

Laponite RDS also exhibits similar anisotropic conductivity.

4.8.3 Activation Energy Measurements

The activation energy of a.c. conductivity for pressed powder discs has been calculated in section 4.6. This treatment can be extended to the thin films to measure the activation energy of the anisotropic conductivities. The films were placed in a sealed container containing a thermometer and immersed in a water bath. The temperature of the water bath was raised and the capacitance and resistance measured. At temperatures above 60°C condensation was observed on the inside of the vessel, indicating that water loss from the film had occurred. Only measurements below 50°C were considered as the water content of the film is critical to the conductivity.

Frequency/kHz	Activation Energy/kJmol^{-1} ± 2 kJmol^{-1}	
	perpendicular	parallel
100	+14	+12
50	+16	+10
10	+14	+ 8
5	+17	+ 8

Table 4.10 Anisotropic activation energies for films of laponite RD

In both the parallel and perpendicular cases the plots of $\log_e \sigma$ against 1/T were straight lines at measured a.c. frequencies, in the range 100 kHz to 12 Hz. As only the low temperature process (20-40°C) can be investigated using this system. This allows a more simple treatment of the results, and a single value for the activation energy at each a.c. frequency. These values are shown in table 4.10.

It can be seen from table 4.10 that while the magnitude of the conductivity differs by two orders, the activation energy does not differ significantly in magnitude, since the conductivity depends on the exponential of the activation energy. The activation energy for the parallel measurement is lower than for the perpendicular measurement, reflecting the higher conductivity in the parallel system.

In the case of the parallel measurements, it can be seen that the activation energy falls as the frequency decreases, as in the case of the pressed powder disc of laponite RD. The magnitude of the parallel activation energy is much lower than the activation energy of the pressed powders as the conductivity of the film is higher than that of the powder.

The frequency dependence of the parallel measurement is similar to the high temperature process observed for the pressed powder disc. The high hydration of the system and the improved interparticle contact should promote charge carrier mobility in this system. There is little frequency dependence in the case of the perpendicular measurements.

4.9 Conclusions

Previous investigations [43, 44] of the conductivity of smectite clays has not attempted to discover the mechanism of conductivity, believing it to be ionic in nature. It has been shown here that a.c. measurements can accurately determine the conductivity over a range of a.c. frequencies, using different electrode materials. The a.c. measurements allow effects of polarization, which can dominate d.c. measurements, to be observed without affecting the whole range of frequency measurements.

For a sample of laponite RD measured using silver-paste electrodes the impedance of the sample is dominated by a reactive component, suggesting very little contribution from ionic conductivity. Measurements of the Hall effect indicate a low level of electronic, n-type conduction.

In a series of experiments in which 17 mm diameter stainless-steel electrodes were utilized, the magnitude of a.c. conductivity increased with increasing temperature. This dependence of conductivity on temperature could arise from the change in position of a free ion - ion pair equilibrium or from a semi-conductor type conductivity. From the shape of the curves of conductivity against frequency the dominant component of the a.c. conductivity appears to be ionic, since the conductivity is almost independent of frequency between 100 kHz and 10 kHz. This is confirmed by calculating the components of the impedance. Resistance rather than reactance is dominant in this case. Therefore the ionic mechanism is more likely when stainless-steel electrodes are utilized.

The series of measurements made at elevated temperature utilized a stainless-steel die as the electrode system and measurements were carried out whilst applying a pressure of 0.5 tonnes. The effect of applied pressure on conductivity was determined. As the applied pressure is increased (up to 7 tonnes), the a.c. conductivity increased. This is probably because of improved interparticle contact and sample-electrode contact.

The measured activation energies reflect the observed conductivities and two activation energies were calculated, one for low temperature, the other for higher temperatures. The activation energy is lower at higher temperatures. There is little frequency dependence of the activation energy at low temperatures. This increased free volume available to charge carriers at higher temperatures has probably increased their mobility and displaced them to higher frequencies, that are outside the measurement window,

thus allowing only the observation of low mobility charge carriers at the low frequencies.

When aluminium is sputtered onto the surface of the sample the a.c. conductivity has a higher magnitude ($10^{-4}\ \Omega^{-1}\ mm^{-1}$) than previously measured for silver-paste electrodes. However, the level of conductivity is similar to that measured when the stainless-steel electrode system is used. The conductivity is almost independent of frequency (for f > 10 kHz) which suggests that the conductivity is ionic in origin.

The a.c. conductivity of laponite also increases with relative humidity. As the relative humidity is increased more water enters the interlayer region, and this may increase the ionic conductivity as water has a high dielectric constant and this parameter effects the magnitude of the ionic conductivity in an exponential manner. Also, as the humidity increases the exchangeable cations will hydrate, including the cations at the edges of the clay crystal. These hydrated cations at the crystal edges could increase interparticle contact and may help to provide a pathway from crystal to crystal for electrical charge carriers.

Therefore, it can be seen that the a.c. conductivity of laponite consists of two components, reactive (minor component) and ionic (major component), which can be observed almost independently by utilizing different electrode systems.

Measurements of the a.c. conductivity of thin films of laponite show that the conductivity is anisotropic in nature. The conductivity in the plane parallel to the interlayer region of the clay is two orders of magnitude higher than the conductivity in the plane perpendicular to the interlayer. This is as expected for a sheet structure, such as a smectite clay or graphite, suggesting that the a.c. conductivity of laponite arises from within the interlayer region.

4.10 Further Work

Further experiments are required to confirm the presence of the two competing components of the a.c. conductivity of laponite and to confirm their origin.

The silver-paste electrodes used at the beginning of this study were convenient and gave reproducible results. Studies using different electrode systems have revealed a further competing conduction mechanism (ionic). However, these electrode systems are inconvenient when measuring many samples. Therefore, an electrode system is

required that combines the ease of use and reproducibility of silver-paste electrodes and the promotion of ionic conduction of through the steel or aluminium electrodes. Gold blocking electrodes, for example, allow no discharge or reaction at the sample-electrode interface, and thus the interface may simply be represented as a double layer capacitance in series with the sample.

The Digibridge allows the sample to be considered as a capacitor and a resistor in parallel (fig. 4.3). This appears to be appropriate as, in some cases, the a.c. conductivity has significant reactive and resistive components. However, this configuration takes no account of the grain boundary. The grain boundary has an associated capacitance in parallel with a grain boundary resistance. The grain boundary resistance is typically larger than that of the bulk, but the grain boundary is significantly thinner than the bulk sample being measured. Therefore, a more complex measurement configuration should be considered, figure 4.21, with the double layer capacitance, C_{dl}, in series with the parallel grain boundary components, R_{gb}, C_{gb} and the bulk components, C_b and R_b.

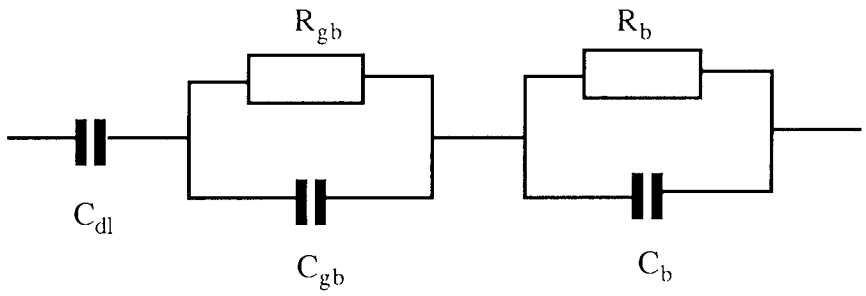

Figure 4.21 Proposed measuring circuit to compensate for interface effects

To remove some of the complications associated with the sample - electrode interface a four point system could be used. The four point probe uses four, small, pin-electrodes which are equal distances apart. The electrodes are lowered onto the sample surface, and a constant current is injected through the end electrodes. A voltage drop is measured across the two middle electrodes using a very high impedance voltmeter. From the voltage drop, knowing the electrode separation distance, the resistivity can be calculated without the problem of electrode polarization encountered previously.

Unsuccessful attempts to measure the conductivity of laponite using a four point probe system specifically constructed for clay discs failed because the voltage drop across the central probes was small compared to background electrical noise. A larger, better shielded instrument with a grounded voltmeter could prove successful.

Utilization of a suitable standard should be considered. Laponite RD has been used as a standard for measurements using silver-paste electrodes. Also, the opportunity to compare the conductivity of other poorly conducting materials should be taken to allow comparison with laponite and other modified clays.

Chapter Five

THE FORMATION OF NOVEL TIN(IV) OXIDE PILLARED LAPONITE

5.1 Introduction

The capacity of inorganic solids with layered structures, including clay minerals, to intercalate guest species within the layers is well known [16]. One simple implication from previous work [43] (see section 1.7) was that the intercalation of suitable large organic or organometallic molecules may be effective in increasing the conductivity of smectite clays. The work presented here describes the intercalation of phenyltin compounds into laponite, a white, synthetic smectite clay, using a conventional method and a novel microwave heating method, and the nature of the resulting clays.

Phenyltin compounds were used for a number of reasons. They are white and therefore will not affect the colour of the resulting clay. They are readily available and the chemistry of phenyltin compounds is well known and understood [88,89]. ^{119}Sn is suitable for Mössbauer spectroscopic studies and both ^{117}Sn and ^{119}Sn ($I=^{1}/_{2}$) are n.m.r. nuclei, therefore powerful spectroscopic techniques are available to probe the nature of the intercalated phenyltin species.

Mössbauer spectroscopy has been used recently to investigate organotin compounds sorbed by montmorillonite [90]. Of more relevance is work describing the formation of tin oxide pillared clays [91] and an associated ^{119}Sn Mössbauer study [92]. The pillaring was achieved by complete ion exchange of cationic hydroxo complexes derived from the hydrolysis of $(CH_3)_2Sn^{2+}$, at a carefully controlled pH to ensure the optimum formation of large oligomeric cations, followed by heat treatment at >200°C for 12 hours to give tin (IV) oxide pillars.

5.2 Chemicals

Laponite was obtained from Laporte Industries Limited and used in the RD form (see section 4.2). Ph_3SnCl and Ph_2SnCl_2 were obtained from the Aldrich Chemical Company Limited. Triphenyltin oxide, $(Ph_3Sn)_2O$, was prepared following a literature method [93] via the hydrolysis of triphenyltin chloride, m.p. 122°C (lit., 123-124°C). Absolute ethanol was dried according to a literature method [94] by refluxing with magnesium turnings followed by distillation.

5.3 Intercalation of Phenyltin Compounds

Two methods were used for the intercalation of phenyltin compounds. Three chosen phenyltin compounds, Ph_2SnCl_2, Ph_3SnCl and $(Ph_3Sn)_2O$, were intercalated using each method.

5.3.1 Mechanical Shaker At Ambient Temperature

Laponite RD (5 g) and the phenyltin compound (1 g) were mixed with dry absolute ethanol (100 ml) in a 250 ml quickfit conical flask. The flask was placed on a Gallenkamp mechanical flask shaker for one week. The clay was filtered and washed with 4 x 25 ml aliquots of ethanol. The combined washings and filtrate were evaporated and the remaining phenyltin compound weighed. The amount of phenyltin compound intercalated was calculated by difference, and expressed as a percentage.

Precursor	% uptake
Ph_2SnCl_2	38%
Ph_3SnCl	45%
$(Ph_3Sn)_2O$	10%

Table 5.1 Percentage of phenyltin precursors intercalated using a mechanical shaker

Amount of Ph_3SnCl used	Uptake
1 g	0.4 g
2 g	0.4 g
3 g	0.5 g
4 g	0.7 g
5 g	1.0 g

Table 5.2 Uptake of Ph_3SnCl as amount of precursor is increased

The amount of intercalation was dependent on the phenyltin precursor, the percentage intercalation for different precursors is shown in table 5.1. Different weights of precursor were also used. Table 5.2 shows the amounts of intercalation achieved by

using different amounts of Ph_3SnCl, while keeping the weight of laponite used constant at 5 g.

Table 5.2 shows that the amount of intercalation can be increased by increasing the amount of starting material used four or five fold. While this leads to a higher weight of precursor intercalated, it also leads to much more waste starting material. The percentage of starting material intercalated is highest when 1 g of phenyltin compound is used. A further experiment was carried out using only 0.6 g of precursor, again the percentage intercalated was lower than when 1 g was used. Therefore, we can conclude that, in percentage terms the most efficient intercalation achieved is when 1 g of phenyltin precursor was used with 5 g of laponite. However, the amount of intercalation can be increased by simply increasing the amount of phenyltin precursor used four of five fold.

5.3.2 Microwave Heating

It has been demonstrated recently [95] that layered inorganic materials intercalated greater quantities of host material more rapidly when the reaction was carried out in a microwave oven. Also, the rapidity of microwave processes may reveal chemistry which may not be observed using conventional methods [70].

	Percentage uptake	
Precursor	shaker	microwave
Ph_2SnCl_2	38%	44%
Ph_3SnCl	45%	75%
$(Ph_3Sn)_2O$	10%	33%

Table 5.3 Comparison of shaker and microwave methods for the intercalation of phenyltin compounds

Laponite RD (1 g) and the phenyltin compound (0.2 g) were mixed with dried absolute ethanol (10 ml) and sealed in a 120 ml Teflon container with a screw cap (from the Savillex Corporation, Minnetonka, Minnesota 55345, U.S.A.) and placed in a Sharp Carousel 650 W domestic microwave oven. The temperature of the oven space was set at 40°C and the mixture was subjected to five one minute bursts of microwave radiation at a medium-high setting. The vessel was allowed to cool before being opened in a fume cupboard. The clay was washed with 4 x 25 ml aliquots of ethanol. The combined

washings and filtrate were evaporated and the remaining phenyltin compound was weighed. The amount of phenyltin compound intercalated was calculated, and expressed as a percentage. It can be seen from table 5.3 that spectacular enhancements for the rate of sorbtion of phenyltin compounds can be achieved using microwave heating.

Experiments with both Ph_3SnCl [96] and $(Ph_3Sn)_2O$ in which microwave irradiation times ranging between 1 and 30 minutes were used, established 5 minutes as the optimal irradiation period in both cases. In the case of $(Ph_3Sn)_2O$ the amount of uptake of the precursor reached a plateau at 5 minutes irradiation. The clay appears to have a higher affinity for Ph_3SnCl than for $(Ph_3Sn)_2O$ (table 5.3) and after 5 minutes irradiation the uptake of Ph_3SnCl had reached a maximum, above that for $(Ph_3Sn)_2O$. On further irradiation it began to decline from the maximum, to approach the $(Ph_3Sn)_2O$ uptake. An uptake versus time curve, with a maximum followed by progress to a lower plateau value, is characteristic of a reaction on a clay surface [97] of one sorbed species to give another which in turn must establish an equilibrium distribution between clay and solvent. Also, organometallic material recovered from these experiments showed clear infra red evidence for the presence of $(Ph_3Sn)_2O$ [96]. This seems to indicate that the Ph_3SnCl hydrolyses on the clay surface to form $(Ph_3Sn)_2O$. This is confirmed by a simple experiment in which Ph_3SnCl was intercalated using the mechanical shaker along with a blank experiment in which an identical quantity of Ph_3SnCl was treated only with solvent. In both cases a lowering of pH was observed, indicating the release of acid (HCl), see table 5.4. However this effect was greatest in the presence of laponite, suggesting that the presence of the clay can enhance the hydrolysis reaction.

	pH
solvent only	6.1
solvent + Ph_3SnCl	5.9
solvent + Ph_3SnCl + clay	4.2

Table 5.4 Measurement of HCl release during intercalation

5.4 Analysis of the Intercalated Clays

5.4.1 ^{119}Sn Mössbauer Spectroscopy

The ^{119}Sn Mössbauer parameters are collected in table 5.5. The ^{119}Sn Mössbauer parameters of the phenyltin compounds were found to be in agreement with literature values [98,99], many of which were determined in the early days of the technique. Each spectrum shows a doublet (fig. 5.1a). ^{119}Sn Mössbauer spectroscopy suggests that the phenyltin compounds undergo a reaction with the laponite. It can be seen from ^{119}Sn Mössbauer spectroscopy that the extent of this reaction depends on the precursor, thus Ph_3SnCl > $(Ph_3Sn)_2O$, Ph_2SnCl_2. In each case the absorption was characterised by a singlet at $\delta = 0$ mms^{-1}. This is similar to SnO_2 [100,101], implying an "SnO_6" environment for these tin atoms. This is the case both for clays prepared using the shaker and for clays prepared using the microwave method, which have very similar parameters. However, the quality of the ^{119}Sn Mössbauer spectrum was superior when the clay was intercalated using the shaker. This is probably because the increase in phenyltin uptake, when the microwave heating method is used, is due to surface sorbtion (see below), therefore the sample is more homogeneous and there are fewer tin microenvironments when the shaker method is used. The data presented in table 5.5 refers to clays intercalated using the shaker method unless otherwise stated.

Material	$\delta \pm 0.15$ (mms^{-1})	$\Delta \pm 0.2$ (mms^{-1})
Ph_3SnCl	1.39	2.62
Ph_3SnCl+ laponite	0.00	
Ph_2SnCl_2	1.46	2.95
Ph_2SnCl_2 + laponite	-0.05	
	1.21	2.66
$(Ph_3Sn)_2O$	1.21	2.52
$(Ph_3Sn)_2O$ + laponite	-0.06	
	1.09	2.04
$(Ph_3Sn)_2O$ + laponite	0.20	
(microwave 5 mins)	1.33	2.54

Table 5.5 ^{119}Sn Mössbauer parameters of phenyltin compounds and the products of their intercalation with laponite

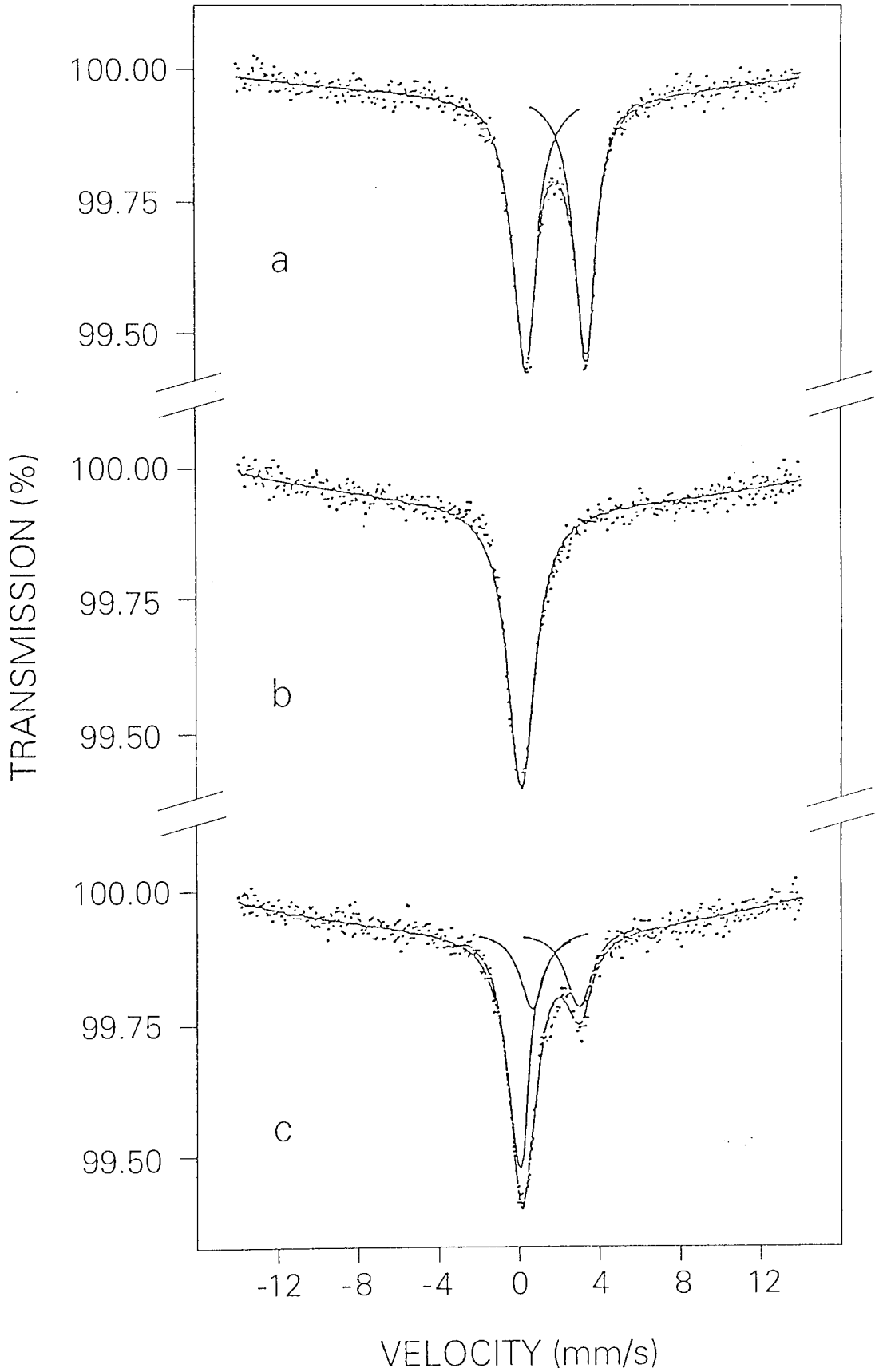

Figure 5.1 ^{119}Sn Mössbauer spectra recorded at 77 K from (a) crystalline Ph_2SnCl_2 (b) Ph_3SnCl + laponite RD (c) Ph_2SnCl_2 + laponite RD

The ^{119}Sn Mössbauer spectrum of laponite intercalated with Ph_3SnCl (fig 5.1b) shows only a singlet at $\delta = 0$ mms^{-1}. Therefore, it can be said that all of the intercalated phenyltin has been converted to "SnO_2".

This is not the case for the intercalation of Ph_2SnCl_2 and $(Ph_3Sn)_2O$. When Ph_2SnCl_2 is intercalated the spectrum (fig 5.1c) shows the combined presence of a phenyltin compound and "SnO_2", see table 5.5. The phenyltin component has Mössbauer parameters $\delta = 1.21$, $\Delta = 2.66$ mms^{-1} which, within the cited experimental errors, could agree with those for Ph_2SnCl_2. However, the values of $\delta(\delta)$ (0.25 mms^{-1}) and $\delta(\Delta)$ (0.35 mms^{-1}) may arise from the intercalation within the clay lattice since some minor structural changes might occur compared with Ph_2SnCl_2 molecules in the bulk crystal. At the very least the next nearest neighbour contribution to the electric field gradient will be different in the two cases. The observed parameters are however close to those of $(Ph_3Sn)_2O$ ($\delta = 1.21$ and $\Delta = 2.52$ mms^{-1}, from table 5.5). $(Ph_3Sn)_2O$ may arise from a rearrangement reaction, common in organotin chemistry [88], of Ph_2SnCl_2 to form $PhSnCl_3$ and Ph_3SnCl, followed by hydrolysis.

The spectrum of intercalated $(Ph_3Sn)_2O$ also shows a combination of "SnO_2" and a phenyltin compound. For the sample prepared using the shaker the Mössbauer parameters of the phenyltin component, δ (δ) (0.12 mms^{-1}), $\delta(\Delta)$ (0.48 mms^{-1}) could agree, within experimental error, with those for $(Ph_3Sn)_2O$ when minor structural changes due to intercalation are considered. However, the Mössbauer parameters for the sample prepared in the microwave oven are more similar to those of crystalline $(Ph_3Sn)_2O$, $\delta(\delta)$ (0.12 mms^{-1}), $\delta(\Delta)$ (0.02 mms^{-1}). This suggests that much of the extra $(Ph_3Sn)_2O$ taken up by the clay in the microwave experiment is surface sorbed rather than truly intercalated.

5.4.2 ^{119}Sn Magic Angle Spinning Nuclear Magnetic Resonance Spectroscopy

^{119}Sn is both a Mössbauer active nucleus and an n.m.r. nucleus. The ^{119}Sn m.a.s. n.m.r. spectrum of the Ph_3SnCl + laponite sample provides further evidence for formation of SnO_2. The spectrum shows a single line at $\delta = -15.5$ ppm (versus a SnO_2 standard). The chemical shift range for ^{119}Sn is very large (approx 3000 ppm), therefore this peak at $\delta = -15.5$ ppm can be considered as arising from a "SnO_2" environment. The peak was obtained from 212,160 transients, which demanded a considerable amount of instrument time. Therefore, it is interesting to note that for these materials ^{119}Sn Mössbauer spectroscopy, rather than ^{119}Sn m.a.s.n.m.r., is the superior analytical tool.

5.4.3 Powder X-Ray Diffraction

The results shown in table 5.6 show an increase in basal spacing when phenyltin compounds are intercalated. This, along with the ^{119}Sn Mössbauer spectroscopic data, suggests that tin(IV) oxide pillars have been formed in the laponite interlayer.

Material	$d_{001} \pm 0.1$ Å
laponite RD	13.5 Å
Ph_3SnCl+ laponite	21.5 Å
$(Ph_3Sn)_2O$ + laponite	20.5 Å
Ph_2SnCl_2 + laponite	15.8 Å

Table 5.6 Powder XRD data for intercalated laponites

The basal spacings correlate well with the ^{119}Sn Mössbauer evidence for the extent of the conversion (pillaring) reaction. It can be seen from table 5.6 that the basal spacings become greater with the increasing efficiency of conversion of phenyltin compounds to tin(IV) oxide.

If the amount of phenyltin compound intercalated is increased by using more starting material, table 5.2, the basal spacing can be increased by up to a further 2 Å in the case of 5 g of Ph_3SnCl. This suggests that when the amount of intercalation is increased, pillars with greater dimensions are produced, rather than more pillars with the same dimensions being produced.

Relative Humidity	$d_{001} \pm 0.1$ Å
15%	15.8 Å
32%	15.8 Å
52%	15.8 Å
79%	16.4 Å
93%	16.4 Å

Table 5.7 Dependence of basal spacing of a pillared clay on relative humidity (laponite RD + Ph_2SnCl_2)

The dependence of the basal spacing of the tin(IV) oxide pillared clay, prepared from Ph_2SnCl_2, on relative humidity can be measured as before (see section 4.5.1). The results (table 5.7) indicate a much reduced dependency on relative humidity, compared to laponite RD (table 4.2). The basal spacing of tin(IV) oxide pillared clays prepared from Ph_3SnCl is almost independent of relative humidity. This is because the pillars tend to hold successive silicate layers together as the pillars are attached to the silicate layers. When the pillaring precursor is Ph_2SnCl_2 ^{119}Sn Mössbauer spectroscopy shows that there is some intercalated phenyltin compound in the interlayer region. Some interlayer regions may contain no pillars, only intercalated Ph_2SnCl_2, leading to some humidity dependence of the basal spacing. Also, the presence of the pillars and the benzene (see below) associated with the pillar formation will lead to the interlayer region of the clay being more hydrophobic than usual.

5.5 Mechanism of Tin(IV) Oxide Pillaring

The formation of tin(IV) oxide pillars under ambient conditions and using microwave heating requires some mechanistic investigation. The fate of the organic component of the phenyltin precursor must be addressed. Proton attack on aryltin bonds is well known [102]. Sites of Brønsted acidity on the clay may provide protons to electrophilically attack the carbon atom bonded to the tin, giving benzene as the product. Strenuous efforts to locate benzene in the washings from the clay, using g.l.c., were unsuccessful. However, measurement of the ^{13}C m.a.s.n.m.r. spectrum of a clay intercalated with Ph_3SnCl, for which the Mössbauer data indicated tin(IV) oxide to be the only tin species present, revealed a single resonance at 128 ppm (versus $(CH_3)_4Si$) which is characteristic of benzene. This indicates that the benzene is formed in situ and is tenaciously held within the lattice. Either the pore size is not large enough for the benzene to diffuse out of the lattice, or it is associated with an interlayer cation. This association is well known in smectite clays [103,104].

When phenyltin chlorides are used as precursors for the pillaring process it has already been demonstrated above that there is a surface sorbtion step and some hydrolysis involved (see section 5.3.2 and table 5.4). This hydrolysis leads to the formation of HCl. These protons could provide a further source of exchangeable ions in the interlayer of the clay. This was confirmed by atomic absorption spectroscopy. When 5 g of laponite was shaken for a week with dry absolute ethanol 15 ppm of Na^+ was released into solution. The same experiment was repeated in the presence of different quantities of Ph_3SnCl and the filtrate was analysed for the presence of sodium ions. The results are presented in table 5.8. The total amount of exchangeable sodium ions

measured by exchange of $(CH_3)_4NCl$ is found to be 580 ppm. Therefore, it can be seen from table 5.8 that the pillaring reaction is accompanied by some sodium release. However, the pillaring process does not require total sacrificial exchange of the interlamellar cations as in other methods of pillaring [91] (see section 1.4.5).

Similar experiments were carried out using 1 g and 5 g of Ph_2SnCl_2. The concentration of sodium released was 138 ppm and 176 ppm. It can be seen that these values are higher than the values for Ph_3SnCl shown in table 5.8, but not as high as double as there is less conversion of Ph_2SnCl_2 to tin(IV) oxide pillars (table 5.1). This suggests that the protons produced by ion exchange are not involved in the pillaring reaction, the Brønsted acid sites provide the sites for electrophilic attack of the Sn—C bond.

Amount of Ph_3SnCl used	Concentration of sodium released
1 g	97 ppm
4 g	126 ppm
5 g	146 ppm

Table 5.8 Sodium release on pillaring with different amounts of Ph_3SnCl

The first step of the pillaring reaction is surface sorbtion of the phenyltin compound, followed by hydrolysis. In the case of Ph_2SnCl_2 the hydrolysis will be preceded by a reversible rearrangement reaction to form Ph_3SnCl and $PhSnCl_3$. The Ph_3SnCl will then undergo hydrolysis, which gives rise to HCl, which can ion exchange H^+ for interlayer sodium ions, releasing them into solution. The presence of Cl^- in the washings can be confirmed using silver nitrate.

The dependence of the pillaring process on the presence of Brønsted acid sites in the clay structure leads to a potential problem. The pillaring process only proceeds efficiently when the clay has sufficient acid sites. As laponite is a synthetic clay there is a batch to batch variation in many properties of the clay. This can affect the amount of pillaring that takes place in a particular batch of clay. Pillaring takes place in all the grades of laponite available to us, RD, RDS, B and S. It has also been shown that this pillaring process can take place in a natural wyoming bentonite [105] (a montmorillonite clay).

The pillaring process was carried out in dry absolute ethanol, since it is important that the solvent is dried as water may compete for the sites of acidity within the clay. The

pillaring process has now been carried out successfully in other solvents, acetonitrile and chloroform.

5.6 Conclusions

^{119}Sn Mössbauer spectroscopy and powder X-ray diffraction studies have shown that attempts to intercalate three phenyltin compounds, Ph_2SnCl_2, Ph_3SnCl and $(Ph_3Sn)_2O$, into laponite under ambient conditions result in the formation of tin(IV) oxide pillars. ^{119}Sn Mössbauer data indicates that the effectiveness of conversion to tin(IV) pillars is in the order:-

$$Ph_3SnCl > (Ph_3Sn)_2O,\ Ph_2SnCl_2$$

The organic product of the pillaring reaction is benzene and has been identified as held tenaciously within the pillared lattice.

The first step of the reaction is surface sorbtion followed by hydrolysis of the phenyltin compound. This results in the release of HCl, which has been identified by a lowering of the pH of the solvent. Some release of Na^+ ions accompanies the pillaring process, but this is probably a result of ion exchange with H^+ ions present and not as part of the pillaring process. Most of the interlayer ions remain in the lattice after pillaring.

The amount of pillaring can be increased by increasing the amount of phenyltin precursor used in the pillaring reaction.

Microwave heating can dramatically accelerate the pillaring process. When the reaction is carried out in a sealed Teflon vessel in a domestic microwave oven a greater degree of pillaring is achieved in 5 mins. than in a week on the mechanical shaker.

These tin(IV) oxide pillared materials are novel materials, since the pillaring was achieved using neutral precursors rather than by sacrificial ion exchange and heat treatment. Unlike previously prepared pillared clays these novel pillared clays contain exchangeable cations within the newly created pores. Therefore, these novel pillared clays resemble zeolite more closely than conventional pillared clays.

5.7 Further Work

This study has only considered a small number of potential precursors to the pillaring process, namely phenyltin compounds. One unfortunate side effect of the use of these precursors is the presence of benzene in the pillared lattice. In view of the toxic nature of benzene other organotin systems that could produce tin(IV) oxide pillars in this way should be considered.

As the pillaring process involves the electrophilic attack at the tin carbon bond of the phenyltin precursor, using a more electron donating ligand, such as 4-methoxyphenyl, would produce a more electron rich tin carbon bond and should promote the electrophilic attack. This would also yield a less toxic organic fragment.

As the pillaring process depends on Brønsted acid sites within the clay structure, the suitability of a particular clay sample for this pillaring reaction could be tested by measuring the surface acidity using Hammett indicators [106,107]. In this way the optimal conditions for pillaring, with respect to the Brønsted acidity, could be determined.

The acidity of the clay surface has been shown to increase as the water content in the interlayer decreases [108], therefore placing the clay in a low relative humidity atmosphere (15%, 32%) before pillaring may increase the degree of pillaring.

Also, the exchangeable ion is a major factor in the protonation of some organic bases on the clay [109], therefore exchange of cations that promote this protonation may increase the degree of pillaring.

Chapter Six

ELECTRICAL PROPERTIES OF MODIFIED LAPONITES

6.1 Introduction

Previous work [43] has indicated that the conductivity of laponite can be increased by the intercalation of a suitable large organic molecule. No mechanism of conductivity was presented although it was suggested [43,44] that the conductivity may be ionic in origin. It has been shown (Chapter Four) that under some conditions there may be two components to the a.c. conductivity of laponite, namely reactive and ionic. Two approaches were taken to increase the a.c. conductivity of laponite:- ion exchange and intercalation of large molecules. During the intercalation of phenyltin compounds the novel formation of tin(IV) oxide pillars was observed (Chapter Five).

6.2 Alkali Metal Exchange

6.2.1 Experimental Methods

Laponite RD was supplied with sodium as the sole interlamellar cation. Conversion of laponite RD to other monoionic forms can be achieved using a method based on that of Posner and Quirk [71].

Laponite RD (5 g) was washed with 1M solution of the chosen alkali metal chloride and separated by decantation. This was repeated five times. The clay was then suspended in 1M solution of the alkali metal salt at pH 3, adjusted with 1M hydrochloric acid. Separation was achieved by settling. After this procedure was repeated three times, the clay was resuspended in 1M solution of the alkali metal at pH 3 and stirred for 36 hours. After separation by standing, the clay was dialysed against deionized water until no Cl^- was observed in the water, using the silver nitrate test. This procedure may last several weeks in total.

The above method was used to prepare monoionic lithium, potassium, rubidium and caesium exchanged laponite samples. Previous work in the laboratory of the sponsoring organization has shown that naturally occurring smectite clays containing group I metals are better electrical conductors than those containing group II metals [110]. This observation has been confirmed in our laboratory [105] using a monoionic copper(II) exchanged laponite.

6.2.2 Conductivity of Alkali Metal Exchanged Laponite Samples

Samples were prepared for conductivity measurements as described in Chapter Two, silver-loaded epoxy resin (paste) electrodes were used. The conductivity of lithium, sodium, potassium, rubidium and caesium ion exchanged laponite samples is shown in figure 6.1.

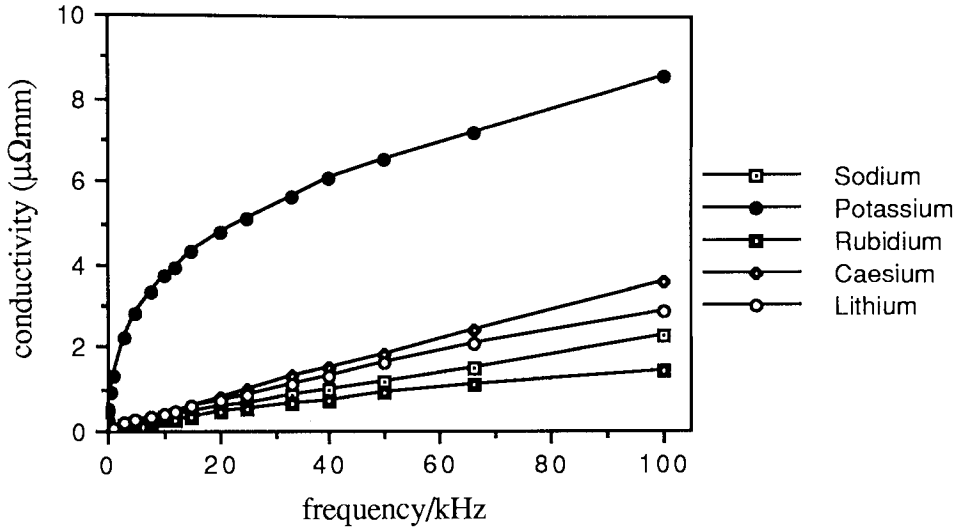

Figure 6.1 Conductivity of alkali metal exchanged laponite samples

It can be seen that the potassium exchanged laponite sample is more conductive than the other four samples. This represents at least a four fold increase in the a.c. conductivity over the whole frequency range. The other four clay samples show similar conductivities and a similar a.c. frequency response. This suggests that when the interlamellar cation is lithium, sodium, rubidium or caesium, the a.c. conductivity is dominated by the capacitive component, as the impedance of the sample is dominated by the capacitive reactance. It is not profitable to speculate about the order of conductivity within this group as the conductivity values are close together, within the limits of possible experimental error.

Potassium exchanged laponite has a different frequency dependence of a.c. conductivity to the other samples. The components of the impedance of the sample are expressed graphically in figure 6.2. While the major component of the impedance is the resistive component there is a significant reactance contribution (c.f. fig. 4.7). Also, there is significant deviation from the plot of conductivity against frequency obtained for laponite RD (fig. 4.5). This also suggests an ionic contribution. Therefore, the a.c. conductivity is comprised of both capacitive and ionic components.

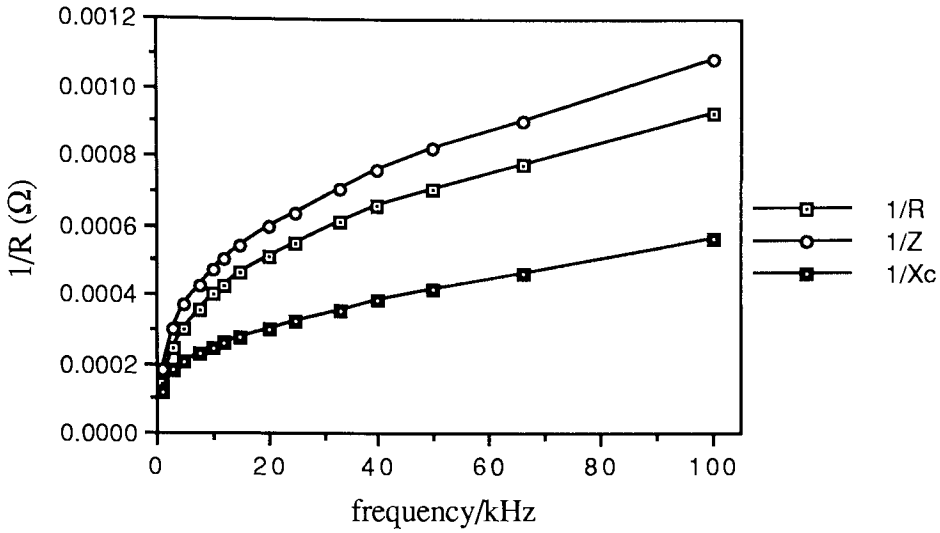

Figure 6.2 Components of the impedance of potassium exchanged laponite

As the alkali metal ions are hydrated in the interlayer region of the clay the hydrated radius of the metal and its degree of hydration (hydration number) must be considered when considering the mobility of ions in the interlayer region (see table 6.1). While lithium and sodium are the smallest unhydrated ions, due to their high hydration number, they are the largest of the alkali metals when hydrated. This will make the ions less mobile than potassium ions which have a much lower hydration number and smaller hydrated radius.

	ionic radius / Å	hydrated radius /Å	hydration number
lithium	0.68	3.00	15.0
sodium	0.95	2.76	16.6
potassium	1.33	2.32	10.5
rubidium	1.48	2.28	-
caesium	1.69	2.28	9.9

Table 6.1 Properties of alkali metal ions [111,112]

Rubidium and caesium are larger unhydrated ions than potassium. However, when they are hydrated they are approximately the same size. It appears that in the case of potassium an optimum mobility is achieved, as potassium is less hydrated, and therefore smaller, than lithium and sodium. Also, the potassium appears to be more mobile than either rubidium or caesium.

As potassium exchanged laponite shows a significantly increased conductivity, larger batches (100 g) were prepared for further investigations.

6.2.3 Temperature Dependence of Potassium Exchanged Laponite RD Conductivity

The same experimental technique as previously used (see section 4.6) was employed to investigate the change in conductivity as the temperature is increased.

As the temperature is increased, as in the case of laponite RD, the a.c. conductivity of the potassium exchanged laponite rises. Similarly, the rate of the conductivity rise increases as the temperature rises. Both ionic and semi-conductor type models of conductivity predict an increase in conductivity as the temperature rises (see section 4.5.1). As the rise is not linear the activation energies were calculated for each curve as a high temperature value (High T) and a low temperature value (Low T) as in section 4.5.4. The results of these calculations are presented in table 6.2.

Frequency/kHz	Activation Energy/kJmol^{-1} ± 2 kJmol^{-1}	
	High T	Low T
100	+20	+30
40	+20	+29
20	+22	+35
10	+22	+38
5	+21	+39

Table 6.2 Variation of activation energy with frequency for potassium exchanged laponite RD

The magnitude of the activation energy is similar to the values obtained for laponite RD suggesting that the mechanism of a.c. conductivity is similar when a similar electrode system (stainless-steel electrodes) is employed. Using this electrode system the a.c. conductivity appears to be predominantly ionic, as in the case of laponite RD. Similarly, the activation energy is higher in the case of the low temperature measurements. This is consistent with the increase in conductivity as the temperature rises.

At the higher temperatures there is little variation in activation energy, reflecting the increased frequency independence of conductivity and the dominance of ionic conductivity when stainless-steel electrodes are used. At lower temperatures the

activation energy is higher, as previously observed (section 4.5.4). As the frequency decreases the activation energy increases. This is not observed for laponite RD and is probably due to a decrease in the mobility of the charge carrier. In the case of potassium exchanged laponite, the ionic conduction is probably due to potassium ions whereas in laponite RD it is probably due to sodium ions. A change in charge carrier or a change in the electrode material could possibly lead to different interface effects.

6.2.4 Dependence of Potassium Exchanged Laponite RD Conductivity on Humidity

The conductivity of laponite RD is highly dependent on the relative humidity (see section 4.6). It can be seen from table 6.3 that this is not the case for potassium exchanged laponite RD. Table 6.3 shows that the conductivity is independent of frequency. This is because of the lower hydration of the potassium ion. At higher humidities the potassium ion does not increase its hydration number and the separation of the ion from the silicate surface is not increased significantly.

Relative Humidity	conductivity/ $\Omega^{-1}mm^{-1}$
32%	5.5×10^{-6}
52%	5.5×10^{-6}
79%	5.6×10^{-6}
93%	5.4×10^{-6}

Table 6.3 Conductivity of potassium exchanged laponite RD at 100 kHz

The observation recorded in table 6.3 is confirmed when the basal spacings of this clay are investigated (see section 6.2.5 below).

6.2.5 Physical Properties of Potassium Exchanged Laponite RD

The physical properties, particularly swelling and hydration (see section 1.4.1), of smectite clays are dependent on the interlayer cation. When potassium exchanged laponite is added to water it behaves differently to sodium exchanged laponite. It does not swell as readily and does not form a clear solution or a gel like its sodium analogue. It forms a suspension in water. However, unless the clay is a fine powder (< 100 μm) it will not remain in suspension. If the suspension is stirred thoroughly (> 8 hours), or subjected to ultrasound (50 Watts, 10 minutes), the clay will remain in suspension for several weeks.

This suggests that the ability of potassium exchanged laponite to form a suspension is a function of particle size since both prolonged stirring and ultrasound will decrease the particle size. Table 6.1 shows that the hydration of a potassium ion is less than a sodium ion, therefore it would be expected that a potassium exchanged clay will swell to a lesser degree than its sodium analogue. This can be confirmed using powder X-ray diffraction to investigate the basal spacing of the potassium exchanged laponite over a range of relative humidities. Table 6.4 shows that the basal spacing of potassium exchanged laponite RD is independent of relative humidity, since the low hydration of interlayer potassium ions does not cause further swelling of the clay, as humidity increases.

Relative Humidity	Basal Spacing ± 0.1 Å
15%	13.7 Å
32%	13.7 Å
52%	13.7 Å
79%	13.7 Å
93%	13.7 Å

Table 6.4 Basal spacing of potassium exchanged laponite RD

6.3 Tin(IV) Oxide Pillared Laponite

6.3.1 Introduction

Pillared clays are well known and have been widely studied (see section 1.4.5). Pillared clays are produced by the ion exchange of large cations which then form the appropriate oxide pillars on heating. Tin(IV) oxide pillared clays have been prepared [91] by ion exchange of cationic hydroxo complexes derived from the hydrolysis of $(CH_3)_2Sn^{2+}$, followed by heat treatment at >200°C. Two novel methods for preparing tin(IV) oxide pillared clays have been described above (Chapter Five). These methods are not based on a sacrificial exchange of the interlayer sodium ions. The pillars are formed when Brønsted acid sites on the clay cleave the aryltin bond of phenyltin compounds by electrophilic attack (see section 5.5). These pillared laponites resemble zeolites more closely than previous pillared clays because they have exchangeable cations available for reaction within a pore channel.

The conductivity of pillared clays has not been investigated previously. One implication from previous work [43] was that increasing the basal spacing of a smectite clay may increase its conductivity. The formation of tin(IV) oxide pillars in the interlayer region of laponite increases the basal spacing of the clay and also introduces to the interlayer a potentially semi-conducting material, SnO_2.

The conductivity of naturally occurring tin(IV) oxide, cassiterite, has been reviewed [87] and it has been shown that it is an n-type semi-conductor. The conductivity is due to structural defects caused by oxygen deficiency. Variation in defect concentration causes the conductivity of cassiterite, and synthetically prepared SnO_2, to vary by several orders of magnitude.

6.3.2 Conductivity of Novel Tin(IV) Oxide Pillared Laponite Samples

Powder X-ray diffraction (table 5.6) and ^{119}Sn Mössbauer spectroscopy (table 5.5) show that the degree of pillaring depends on the phenyltin precursor, Ph_3SnCl > $(Ph_3Sn)_2O$, Ph_2SnCl_2. Figure 6.3 shows the conductivity of pillared clays prepared from three different precursors using the mechanical shaker method (see section 5.3.1). It can be seen that the order of a.c. conductivity is not the same as the order of pillaring or the same as the order of uptake of precursor (table 5.1).

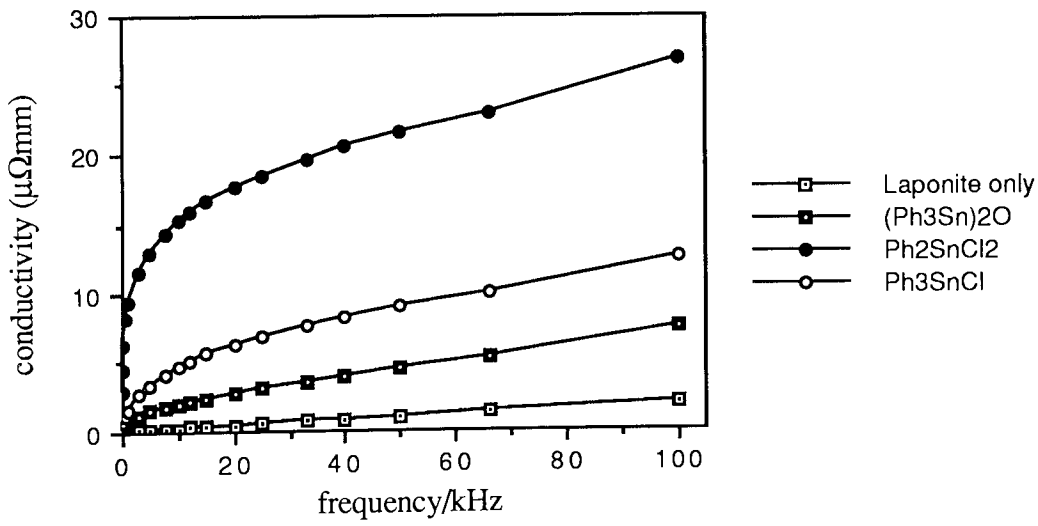

Figure 6.3 Conductivity of pillared clays from different precursors

To assess whether an increase in the uptake of phenyltin precursor increases the a.c. conductivity, samples were prepared on the shaker with 1 g, 4 g and 5 g of Ph_3SnCl and their conductivity measured. Table 5.2 shows the increase in uptake of precursor with the increase in weight of starting material used. The increased pillaring is confirmed by increased basal spacings determined by powder X-ray diffraction (see section 5.4.3). Figure 6.4 shows the increase in the a.c. conductivity as the amount of tin(IV) oxide incorporated into the clay increases. Ph_3SnCl was used in this experiment as the ^{119}Sn Mössbauer spectrum of laponite pillared with Ph_3SnCl shows only one peak, suggesting that all of the precursor is converted to pillars.

The a.c. conductivity of pillared clays prepared using the microwave heating method (see section 5.3.2) shows the same order of conductivity as that in figure 6.3. An increase in the conductivity of each sample is noted. This is consistent with an increased uptake of phenyltin compound in each case.

Therefore, in terms of the conductivity, the only difference in the two novel methods of preparation of tin(IV) oxide pillared clays is that the uptake of precursor using the microwave heating method is higher and this increase causes an increase in conductivity. However, it has been shown, by ^{119}Sn Mössbauer spectroscopy, that the increase in uptake of phenyltin precursor in the microwave experiment is not entirely due to an increase in pillaring (see section 5.4.1). Table 5.5 suggests that much of the extra organotin precursor taken up by the clay does not form pillars.

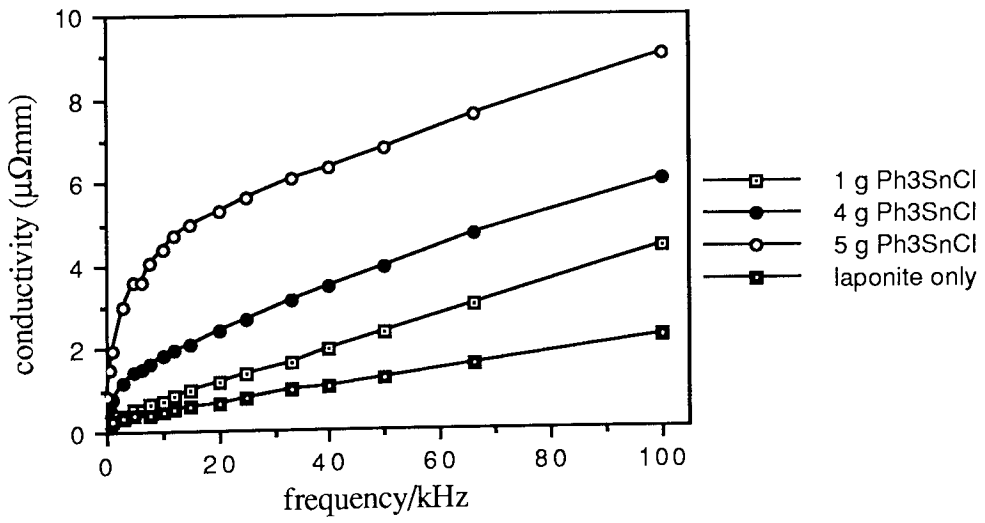

Figure 6.4 Conductivity of clays after treatment with different weights of Ph_3SnCl

The shape of the curve shown in figure 6.3 (and those in figure 6.4) suggests that the a.c. conductivity may contain a significant ionic component. This is confirmed by calculating the resistive and reactive components of the impedance of the most conductive sample (prepared from Ph_2SnCl_2 precursor), see table 6.5. It was found that the reactive component of the impedance is large compared to the purely resistive component. Therefore, it appears that the pillars are not behaving as semi-conductors within the interlayer.

Frequency/kHz	Resistance/Ω	Reactance/Ω	Impedance/Ω
100	353	1520	344
40	459	1772	444
20	536	1874	515
10	623	1984	594
5	730	2174	692

Table 6.5 Components of impedance for tin(IV) oxide pillared laponite RD

It can be seen from table 6.5 that as the resistive component of the impedance is much lower than the reactive component, then it may be concluded that the a.c. conductivity is dominated by the ionic component. It is probable that the interlayer sodium ions are the charge carriers. The pillars provide a permanent increase in the basal spacing of the clay, thereby increasing the mobility of the charge carrying ions. However, reaction with Ph_3SnCl produces the largest increase in basal spacing but not the largest increase in conductivity.

The greatest enhancement of the a.c. conductivity was found when Ph_2SnCl_2 is the precursor. The reason for this is not clear, however the amount of sodium released is greatest when Ph_2SnCl_2 is the precursor. This will lead to a greater number of hydrogen ions, which may act as potential charge carriers in the interlayer and this may be the cause of the increase in the a.c. conductivity.

Alternatively, the significant amount of residual Ph_2SnCl_2 in the clay observed by ^{119}Sn Mössbauer spectroscopy, could be a factor the increase of the a.c. conductivity. This residual Ph_2SnCl_2 can be considered to be intercalated into the clay interlayer and one simple implication from earlier work [43] was that the intercalation of large molecules can lead to an increase in conductivity. This observation is consistent with the increased uptake of precursor, without conversion to tin(IV) oxide pillars, during the microwave experiment (section 5.4.1).

It appears that when Ph_2SnCl_2 is used as a pillaring precursor, an optimum conductivity is achieved by a balance of the degree of efficiency of pillaring, intercalation of precursor and concentration and mobility of charge carrying ions.

The a.c. conductivity of thin films of tin(IV) oxide pillared clays show that the pillared clays show approximately the same degree of anisotropy as laponite RD (see section 4.8).

Samples of tin(IV) oxide pillared laponite have been produced [105] using the method previously reported [91]. The a.c. conductivity of these samples has been shown to be two orders of magnitude lower [105] than any pillared clay produced using the novel method of pillaring. The implication of this observation is that the exchange of the interlayer sodium ions during the pillaring process has removed the ionic charge carriers.

6.3.3 Temperature Dependence of Tin(IV) Oxide Pillared Laponite RD Conductivity

The temperature dependence of the a.c. conductivity the tin(IV) oxide pillared laponite exhibiting the greatest a.c. conductivity (produced using Ph_2SnCl_2 as the precursor) was investigated using the analysis adopted for previous samples, using a stainless-steel electrode system (section 4.6). The frequency independence of the a.c. conductivity, using this electrode system, confirmed that the a.c. conductivity of tin(IV) oxide pillared laponite RD is dominated by an ionic component.

Frequency/kHz	Activation Energy/kJmol^{-1} ± 2 kJmol^{-1}	
	High T	Low T
100	+24	+28
40	+24	+33
20	+24	+32
10	+22	+33
5	+23	+33

Table 6.6 Variation of activation energy with frequency for tin(IV) oxide pillared laponite RD

The a.c. conductivity increased with increasing temperature. As the dominant component of the a.c. conductivity in this case is ionic, the increase in conductivity can

be attributed to an increase in the number of charge carrying ions because of dissociation of ion pairs at the higher temperatures. The ion pair can be regarded as an ion held at the surface of the silicate sheet. When the temperature increases the ion is more mobile as the free volume available to the ions at elevated temperatures is higher. In common with previous samples this increase in a.c. conductivity was not linear, thus requiring an analysis of the results similar to that used previously (section 4.5.4).

The activation energies are presented in table 6.6. The activation energies determined for the high and low temperatures are largely frequency independent at both higher and lower temperatures. This is probably because of the high degree of ionic conductivity in this sample, as deduced from the components of the impedance (table 6.5).

The activation energies are lower at higher temperatures, as observed previously, reflecting the higher degree of conductivity at higher temperatures and the increased free volume available to charge carriers at elevated temperatures. The magnitude of the activation energy is similar to that of laponite RD, suggesting a similar mechanism of conductivity. In both cases the charge carriers are probably sodium ions.

At the lower temperatures the activation energy is higher than for laponite RD. This is probably because the free volume for the conducting ions is low, as a consequence of the increased occupancy of the interlayer. The pillars and the intercalated Ph_2SnCl_2 will reduce the free volume available within the interlayer at low temperatures and thereby reduce the conductivity.

6.3.4 Dependence of the Conductivity of Tin(IV) Oxide Pillared Laponite on Humidity

The dependence of conductivity on relative humidity of the most conducting sample of tin(IV) oxide pillared laponite (produced using Ph_2SnCl_2 as the precursor) was investigated using the method previously described (section 4.6). The results are presented in table 6.7. Several unsuccessful attempts were made to measure the a.c. conductivity of this sample at 93% relative humidity, but failed due to loss of sample integrity.

From an examination of the conductivities listed in table 6.7 is can be seen that the a.c. conductivity shows a strong dependence on humidity. This is more significant at relative humidities greater than 52%. Table 5.7 shows that the basal spacing of tin(IV) oxide pillared laponite is constant between 15% and 52%, but it is larger at 79%. The basal spacing at 93% relative humidity is the same as that obtained at 79%.

Relative Humidity	conductivity/ $\Omega^{-1}mm^{-1}$
32%	22×10^{-6}
52%	26×10^{-6}
79%	91×10^{-6}

Table 6.7 Conductivity of tin(IV) oxide pillared laponite RD at different humidities

Therefore, as the relative humidity increases there is only a small increase in basal spacing, but the amount of water in the interlayer and at crystal edges increases due to ion hydration. The increase in hydration of ions at the crystal edges will increase interparticle contact, which will give rise to an increase in the a.c. conductivity.

As the relative humidity increases both the interlayer ion and the silicate sheet become more hydrated. The effect of this will be to increase the distance of separation of the cation from the silicate layer. At high relative humidities the mobility of the ions will be greater as the ions will not be held as strongly at the silicate surface, compared to that at low relative humidity when there is little hydration of either the ion or the silicate layer. This increase in ion mobility leads to an increase in the ionic component of the a.c. conductivity.

The higher degree of incorporation of water in the interlayer region can lead to rise in the ionic conductivity, due to the high dielectric constant of water which promotes dissociation of ion pairs (see section 4.6.3).

6.4 Conclusions

The original aim of this work was to produce a smectite clay with an increased conductivity for use in the production of electrographic paper. Two methods of interlamellar modification have been successful in producing modified laponite samples with significantly increased a.c. conductivity.

Exchange of the interlamellar sodium ions for potassium ions produces a monoionic clay with a.c. conductivity enhanced by at least four times compared to laponite RD, over a wide range of a.c. frequencies. This increase in a.c. conductivity can be attributed to the appearance of an ionic component of a.c. conductivity. From the analysis of the components of the impedance in this system (silver-paste electrodes) it

appears that while the ionic component of the a.c. conductivity is dominant, the reactive component is significant in determining the overall magnitude of the a.c. conductivity.

A stainless-steel electrode system was used to measure the conductivity as the temperature was increased. When this electrode system is used the is a large increase in the magnitude of the a.c. conductivity and the dominant component of the a.c. conductivity is the ionic component. When the temperature is raised, the conductivity increases but the increase is not linear and this necessitates the defining of a high temperature and a low temperature value for the activation energy of a.c. conduction.

At the higher temperatures the activation energy is lower than at low temperatures and is almost frequency independent, reflecting the increased ionic conductivity of the sample. At the lower temperatures, as the frequency decreases, the activation energy increases. This is probably because the charge carriers are less mobile at low temperatures and low frequencies.

In contrast to the parent sodium exchanged laponite, the basal spacing of the potassium exchanged laponite remains constant over a wide range of relative humidities. This is a reflection of the lower hydration of potassium ions. This humidity independence of the basal spacing is accompanied by a constant a.c. conductivity over the same range of humidities.

As the hydration of the potassium ion in the interlayer region of laponite is lower than that of the sodium ion the potassium exchanged laponite will have different swelling properties. Potassium exchanged laponite does not form a gel in aqueous solution and forms an unstable aqueous suspension unless the particle size of the clay is below 100 μm and the suspension is stirred for 8 hours or subjected to ultrasound.

It has been shown in Chapter Five above, that the intercalation of three phenyltin compounds, namely Ph_2SnCl_2, Ph_3SnCl and $(Ph_3Sn)_2O$, can lead to the formation of tin(IV) oxide pillared laponite. This occurs without the total sacrifice of the interlayer sodium ions. It has also been shown that this pillaring can be achieved using two methods, one at room temperature using a conventional flask shaker and the second using a microwave heating method.

All of the tin(IV) oxide pillared laponite samples prepared show an increased a.c. conductivity compared to laponite RD. The a.c. conductivity of the samples prepared using the microwave heating method is higher than the corresponding samples prepared

using the flask shaker. This is probably because the uptake of phenyltin precursor during the pillaring reaction is higher. However, ^{119}Sn Mössbauer spectroscopy shows that not all of the extra phenyltin precursor sorbed by the clay in the microwave heating experiment is converted to tin(IV) oxide pillars.

The a.c. conductivity of the tin(IV) oxide pillared laponite samples is dependent on the precursor used in the pillaring experiment. When Ph_3SnCl is used, complete conversion of the phenyltin precursor to tin(IV) oxide pillars is achieved, and this sample also shows the largest increase in basal spacing. However, the largest increase in conductivity, of over an order of magnitude, is observed when Ph_2SnCl_2 is used as the pillaring precursor. In this case, the conversion of Ph_2SnCl_2 to tin(IV) oxide pillars is incomplete and a significant amount of Ph_2SnCl_2 is observed as intercalated into the interlayer, by ^{119}Sn Mössbauer spectroscopy.

Analysis of the components of the impedance for the tin(IV) oxide pillared laponite samples indicates that an ionic component dominates the a.c. conductivity when silver-paste electrodes are used. This observation is supported by analysis of the shape of the a.c. conductivity against frequency plot, which shows a degree of frequency independence for the a.c. conductivity (for $f > 10$ kHz).

Stainless-steel electrodes were used to investigate the temperature dependence of the a.c. conductivity of tin(IV) oxide pillared laponite prepared from Ph_2SnCl_2. The a.c. conductivity is again dominated by an ionic component. The a.c. conductivity increased with temperature, suggesting that as the temperature increased more ions were released, as the ion pair - free ions equilibrium moved towards free ions at higher temperatures. As previously, two activation energy calculations were made due to the curvature of the plot of $\log_e \sigma$ against $1/T$ plot.

Exposing the tin(IV) pillared laponite prepared from Ph_2SnCl_2 to increasing relative humidity atmospheres produced only a small increase in the basal spacing at high relative humidity. Up to 52% relative humidity the basal spacing remains constant. It increases slightly at 79% and remains at this higher value up to 93% relative humidity. This is accompanied by a small increase in the a.c. conductivity when the relative humidity is raised from 32% to 52% and a much larger increase in the a.c. conductivity when the relative humidity was raised from 52% to 79%, as the silicate surface and the interlayer sodium ions become more hydrated and the ions become more separated from the silicate surface and become more mobile.

6.5 Further Work

The hydration of the potassium exchanged laponite sample could be increased by the back-exchange of a controlled amount of an ion that has a higher hydration number, for example, sodium (or lithium). This may occur without significantly reducing the conductivity of the sample.

The a.c. conductivity of the novel tin(IV) oxide pillared laponite is dominated by an ionic component. It appears that the potentially semi-conducting pillars are not contributing to the overall a.c. conductivity of the clay, therefore the conductivity of the clay could still be increased by increasing the conductivity of the pillars. The pillaring material, tin(IV) oxide, is known to be a semiconductor [87], doping tin(IV) oxide with antimony is known to increase its conductivity greatly [113]. Antimony doped tin(IV) oxide pillars could be prepared by adding a small amount of organoantimony compound to the pillaring reaction or using mixed tin antimony compounds as the organic precursor. Also, it is known that at elevated temperature antimony can diffuse into the tin(IV) oxide lattice [114], therefore if the pillaring reaction was carried out in the microwave oven a more conducting pillared system may be achieved.

The novel formation of tin(IV) oxide pillars depends on the electrophilic cleavage of the aryltin bond by sites of Brønsted acidity from within the clay. Therefore, the formation of clays pillared in the same manner, with different metal oxides, could be possible. This would require organometallic precursor compounds that are susceptible to a similar electrophilic attack.

The increased conductivity achieved when a significant quantity of Ph_2SnCl_2 is intercalated during the pillaring reaction suggests that the intercalation of neutral compounds into the interlayer of laponite may increase the a.c. conductivity of the clay. If intercalation could be achieved independently of the pillaring process the intercalated species could increase the basal spacing of the clay and increase the mobility of the interlayer sodium ions, increasing the a.c. conductivity. Care must be taken to select a compound that can be observed by a spectroscopic technique, to ensure that no reaction has occurred on intercalation.

REFERENCES

1) R.E. Grim. Clay Mineralogy. McGraw-Hill. New York, 1953.

2) R.W. Grimshaw. The Chemistry and Physics of Clay Minerals and Allied Ceramic Minerals. 4th Edition. Ernst Benn, 1971.

3) J. Konta. The present state and development trends of clay science. Developments in Sedimentology, **35**, International Clay Conference 1981. Eds. H. van Olphen and F. Veniale. Elsevier, Amsterdam, 1982, 1 - 14.

4) B.K.G. Theng. The Chemistry of Clay-Organic Reactions. Adam Hilger, London, 1974.

5) I. E. Odom. Smectite clay minerals: properties and uses. *Phil. Trans. R. Soc. Lond.* 1984, A **311**, 391-409.

6) G.W. Brindley and G. Brown. Crystal Structures of Clay Minerals and their X-Ray Identification. Mineralogical Society, London, 1984.

7) G. Brown. Crystal Structures of Clay Minerals and Related Phyllosilicates. *Phil. Trans. R. Soc. Lond.*, 1984, A **311**, 221-240.

8) C. E. Weaver and L. D. Pollard. The Chemistry of Clay Minerals. Elsevier, Amsterdam, 1973.

9) H. van Damme, P. Levitz, J. J. Fripiat, J. F. Alcover, L. Gatineau, and F. Bergaya. Clay Minerals: A Molecular Approach to Their (Fractal) Microstructure. Physics of Finely Divided Matter. Proceedings of the Winter School, France, 1985. Eds. N. Boccara and M. Daoud. Springer Verlag, Berlin, 1985, 24-30.

10) J. Fripiat, J. Cases, M. Francois and M. Letellier. Thermodynamic and Microdynamic Behaviour of Water in Clay Suspensions and Gels. *J. Colloid Interf. Sci.*, 1982, **89**, 378-400.

11) D. J. Cebula and R. K. Thomas. Small Angle Neutron Scattering from Dilute Aqueous Dispersions of Clay. *J. Chem. Soc. Faraday I.* 1980, **76**, 314-321.

12) C. H. Pons, F. Rousseaux and D. Tchoubar. Utilisation du Rayonnement Synchroton en Diffusion aux Petits Angles pour L'Etude du Gonflement des Smectites. *Clay Minerals,* 1981, **16**, 23-42.

13) H. van Olphen. An Introduction to Clay Colloid Chemistry. Interscience, New York, 1963.

14) C. H. Pons, D. Tessier, H. B.Rahiem and D. Tchoubar. Electron Microscopy Study of Na Smectite Fabric. Developments in Sedimentology, **35**, International Clay Conference 1981. Eds. H. van Olphen and F. Veniale. Elsevier, Amsterdam, 1982, 177 - 185.

15) J. J. Fripiat. Internal Surface of Clays and Constrained Chemical Reactions. *Clays and Clay Minerals*. 1986, **34,** 501-506.

16) A. J. Jacobson and M. S. Whittington. Intercalation Chemistry. Academic Press Inc., London, 1982.

17) G. Lagaly. Clay-Organic Interactions. *Phil. Trans. R. Soc. Lond.* 1984, A **311**, 315-332.

18) M. M. Mortland. Clay-Organic Complexes and Interactions. *Adv. Agron.* 1970, **23**, 75-117.

19) P. Monsef-Mirzai and W. R.McWhinnie. Transition Metal Ion (Cu^{2+}, Mn^{2+}, VO^{2+}) - Montmorillonite Interactions. *Inorg. Chim. Acta,* 1983, **73**, 41-44.

20) N. Davison and W. R. McWhinnie. The Formation of Cobalt and Nickel Complexes on Clay Surfaces. *Polyhedron*, 1990, **9**, 2273-2283.

21) M. I. Knudson and J. L. McAtee. The Effect of Cationic Exchange of Tris (Ethylenediamine)Cobalt(III) for Sodium on Nitrogen Sorbtion by Montmorillonite. *Clays and Clay Minerals*, 1973, **21**, 19-26.

22) V. E. Berkhieser and M. M. Mortland. Hectorite Complexes with Cu(II) and Fe(II) - 1,10-Phenanthroline Chelates. *Clays and Clay Minerals*, 1977, **25**, 105-112.

23) P. Peigneur, A. Maes and A. Cremers. Ion Exchange of Poly-amine Complexes of Some Transition Metals in Montmorillonite. Developments in Sedimentology, **27**, International Clay Conference 1978. Eds. M. M. Mortland and V. C. Farmer. Elsevier, Amsterdam, 1979, 207-216.

24) M. F. Traynor, M. M. Mortland and T. J. Pinnavaia. Ion Exchange and Intersalation Reactions of Hectorite with Tris(Bipyridyl) Metal Complexes. *Clays and Clay Minerals*, 1978, **26**, 318-326.

25) N. Davison and W. R. McWhinnie. Clay Supported Redox Catalysts. *Inorg. Chim. Acta*, 1987, **131**, 9-10.

26) W. Jones. The Structure and Properties of Pillared Clays. *Catalysis Today*, 1988, **2**, 357-367.

27) R. M. Barrer and D. M. MacLeod. Activation of Montmorillonite by Ion Exchange and Sorption Complexes of Tetra-Alkyl Ammonium Montmorillonites. *Trans. Faraday Soc.*, 1955, **51**, 1290-1300.

28) R. M. Barrer and S. S. Reay. Sorption and Intercalation by Methyl-Ammonium Montmorillonites. *Trans. Faraday Soc.*, 1957, **53**, 1253-1261.

29) R. H. Leoppert, M. M. Mortland and T. J. Pinnavaia. Synthesis and Properties of Heat-Stable Expanded Smectite and Vermiculite. *Clays and Clay Minerals*, 1979, **27**, 201-208.

30) S. L. Jones. The Preparation and Solution Chemistry of Al(III) and Zr(IV) Pillaring Species. *Catalysis Today*, 1988, **2**, 209-217.

31) S. Yamanaka and G. W. Brindley. High Surface Area Solids Obtained by Reaction of Montmorillonite with Zirconyl Chloride. *Clays and Clay Minerals*, 1979, **27**, 119-124.

32) J. J. Fripiat. High Resolution Solid State N.M.R. Study of Pillared Clays. *Catalysis Today*, 1988, **2**, 281-295.

33) G. J. J. Bartley. Zirconium Pillared Clays. *Catalysis Today*, 1988, **2**, 233-241.

34) M. S. Tzou and T. J. Pinnavaia. Chromia Pillared Clays. *Catalysis Today*, 1988, **2**, 243-259.

35) K. Bornholdt, J. M. Corker, J. Evans and J. M. Rummey. EXAFS Studies of the Formation of Chromia Pillared Clay Catalysts. *Inorg. Chem.*, 1991, **30**, 1-2.

36) S. Yamanaka and M. Hattori. Iron Oxide Pillared Clay. *Catalysis Today*, 1988, **2**, 261-270.

37) S. P. Christano, J. Wang and T. J. Pinnavaia. Intercalation of Niobium and Tantalum $M_6Cl_{12}^{n+}$ Cluster Cations in Montmorillonite: A New Route to Pillared Clays. *Inorg. Chem.*, 1985, **24**, 1222-1227.

38) W. B. Jepson. Kaolins: Their Properties and Uses. *Phil. Trans. R. Soc. Lond.*, 1984, A **311**, 411-432.

39) Laporte Industries Ltd., Technical Document L51. Laponite. Chemistry, Properties and Applications.

40) E. Anczurowski, J. Oliver and R. H. Marchessault. New Papers For New Printers. *Chemtech*, May 1986, 304-310.

41) K. W. Barr and V. D. Royston. Aqueous Conductivizing Composition for Conductivizing Sheet Material. United States Patent 4,739,003. 1988, and European Patent Appliction 86306547.0, 1986.

42) Versatec 8500 Series Plotter Operator Guide. Versatec. A Xerox Company, Santa Clara, California. 1989.

43) A.-P. S. Mandair, W. R. McWhinnie and P. Monsef-Mirzai. Charge Transfer Interactions in Smectite Clays. *Inorg. Chim. Acta*, 1987, **134**, 99-103.

44) H. van Damme, F. Obrecht and M. Letellier. Intercalation of Tetrathiafulvalene in Smectite Clays: Evidence for Charge Transfer Interactions. *Nouv. J. Chim.*, 1984, **8**, 681- 683.

45) F. E. M. O'Brien. The Control of Humidity by Saturated Salt Solutions. *J. Sci. Instr.*, 1948, **25**, 73-76.

46) A. R. Blythe, Electrical Properties of Polymers. Cambridge University Press. 1980.

47) Genrad RLC 1689 Precision Digibridge Manual. Genrad Corparation, Boston, U.S.A., 1983.

48) W. E. Rudzinski and A. J. Bard. Clay Modified Electrodes. Part VI. Aluminium and Silicon Pillared Clay-Modified Electrodes. *J. Electroanal. Chem.*, 1986, **199**, 323-340.

49) C. Sui, J. F. Rusling, Z. Wang, W.S. Willis, A. M. Winiecki and S. L. Suib. Electrocatalytic Reactions in Organised Assemblies. 6. Electrochemical and Spectroscopic Studies of Catalytic Clay/Micelle Electrodes. *Langmuir*, 1989, **5**, 650-660.

50) W. R. McWhinnie, G. C. Kulasingam and J. C. Draper. Complexes of Tri-(2-pyridyl)amine. Part 1. Complexes with Cobalt(II), Nickel(II) and Copper(II) perchlorates. *J. Chem. Soc. (A)*, 1966, 1199-1203.

51) P. F. B. Barnard, A. T. Chamberlain, G. C. Kulasingam, W. R. McWhinnie and R. C. Dosser. Infrared, Raman, and Magnetic Evidence for a $^4T \leftrightarrow {}^2E$ Equilibrium in Bis[tri-(2-pydridyl)amine]cobalt(II) Perchlorate. *J. Chem. Soc. Chem. Commun.*, 1970, 520-521.

52) E. S. Kucharski, W. R. McWhinnie and A. H. White. Crystal Structure of Bis(tri-2-pyridylamine)cobalt(II) Diperchlorate. *Aust. J. Chem.*, 1978, **31**, 2647-2650.

53) E. S. Kucharski, W. R. McWhinnie and A. H. White. Crystal Structure of Bis(tri-2-pyridylamine)iron(II) Diperchlorate. *Aust. J. Chem.*, 1978, **31**, 53-56.

54) J. C. Lancaster and W.R. McWhinnie. The Chemistry of the Isomeric Complexes Obtained from the Reaction of Copper(II) Perchlorate with Substituted Tri-(2-pyridyl)amines. *Inorg. Chim. Acta.*. 1971, **5**, 515-519.

55) P. K. Ghosh and A. J. Bard. Clay Modified Electrodes. *J. Am. Chem. Soc.*, 1983, **105**, 5691-5693.

56) J. Heinze. Cyclic Voltammetry — "Eletrochemical Spectroscopy". *Angew. Chem. Int. Ed. Engl.*, 1984, **23**, 831-918.

57) P. K. Ghosh, A. W.-H. Mau and A. J. Bard. Clay Modified Electrodes. Part II. Electrocatalysis at bis(2,2'-bipyridyl)(4,4'-dicarboxy-2,2'-bipyridyl)Ru(II)-Dispersed Ruthenium Oxide-Hectroite Layers. *J. Electroanal. Chem.*, 1984, **169**, 315-317.

58) D. Ege, P. K. Ghosh, J. R. White, J.-F. Equey and A. J. Bard. Clay Modified Electrodes. Part III. Electrochemical and Electron Spin Resonance Studies of Montmorillonite Layers. *J. Am. Chem. Soc.*, 1985, **107**, 5644-5652.

59) J. R. White and A. J. Bard. Clay Modified Electrodes. Part IV. The Electrochemistry and Electron Spin Resonance Spin Resonance of Methyl Viologen Incorparated into Montmorillonite. *J. Electroanal. Chem.*, 1986, **197**, 233-244.

60) K. Itaya and A. J. Bard. Clay Modified Electrodes. Part V. Preparation and Electrochemical Characterisation of Pillared Clay-Modified Electrodes and Membranes. *J. Phys. Chem.*, 1985, **89**, 5565-5568.

61) R. D. King, D. C. Nocera and T. J. Pininavaia. The Nature of Electroactive sites in Clay Modified Electrodes. *J. Electroanal. Chem.*, 1987, **236**, 43-53.

62) J. P. Wibaut and G. L. C. La Bastide. Tri-(2-Pyridyl)amine. *Res. Trav. Chim.*, 1933, **52**, 493-498.

63) J. C. Lancaster and W. R. McWhinnie. The Synthesis and Spectra of Some Mono-substituted Tri-(2-pyridyl)amines. *J. Chem. Soc. (C)*, 1970, 2435-2436.

64) C. J. McNerlin. Cobalt and Iron Complexes and their Intercalation With the Smectite Clay Laponite. Final Year B.Sc. Project Report. Aston University, Birmingham. 1990.

65) D. F. B. Barnard, J. C. Lancaster, M. E. Fernandopullé and W. R. McWhinnie. The Chemistry of 2-Pyridylamine Complexes of Cobalt(II) and Cobalt(III). *J. Chem. Soc., Dalton Trans.*, 1973, 2172-2176.

66) W. R. McWhinnie, R. C. Poller and M. Thevarasa. Vibrational, Electronic and Mössbauer Spectra of Some Complexes of Iron(II) with Tri- and Di-2-Pyridylamine. *J. Chem. Soc. (A).*, 1967, 1671-1674.

67) R. N. Gedye, F. E. Smith and K. C. Westaway. The Rapid Synthesis of Organic Compounds in Microwave Ovens. *Can. J. Chem.*, 1988, **66**, 17-26.

68) M. Ali, S. P. Bond, S. A. Mbogo, W. R. McWhinnie and P. M. Watts. Use of a Domestic Microwave Oven in Orgaonmetallic Chemistry. *J. Organometal. Chem.*, 1989, **371**, 11-13.

69) D. R. Baghurst and D. M. P. Mingos. Application of Microwave Heating Techniques for the Synthesis of Solid State Inorganic Compounds. *J. Chem. Soc., Chem. Commun.*, 1988, 829-830.

70) S. P. Bond, A. Gelder, J. Homer, W. R. McWhinnie and M. C. Perry. ^{6}Li m.a.s.n.m.r.: A Powerful Probe for the Study of Lithium Containing Materials. *J. Mater. Chem.*, 1991, **1**, 327-330.

71) A. M. Posner and J. P Quirk. The Adsorption of Water from Concentrated Electrolyte Solutions by Montmorillonite and Illite. *Proc. R. Soc. Lond.*, 1964, A **278**, 35-56.

72) F. H. Burstall and R. S. Nyholm. Studies in Co-ordination Chemistry Part XIII. Magnetic Moments and Bond Types of Transition Metal Complexes. *J. Chem. Soc.*, 1952, 3570-3579.

73) G. C. Kulasingam, Ph.D. Thesis, University of London, 1967.

74) A. Fitch. Clay Modified Electrodes: A Review. *Clays and Clay Minerals.* 1990, **38**, 391-400.

75) A. R. West. Solid State Chemistry and its Applications. John Wiley and Sons. 1984.

76) Laporte Industries Ltd. technical document 64. Laponite. Chemistry, properties and applications.

77) P. Debye and H. Falkenhagen. Dispersion von Leitfähigkeit und Dielektrizitätskonstante bei Starken Elektrolyten. *Physikal. Z.*, 1928, **29**, 121-132.

78) H. Sack. Experimentelles zur Dispersion der Leitfähigkeit. *Physik. Z.*, 1928, **29**, 627-629.

79) S. Glasstone and D. Lewis. Elements of Physical Chemistry. 2nd Edition. MacMillan, London, 1960.

80) The Handbook of Chemistry and Physics. 69th Edition. Chemical Rubber Company Press Inc., Florida, U.S.A., 1988.

81) E. H. Putley. The Hall Effect and Related Phenomena. Butterworths, London. 1960.

82) R. B. Adler, A. C. Smith and R. L. Longini. Introduction to Semiconductor Physics. John Wiley and Sons, New York. 1964.

83) H. Teichmann. Semiconductors. Butterworths, London. 1964.

84) E. E. Kohnke. Electrical and Optical Properties of Natural Stannic Oxide Crystals. *J. Phys. Chem.* Solids. 1962, **23**, 1557-1562.

85) W. Ehrenberg. Electric Conduction in Semiconductors and Metals. Clarendon Press, London. 1958.

86) G. Wagoner. Spin resonance of Charge Carriers in Graphite. *Phys. Rev.*. 1960, **118**, 647-653.

87) R. T. Shuey. Semiconducting Ore Minerals. Developments in Economic Geology, **4**. Elsevier Scientific Publishing Company, Amsterdam. 1975.

88) R. C. Poller. The Chemistry of Organotin Compounds. Logos Press Ltd., London, 1970.

89) G. Wilkinson and F. G. A. Stone. Comprehensive Organometallic Chemistry. Pergamon Press, Oxford, 1982, Volume 2, Chapter 11.

90) K. C. Molloy, C. Breen and K. Quill. Organometallic cation-exchanged phyllosilicates: A high spacing intercalate formed from *N*-methyl-(3-triphenylstannyl)pyridinium exchanged montmorillonite. *App. Organomet. Chem.*. 1987, **1**, 21-27.

91) D. Petridis, T. Bakes, A. Simopoulos and N. H. J. Gangas. Pillaring of Montmorillonite by Organotin Cationic Complexes. *Inorg. Chem.*, 1989, **28**, 2439-2443.

92) A. Simopoulos, D. Petridis, A. Kostikas and N. H. J. Gangas. Intercalation of Dimethyltin (IV) Cationic Complexes in Montmorillonite. *Hyperfine Interactions*, 1988, **41**, 843-846.

93) R. K. Ingham, S. D. Rosenberg and H. Gilman. Organotin Compounds. *Chem. Rev.*, 1960, **60**, 459-539.

94) A. I. Vogel. A textbook of Practical Organic Chemistry. 3rd Edition. Longman, London. 167-168.

95) K. Chatakondu, M. L. H. Green, D. M. P. Mingos and S. M. Reynolds. Application of Microwave Dielectric Loss Heating Effects for the Rapid and Convenient Synthesis of Intercalation Compounds. *J. Chem. Soc., Chem. Commun.*, 1989, 1515-1517.

96) M. A. M. Lawrence. Formation of Tin(IV) Oxide Pillared Laponite. Final Year B.Sc. Project Report, Aston University, Birmingham. 1991.

97) P. Monsef-Mirzia and W. R. McWhinnie. Spectroscopic Studies of Metal Ions Sorbed onto Kaolinite. *Inorg. Chim. Acta.*, 1982, **58**, 143-148.

98) R. H. Herber, H. A. Stöckler and W. T. Reichle. Systematics of Mössbauer Isomer Shifts of Organo-Tin Compounds. *J. Chem. Phys.*, 1965, **42**, 2447-2452.

99) H. A. Stöckler and H. Sano. Nuclear Monopole and Quadrapole Hyperfine Interactions in Organotin Halides and Organoperfluoro Compounds. *Trans. Faraday Soc.*, 1968, **64**, 577-581.

100) N. N. Greenwood and T. C. Gibb. Mössbauer Spectroscopy. Chapman and Hall, London. 1971. p.374.

101) F. J. Berry and A. G. Maddock. A Tin-119 Mössbauer Investigation of the Thermal Decomposition of Tin(IV) Hydroxides. *Radiochim. Acta*, 1977, **24**. 32-33.

102) C. Eaborn and J. A. Waters. Aromatic Reactivity. Part XIV. Cleavage of Aryltincyclohexyl- and Aryltintrimethyl-stannates by Aqueous-ethanolic Perchloric Acid. *J. Chem. Soc.*, 1961, 542-547.

103) W. F. Bradley. Molecular Associations between Montmorillonite and Some Polyfunctional Organic Liquids. *J. Am. Chem. Soc.*, 1945, **67**, 975-981.

104) H. E. Donner and M. M. Mortland. Benzene Complexes with Copper(II) Montmorillonite. *Science*, 1969, **166**, 1406-1407.

105) R. C. Ashcroft. Organometallic Precursors for Pillared Clay Synthesis. Qualifying Report, Aston University, Birmingham. 1991.

106) H. A. Benesi. Acidity of Catalyst Surfaces II. Amine Titration using Hammett Indicators. *J. Phys. Chem.*, 1957, **61**, 970-973.

107) D. H. Soloman, J. D. Swift and A. J. Murphy. The Acidity of Clay Minerals in Polmerizations and Related Reactions. *J. Macromol. Sci. Chem.*, 1971, **A5**, 587-601.

108) M. M. Mortland and K. V. Raman. Surface Acidity of Smectites in Relation to Hydration, Exchangeable Cation and Structure. *Clays and Clay Minerals*. 1968, **16**, 393-398.

109) M. M. Mortland. Protonation of Compounds on Clay Mineral Surfaces. *9th Int. Congr. Soil Sci.* Vol I. 691-699.

110) Keith Webb, James River Graphics. Personal communication.

111) Mellor's Comprehensive Treates on Inorganic and Theoretical Chemistry. Volume II, Supplement II. Longmans, London. 1961.

112) J. C. Bailer, H. J. Emeléus, R. Nyholm and A. F. Trotman-Dickenson. Comprehensive Inorganic Chemistry, Volume 1. Permagon Press, Oxford. 1973.

113) P. A. Cox. Electronic Structure and Chemistry of Solids. Oxford University Press, Oxford. 1987.

114) G. J. Long. Mössbauer Spectroscopy Applied to Inorganic Chemistry. Volume 1. Plenum Press, New York, 1984.

Appendix One

Chapter Four Raw Data

laponite B	13 mm disc	1.18 mm thickness
silver paste	52% RH	
frequency/kHz	capacitance/nF	resistance/Ω
100	2.901	1556
66	3.109	2672
50	3.235	3817
40	3.323	4934
33	3.392	6002
25	3.495	8258
20	3.563	10170
15	3.687	13020
12	3.779	15530
10	3.859	21620
7.5	3.999	21620
6	4.120	24940
5	4.230	27770
3	4.562	38080
1	5.322	79010
0.1	9.059	197000
0.012	18.05	349600

laponite RD	13 mm disc	1.09 mm thickness
silver paste	52% RH	
frequency/kHz	capacitance/nF	resistance/Ω
100	3.109	1509
66	3.337	2266
50	3.500	2900
40	3.636	3413
33	3.755	3831
25	3.928	4964
20	4.071	5830
15	4.277	7026
12	4.454	8050
10	4.615	8949
7.5	4.904	10490
6	5.168	11720
5	5.433	12640
3	6.346	15260
1	9.163	22950
0.1	19.81	77540
0.012	50.87	131000

Figure 4.4 raw data

laponite RDS	13 mm disc	1.03 mm thickness
silver paste	52% RH	
frequency/kHz	capacitance/nF	resistance/Ω
100	2.915	2946
66	3.010	4830
50	3.083	6386
40	3.132	7837
33	3.177	9017
25	3.171	17580
20	3.214	21960
15	3.272	28760
12	3.320	35000
10	3.362	40760
7.5	3.432	51350
6	3.492	60970
5	3.544	69700
3	3.705	99900
1	4.033	222200
0.1	5.369	719800
0.012	7.016	1235000

laponite S	13 mm disc	0.87 mm thickness
silver paste	52% RH	
frequency/kHz	capacitance/nF	resistance/Ω
100	2.635	2615
66	2.754	4469
50	2.832	6359
40	2.891	8221
33	2.932	10190
25	3.001	13760
20	3.056	17100
15	3.127	22210
12	3.186	26800
10	3.236	30970
7.5	3.319	38350
6	3.390	44760
5	3.452	50460
3	3.647	69370
1	4.187	135400
0.1	6.497	455300
0.012	10.50	894500

Figure 4.4 raw data (continued)

laponite RD	13 mm disc	1.29 mm thickness
silver paste	52% RH	
frequency/kHz	capacitance/nF	resistance/Ω
100	1.774	4273
66	1.886	6411
50	1.966	8266
40	2.030	9978
33	2.080	11580
25	2.170	14520
20	2.240	17190
15	2.340	21180
12	2.420	24750
10	2.490	27860
7.5	2.610	33470
5	3.800	42600
3	3.090	63910
1	3.970	134200
0.1	8.750	505900
0.012	22.90	1403000

Figure 4.5 raw data

laponite RD	17 mm disc	1.30 mm thickness
stainless steel	52% RH	3 tonnes
frequency/kHz	capacitance/nF	resistance/Ω
100	0.0007	35.6
66	0.0016	35.7
50	0.0029	35.8
40	0.0043	35.8
33	0.0060	35.9
25	0.0099	36.0
20	0.0146	36.2
15	0.0146	36.2
12	0.0356	36.6
10	0.0489	37.0
7.5	0.0800	37.4
5	0.1577	38.6
3	0.3541	41.2
1	1.5560	54.9
0.1	7.6928	391.4
0.012	19.514	1406.0

laponite RD	17 mm disc	1.30 mm thickness
stainless steel	52% RH	5 tonnes
frequency/kHz	capacitance/nF	resistance/Ω
100	0.0012	31.0
66	0.0026	31.1
50	0.0043	31.1
40	0.0043	31.2
33	0.0086	31.3
25	0.0140	31.3
20	0.0205	31.5
15	0.0331	31.8
12	0.0486	32.0
10	0.0660	32.3
7.5	0.1060	32.9
5	0.2043	34.3
3	0.5404	37.0
1	1.8715	53.4
0.1	8.4585	419.7
0.012	21.555	1418.0

Figure 4.9 raw data

laponite RD	17 mm disc	1.30 mm thickness
stainless steel	52% RH	7 tonnes
frequency/kHz	capacitance/nF	resistance/Ω
100	0.0042	20.3
66	0.0074	20.3
50	0.0111	20.5
40	0.0153	20.6
33	0.0199	20.7
25	0.0307	20.8
20	0.0431	20.9
15	0.0669	21.2
12	0.0939	21.6
10	0.1245	21.8
7.5	0.1944	22.3
5	0.3543	23.6
3	0.7354	25.9
1	2.7608	37.5
0.1	11.592	250.5
0.012	28.191	980.0

Figure 4.9 raw data (continued)

laponite RD	17 mm disc	1.79 mm thickness
stainless steel	52% RH	min pressure
frequency/kHz	capacitance/nF	resistance/Ω
100	0.0048	28.9
66	0.0089	29.8
50	0.0137	29.8
40	0.0191	30.3
33	0.0250	30.7
25	0.0382	31.5
20	0.0528	32.3
15	0.0792	33.6
12	0.1075	34.8
10	0.1370	36.0
7.5	0.1979	38.2
5	0.3222	42.5
3	0.5626	49.8
1	1.5529	77.4
0.1	5.4273	438.5
0.012	16.358	1437.0

laponite RD	13 mm disc	0.77 mm thickness
aluminium	52% RH	
frequency/kHz	capacitance/nF	resistance/Ω
100	0.0021	51.3
66	0.0046	52.9
50	0.0077	52.9
40	0.0117	53.5
33	0.0162	54.2
25	0.0270	55.8
20	0.0396	57.7
15	0.0637	61.4
12	0.0898	65.6
10	0.1166	70.6
7.5	0.1708	81.5
5	0.2672	109.6
3	0.3944	183.3
1	0.5917	748.5
0.1	0.7848	10910.0
0.012	1.0355	56560.0

Figure 4.10 raw data

laponite RD	17 mm disc	2.02 mm thickness
stainless-steel	19°C 52% RH	min pressure
frequency/kHz	capacitance/nF	resistance/Ω
100	0.0009	31.1
66	0.0021	31.2
50	0.0035	31.3
40	0.0052	31.4
33	0.0072	31.5
25	0.0118	31.7
20	0.0172	31.9
15	0.0281	32.2
12	0.0411	32.5
10	0.0558	32.7
7.5	0.0905	33.3
5	0.1774	34.4
3	0.4021	36.7
1	1.8024	49.9
0.1	8.8421	335.7
0.012	20.122	1647.0

laponite RD	17 mm disc	2.02 mm thickness
stainless-steel	23°C 52% RH	min pressure
frequency/kHz	capacitance/nF	resistance/Ω
100	0.0011	27.3
66	0.0025	27.3
50	0.0043	27.4
40	0.0064	27.5
33	0.0088	27.5
25	0.0145	27.7
20	0.0214	27.8
15	0.0352	28.1
12	0.0516	28.3
10	0.0706	28.5
7.5	0.1151	29.0
5	0.2267	30.1
3	0.5130	32.5
1	2.1929	47.0
0.1	9.0345	361.5
0.012	20.161	1701.0

Figure 4.11 Raw data

laponite RD	17 mm disc	2.02 mm thickness
stainless-steel	28°C 52% RH	min pressure
frequency/kHz	capacitance/nF	resistance/Ω
100	0.0014	22.7
66	0.0033	22.8
50	0.0057	22.9
40	0.0085	23.0
33	0.0117	23.1
25	0.0193	23.2
20	0.0284	23.4
15	0.0466	23.6
12	0.0683	23.8
10	0.0931	24.1
7.5	0.1514	24.6
5	0.2958	25.7
3	0.6579	28.1
1	2.6355	42.8
0.1	9.7026	347.5
0.012	21.487	1610.0

laponite RD	17 mm disc	2.02 mm thickness
stainless-steel	33°C 52% RH	min pressure
frequency/kHz	capacitance/nF	resistance/Ω
100	0.0016	19.2
66	0.0039	19.3
50	0.0069	19.4
40	0.0104	19.5
33	0.0144	19.5
25	0.0240	19.7
20	0.0355	19.8
15	0.0586	20.0
12	0.0861	20.2
10	0.1177	20.4
7.5	0.1917	20.9
5	0.3742	21.9
3	0.8244	24.3
1	3.1440	38.4
0.1	10.644	328.4
0.012	23.247	1532.0

Figure 4.11 Raw data (continued)

laponite RD	17 mm disc	2.02 mm thickness
stainless-steel	38°C 52% RH	min pressure
frequency/kHz	capacitance/nF	resistance/Ω
100	0.0019	16.3
66	0.0047	16.4
50	0.0084	16.5
40	0.0127	16.5
33	0.0177	16.6
25	0.0297	16.7
20	0.0442	16.8
15	0.0732	17.0
12	0.1079	17.2
10	0.1478	17.4
7.5	0.2410	17.8
5	0.4688	18.8
3	1.0198	21.0
1	3.7068	34.4
0.1	11.679	309.7
0.012	25.173	1455.0

laponite RD	17 mm disc	2.02 mm thickness
stainless-steel	23°C 52% RH	min pressure
frequency/kHz	capacitance/nF	resistance/Ω
100	0.0020	14.8
66	0.0052	14.9
50	0.0094	15.0
40	0.0143	15.0
33	0.0200	15.1
25	0.0336	15.2
20	0.0500	15.3
15	0.0830	15.5
12	0.1225	15.7
10	0.1679	15.8
7.5	0.2743	16.2
5	0.5306	17.2
3	1.1463	19.4
1	4.0616	32.5
0.1	16.818	167.9
0.012	25.851	1430.0

Figure 4.11 Raw data (continued)

laponite RD	17 mm disc	2.02 mm thickness
stainless-steel	45°C 52% RH	min pressure
frequency/kHz	capacitance/nF	resistance/Ω
100	0.0022	13.6
66	0.0059	13.7
50	0.0106	13.7
40	0.0162	13.8
33	0.0226	13.9
25	0.0381	14.0
20	0.0566	14.1
15	0.0937	14.3
12	0.1380	14.5
10	0.1883	14.7
7.5	0.3055	15.1
5	0.5890	16.1
3	1.2587	18.3
1	4.3486	31.1
0.1	17.487	163.6
0.012	26.473	1410.0

laponite RD	17 mm disc	2.02 mm thickness
stainless-steel	50°C 52% RH	min pressure
frequency/kHz	capacitance/nF	resistance/Ω
100	0.0024	12.1
66	0.0067	12.2
50	0.0122	12.1
40	0.0188	12.3
33	0.0265	12.3
25	0.0447	12.4
20	0.0668	12.5
15	0.1111	12.6
12	0.1639	12.8
10	0.2242	13.0
7.5	0.3642	13.3
5	0.7000	14.2
3	1.4780	16.3
1	4.9502	28.3
0.1	19.256	152.2
0.012	28.477	1337.0

Figure 4.11 Raw data (continued)

laponite RD	17 mm disc	2.02 mm thickness
stainless-steel	56°C 52% RH	min pressure
frequency/kHz	capacitance/nF	resistance/Ω
100	0.0028	10.4
66	0.0082	10.4
50	0.0150	10.5
40	0.0232	10.5
33	0.0554	10.5
25	0.0554	10.6
20	0.0826	10.7
10	0.1371	10.9
12	0.2018	11.0
10	0.2755	11.2
7.5	0.4448	11.6
5	0.8461	12.5
3	1.7579	14.4
1	5.6569	25.8
0.1	20.783	144.1
0.012	62.835	308.5

laponite RD	17 mm disc	2.02 mm thickness
stainless-steel	63°C 52% RH	min pressure
frequency/kHz	capacitance/nF	resistance/Ω
100	0.0036	8.90
66	0.0106	8.91
50	0.0195	8.95
40	0.0302	8.98
33	0.0424	9.02
25	0.0716	9.11
20	0.1063	9.21
15	0.1750	9.38
12	0.2555	9.56
10	0.3458	9.76
7.5	0.5506	10.1
5	1.0230	11.0
3	2.0575	13.0
1	6.3079	23.4
0.1	23.425	124.9
0.012	62.961	352.5

Figure 4.11 Raw data (continued)

laponite RD	13 mm disc	1.29 mm thickness
silver paste	15% RH	
frequency/kHz	capacitance/nF	resistance/Ω
100	0.370	5023
66	0.459	7146
50	0.522	9275
40	0.569	11380
33	0.606	13410
25	-	-
20	-	-
15	0.664	17300
12	0.813	31110
10	0.851	35520
7.5	0.914	43210
6	0.967	49670
5	1.011	55360
3	1.150	73160
1	1.533	117500
0.1	4.246	237300
0.012	14.95	446000

laponite RD	13 mm disc	1.45 mm thickness
silver paste	32% RH	
frequency/kHz	capacitance/nF	resistance/Ω
100	1.026	2852
66	1.133	4019
50	1.216	4996
40	1.285	5832
33	1.344	6571
25	-	-
20	1.529	8948
15	1.653	10420
12	1.753	11740
10	1.842	12900
7.5	1.969	16400
6	2.094	19070
5	2.201	21610
3	2.565	28650
1	3.635	48440
0.1	9.021	105800
0.012	23.44	172600

Figure 4.13 Raw data

laponite RD	13 mm disc	1.29 mm thickness
silver paste	52% RH	
frequency/kHz	capacitance/nF	resistance/Ω
100	1.264	1676
66	1.406	2065
50	1.521	2350
40	1.621	2588
33	1.711	2792
25	1.881	3099
20	2.029	3367
15	2.265	3705
12	2.479	3996
10	2.684	4243
7.5	3.081	4637
6	3.458	4969
5	3.787	5322
3	5.161	6203
1	10.61	8873
0.1	39.33	17700
0.012	134.3	24830

laponite RD	13 mm disc	1.30 mm thickness
stainless steel	79% RH	
frequency/kHz	capacitance/nF	resistance/Ω
100	1.547	1003
66	1.839	1177
50	2.027	1357
40	2.194	1524
33	2.294	1692
25	-	-
20	2.749	1993
15	3.044	2231
12	3.311	2419
10	3.530	2619
7.5	3.966	2895
6	4.344	3120
5	4.647	3371
3	5.869	3849
1	9.906	4922
0.1	35.43	6503
0.012	170.3	7722

Figure 4.13 Raw data (continued)

laponite RD	13 mm disc	1.11 mm thickness
stainless steel	93% RH	
frequency/kHz	capacitance/nF	resistance/Ω
100	2.182	269
66	2.611	337
50	2.969	389
40	3.204	436
33	3.531	477
25	4.000	524
20	4.352	574
15	4.958	640
12	5.479	691
10	5.940	744
7.5	6.877	801
6	7.573	868
5	8.275	926
3	10.94	1023
1	21.89	1168
0.1	128.1	1442
0.012	1159	1683

Figure 4.13 Raw data (continued)

laponite RD film	26 mm slide	0.09 mm thickness
silver paste	20°C	
frequency/kHz	capacitance/nF	resistance/Ω
100	0.0157	20400
66	0.0236	22140
50	0.0320	23490
40	0.0407	24260
33	0.0495	24870
25	0.0666	26110
20	0.0838	26990
15	0.1112	28460
12	0.1387	29670
10	0.1658	30710
7.5	0.2192	32570
6	0.2737	34640
5	0.3275	36090
3	0.5366	41020
1	1.4616	58290
0.1	6.7715	141400
0.012	20.180	224500

laponite RD film	10 x10 mm square	0.1 mm thickness
silver paste	20°C	
frequency/kHz	capacitance/nF	resistance/Ω
100	4.0671	648
66	4.7264	819
50	5.3267	918
40	5.9251	978
33	6.5387	1011
25	7.6475	1084
20	8.8139	1102
15	10.565	1155
12	12.278	1185
10	13.981	1200
7.5	17.054	1258
6	19.796	1319
5	23.271	1125
3	33.756	1264
1	49.000	3925
0.1	156.53	8398
0.012	490.03	15150

Table 4.9/Figure 4.20 Raw data

laponite RD film	26 mm slide	0.015 mm thickness
silver paste	20°C	
frequency/kHz	capacitance/nF	resistance/Ω
100	0.0268	10510
66	0.0404	10780
50	0.0552	11090
40	0.0708	11350
33	0.0869	11590
25	0.1206	12010
20	0.1555	12380
15	0.2166	12920
12	0.2770	13410
10	0.3395	13860
7.5	0.4630	14680
6	0.5850	15440
5	0.7041	16120
3	1.1589	18290
1	3.0000	24860
0.1	22.420	60250
0.012	97.963	148800

laponite RD film	26 mm slide	0.015 mm thickness
silver paste	23°C	
frequency/kHz	capacitance/nF	resistance/Ω
100	0.0316	9240
66	0.0495	9540
50	0.0685	9840
40	0.0884	10110
33	0.1090	10340
25	0.1515	10770
20	0.1950	11160
15	0.2690	11750
12	0.3429	12270
10	0.4159	12730
7.5	0.5597	13580
6	0.6988	14330
5	0.8367	14930
3	1.3320	16980
1	3.3400	22640
0.1	25.910	56190
0.012	109.80	127800

Table 4.10 Raw data

laponite RD film	26 mm slide	0.015 mm thickness
silver paste	26°C	
frequency/kHz	capacitance/nF	resistance/Ω
100	0.0380	9069
66	0.0536	9532
50	0.0733	9910
40	0.0937	10240
33	0.1144	10540
25	0.1566	11070
20	0.1993	11540
15	0.2700	12250
12	0.3396	12870
10	0.4070	13420
7.5	0.5385	14380
6	0.6632	15210
5	0.7823	15930
3	1.2230	18190
1	3.0340	24010
0.1	24.100	60530

laponite RD film	26 mm slide	0.015 mm thickness
silver paste	30°C	
frequency/kHz	capacitance/nF	resistance/Ω
100	0.0411	7893
66	0.0639	8301
50	0.0877	8641
40	0.1123	8938
33	0.1374	9202
25	0.1877	9677
20	0.2384	10110
15	0.3212	10740
12	0.4022	11290
10	0.4813	11770
7.5	0.6317	12630
6	0.7747	13350
5	0.9109	13970
3	1.4100	15910
1	3.5000	20790
0.1	27.306	55980
0.012	86.000	168000

Table 4.10 Raw data (continued)

laponite RD film	26 mm slide	0.015 mm thickness
silver paste	34°C	
frequency/kHz	capacitance/nF	resistance/Ω
100	0.0447	7363
66	0.0696	7760
50	0.0955	8091
40	0.1220	8380
33	0.1493	8649
25	0.2037	9112
20	0.2579	9523
15	0.3465	10130
12	0.4322	10660
10	0.5155	11120
7.5	0.6737	11940
6	0.8233	12640
5	0.9655	13220
3	1.4880	15040
1	3.7123	19610
0.1	28.700	53780

laponite RD film	26 mm slide	0.015 mm thickness
silver paste	36°C	
frequency/kHz	capacitance/nF	resistance/Ω
100	0.0464	7177
66	0.0721	7578
50	0.0989	7906
40	0.1264	8195
33	0.1542	8454
25	0.2097	8925
20	0.2648	9340
15	0.3546	9943
12	0.4414	10480
10	0.5253	10940
7.5	0.6854	11750
6	0.8360	12430
5	0.9790	13010
3	1.5070	14790
1	3.7564	19260
0.1	29.030	53010
0.012	89.700	157700

Table 4.10 Raw data (continued)

laponite RD film	26 mm slide	0.015 mm thickness
silver paste	39°C	
frequency/kHz	capacitance/nF	resistance/Ω
100	0.0475	7030
66	0.0740	7432
50	0.1016	7758
40	0.1296	8049
33	0.1580	8309
25	0.2147	8774
20	0.2708	9186
15	0.3622	9787
12	0.4504	10310
10	0.5354	10770
7.5	0.6977	11560
6	0.8506	12230
5	0.9965	12800
3	1.5313	14550
1	3.8280	18950
0.1	29.700	53800
0.012	88.000	162000

laponite RD film	26 mm slide	0.015 mm thickness
silver paste	42°C	
frequency/kHz	capacitance/nF	resistance/Ω
100	0.0496	6808
66	0.0770	7213
50	0.1054	7542
40	0.1340	7823
33	0.1635	8084
25	0.2216	8550
20	0.2790	8954
15	0.3720	9548
12	0.4620	10060
10	0.5470	10530
7.5	0.7120	11310
6	0.8664	11970
5	1.0140	12520
3	1.5500	14220
1	3.9000	18220
0.1	30.200	52940
0.012	90.700	150500

Table 4.10 Raw data (continued)

laponite RD film	10 x 10 mm square	0.015 mm thick
silver paste	21°C	
frequency/kHz	capacitance/nF	resistance/Ω
100	4.05	910
66	4.46	1330
50	4.74	1692
40	4.96	1990
33	5.16	2234
25	5.49	2659
20	5.75	3003
15	6.03	4605
12	6.41	5341
10	6.68	6015
7.5	6.94	7237
6	7.31	8350
5	7.65	9034
3	8.35	10620
1	13.2	14130
0.1	26.1	75570

laponite RD film	10 x 10 mm square	0.015 mm thickness
silver paste	25°C	
frequency/kHz	capacitance/nF	resistance/Ω
100	4.56	793
66	5.04	1133
50	5.35	1419
40	5.58	1671
33	5.75	1917
25	6.07	2298
20	6.34	2606
15	6.53	4309
12	6.89	5026
10	7.18	5675
7.5	7.66	6692
6	8.06	7541
5	8.43	8093
3	9.90	9240
1	15.24	12150
0.1	29.28	70890

Table 4.10 Raw data (continued)

laponite RD film 10 x 10 mm square 0.015 mm thick
silver paste 30°C

frequency/kHz	capacitance/nF	resistance/Ω
100	4.90	739
66	5.41	1039
50	5.76	1274
40	6.01	1492
33	6.20	1699
25	6.53	2034
20	6.78	2345
15	7.18	2713
12	7.23	4599
10	7.54	5288
7.5	8.05	6257
6	8.50	7033
5	8.93	7519
3	10.61	8534
1	16.74	11190

laponite RD film 10 x 10 mm square 0.015 mm thick
silver paste 34°C

frequency/kHz	capacitance/nF	resistance/Ω
100	5.08	715
66	5.61	1001
50	5.99	1200
40	6.19	1460
33	6.40	1611
25	6.79	1869
20	7.07	2119
15	7.49	2443
12	7.55	4227
10	7.87	4887
7.5	8.44	5739
6	8.92	6450
5	9.39	6894
3	11.24	7913
1	18.22	10470

Table 4.10 Raw data (continued)

laponite RD film	10 x 10 mm square	0.015 mm thick
silver paste	36°C	
frequency/kHz	capacitance/nF	resistance/Ω
100	5.21	687
66	5.75	952
50	6.14	1134
40	6.45	1280
33	6.68	1435
25	7.06	1710
20	7.38	1934
15	7.81	2232
12	7.82	3942
10	8.16	4618
7.5	8.76	5418
6	9.27	6089
5	9.78	6515
3	77.79	7494
1	19.35	10020

Table 4.10 Raw data (continued)

Appendix Two

Chapter Six Raw Data

Li laponite RD	13 mm disc	1.17 mm thick
silver paste	22°C	
frequency/kHz	capacitance/nF	resistance/Ω
100	0.0944	38020
66	0.1023	49230
50	0.1102	58250
40	0.1160	65840
33	0.1212	72520
25	0.1302	83690
20	0.1377	94990
15	0.1488	108300
12	0.1586	119200
10	0.1676	128800
7.5	0.1842	144700
5	0.2132	170200
3	0.2623	208100
1	0.4277	322900
0.1	1.2335	846600
0.012	4.5589	1182000

laponite RD	13 mm disc	1.29 mm thickness
silver paste	52% RH	
frequency/kHz	capacitance/nF	resistance/Ω
100	1.047	4273
66	1.114	6411
50	1.173	8266
40	1.220	9978
33	1.260	11580
25	1.326	14520
20	1.381	17190
15	1.457	21180
12	1.521	24750
10	1.578	27860
7.5	1.674	33470
5	1.829	42600
3	2.057	63910
1	2.701	134200
0.1	4.851	505900
0.012	8.811	1403000

Figure 6.1 Raw data

K laponite RD	13 mm disc	1.23 mm thickness
silver paste	52% RH	
frequency/kHz	capacitance/nF	resistance/Ω
100	0.901	1081
66	1.120	1293
50	1.335	1417
40	1.527	1531
33	1.708	1644
25	2.055	2344
20	2.390	1955
15	2.923	2160
12	3.427	2344
10	3.915	2509
7.5	4.837	2805
5	6.522	3313
3	9.382	4159
1	18.63	7104
0.1	59.16	17780
0.012	191.0	36010

Rb laponite RD	13 mm disc	1.22 mm thick
silver paste	22°C	
frequency/kHz	capacitance/nF	resistance/Ω
100	0.2536	6343
66	0.3254	8385
50	0.3816	10380
40	0.4276	12330
33	0.4664	14250
25	0.5289	17980
20	0.5789	21580
15	0.6438	27270
12	0.6951	32560
10	0.7377	37510
7.5	0.8062	46810
5	0.9078	62740
3	1.0499	87920
1	1.4432	163700
0.1	3.3060	412000
0.012	8.7862	710600

Figure 6.1 Raw data (continued)

Cs laponite RD	13 mm disc	1.27 mm thick
silver paste	22°C	
frequency/kHz	capacitance/nF	resistance/Ω
100	0.6952	2643
66	0.8631	3926
50	0.9600	5146
40	0.9343	6241
33	1.0141	7394
25	1.1385	9708
20	1.2317	12020
15	1.3517	15820
12	1.4429	19510
10	1.5160	23110
7.5	1.6314	29930
5	1.7944	42290
3	2.0048	63500
1	2.5483	131700
0.1	2.5483	405100
0.012	11.007	822100

Figure 6.1 Raw data (continued)

K laponite RD	17 mm disc	1.65 mm thick
stainless steel	19°C	min pressure
frequency/kHz	capacitance/nF	resistance/Ω
100	1.0628	131
66	1.7029	132
50	2.4458	134
40	3.2695	136
33	4.1575	137
25	6.1164	139
20	8.2886	142
15	12.298	145
12	16.706	148
10	21.436	151
7.5	31.705	157
6	42.711	162
5	54.254	168
3	103.43	187
1	344.36	268
0.1	2076.3	806

K laponite RD	17 mm disc	1.65 mm thick
stainless steel	22°C	min pressure
frequency/kHz	capacitance/nF	resistance/Ω
100	0.9074	112
66	1.4985	121
50	2.1846	122
40	2.9502	123
33	3.7858	124
25	5.6528	126
20	7.7466	128
15	11.668	130
12	16.041	133
10	20.789	136
7.5	31.197	140
6	42.561	144
5	54.623	148
3	106.99	162
1	381.45	227
0.1	734.40	305

Table 6.2 Raw data (continued)

K laponite RD	17 mm disc	1.65 mm thick
stainles steel	26°C	min pressure
frequency/kHz	capacitance/nF	resistance/Ω
100	1.0512	94
66	1.7947	95
50	2.5561	96
40	3.4578	97
33	4.4448	98
25	6.6566	99
20	9.1501	100
15	13.837	102
12	19.096	103
10	24.847	105
7.5	37.518	108
6	51.468	110
5	66.407	113
3	132.32	124
1	490.05	170
0.1	3238.6	539

K laponite RD	17 mm disc	1.65 mm thick
stainless steel	31°C	min pressure
frequency/kHz	capacitance/nF	resistance/Ω
100	1.07	78.1
66	1.85	78.9
50	2.77	79.5
40	3.79	80.1
33	4.93	80.6
25	7.49	81.5
20	10.38	82.4
15	15.86	83.7
12	22.03	84.9
10	28.79	86.1
7.5	43.75	88.4
6	60.30	90.6
5	78.10	92.8
3	157.30	101.1
1	595.76	139.2
0.1	3509.6	564.6

Table 6.2 Raw data (continued)

K laponite RD	17 mm disc	1.65 mm thick
stainless steel	35°C	min pressure
frequency/kHz	capacitance/nF	resistance/Ω
100	1.11	67.6
66	1.96	68.2
50	2.95	67.7
40	4.08	69.1
33	5.32	69.5
25	8.12	70.3
20	11.31	71.0
15	17.35	72.1
12	24.17	73.1
10	31.68	74.0
7.5	48.38	75.9
6	66.87	77.7
5	86.88	79.4
3	176.61	86.1
1	685.27	117.0
0.1	4214.2	468.0

K laponite RD	17 mm disc	1.65 mm thick
stainless steel	39°C	min pressure
frequency/kHz	capacitance/nF	resistance/Ω
100	1.09	57.4
66	1.74	57.8
50	2.96	58.2
40	4.10	58.6
33	5.30	58.8
25	8.25	59.4
20	11.50	59.9
15	17.80	60.7
12	25.00	61.5
10	32.90	62.2
7.5	50.70	63.5
6	70.70	64.8
5	92.40	66.1
3	192.2	70.9
1	794.7	93.1
0.1	5394.8	370.0

Table 6.2 Raw data (continued)

K laponite RD	17 mm disc	1.65 mm thick
stainless steel	45°C	min pressure
frequency/kHz	capacitance/nF	resistance/Ω
100	1.14	49.4
66	2.11	49.8
50	3.26	50.1
40	4.56	50.3
33	6.02	50.6
25	9.34	51.0
20	13.15	51.4
15	20.43	52.0
12	28.76	52.6
10	37.99	53.2
7.5	58.76	54.3
6	82.07	55.4
5	107.5	56.4
3	224.3	60.4
1	931.2	79.3
0.1	6355.4	316.8

K laponite RD	17 mm disc	1.65 mm thick
stainless steel	49°C	min pressure
frequency/kHz	capacitance/nF	resistance/Ω
100	1.22	43.1
66	2.27	43.4
50	3.53	43.6
40	4.98	43.8
33	4.95	43.9
25	10.26	44.3
20	14.49	44.6
15	22.60	45.1
12	32.02	45.1
10	43.39	45.8
7.5	65.78	46.7
6	92.16	47.5
5	121.09	48.3
3	254.43	51.6
1	1076.8	67.1
0.1	7549.4	276.4

Table 6.2 Raw data (continued)

K laponite RD	17 mm disc	1.65 mm thick
stainless steel	59°C	min pressure
frequency/kHz	capacitance/nF	resistance/Ω
100	1.45	33.9
66	2.68	34.0
50	4.25	34.1
40	6.06	34.2
33	8.07	34.3
25	12.68	34.6
20	17.98	34.9
15	28.13	35.3
12	39.79	35.6
10	52.74	35.9
7.5	81.97	36.6
6	114.96	37.3
5	151.12	37.9
3	318.45	40.5
1	1364.3	52.3
0.1	9728.2	210.3

K laponite RD	17 mm disc	1.65 mm thick
stainless steel	67°C	min pressure
frequency/kHz	capacitance/nF	resistance/Ω
100	1.47	28.1
66	2.99	28.3
50	4.81	28.4
40	6.90	28.6
33	9.24	28.7
25	14.58	28.9
20	20.74	29.1
15	32.58	29.4
12	46.18	29.7
10	61.32	29.9
7.5	95.54	30.5
6	134.27	31.1
5	176.89	31.6
3	375.19	33.6
1	1637.7	43.2
0.1	11785.0	177.0

Table 6.2 Raw data (continued)

K laponite RD	17 mm disc	1.65 mm thick
stainless steel	75°C	min pressure
frequency/kHz	capacitance/nF	resistance/Ω
100	1.49	24.2
66	3.15	24.3
50	5.16	24.4
40	10.00	24.5
33	12.97	25.0
25	20.18	25.3
20	28.33	25.5
15	43.52	25.9
12	60.40	26.3
10	78.70	26.6
7.5	118.72	27.2
6	162.45	27.8
5	209.29	28.3
3	416.40	30.3
1	1632.3	38.3
0.1	13118.0	110.2

Table 6.2 Raw data (continued)

K laponite RD	13 mm disc	1.49 mm thick
silver paste	20°C / 32% RH	min pressure
frequency/kHz	capacitance/nF	resistance/Ω
100	1.49	2028
66	1.69	3301
50	1.81	4691
40	1.89	4691
33	1.96	7566
25	2.05	10450
20	2.12	13300
15	2.20	17820
12	2.27	22070
10	2.32	26110
7.5	2.40	33520
6	2.47	40150
5	2.53	46330
3	2.71	65490
1	3.22	127300
0.1	5.88	330800
0.012	14.24	686900

K laponite RD	13 mm disc	1.26 mm thick
silver paste	20°C / 52% RH	min pressure
frequency/kHz	capacitance/nF	resistance/Ω
100	1.61	1730
66	1.84	2757
50	1.99	3840
40	2.09	4948
33	2.17	6062
25	2.29	8212
20	2.37	10280
15	2.49	13580
12	2.56	16730
10	2.63	19830
7.5	2.74	25080
6	2.85	29700
5	2.93	34070
3	3.19	48530
1	3.94	96000
0.1	7.13	319100
0.012	15.70	758200

Table 6.3 Raw data (continued)

K laponite RD	13 mm disc	1.55 mm thick
silver paste	20°C / 79% RH	min pressure
frequency/kHz	capacitance/nF	resistance/Ω
100	0.98	2843
66	1.12	4009
50	1.22	5074
40	1.29	6047
33	1.35	6955
25	1.45	8536
20	1.54	9911
15	1.65	11920
12	1.75	13670
10	1.83	15220
7.5	1.97	17900
6	2.10	20110
5	2.20	22100
3	2.56	28280
1	3.78	45130
0.1	11.30	119400
0.012	29.93	244300

K laponite RD	13 mm disc	1.37 mm thick
silver paste	20°C / 93 % RH	min pressure
frequency/kHz	capacitance/nF	resistance/Ω
100	1.60	1926
66	1.80	3108
50	1.92	4376
40	2.00	5679
33	2.07	6982
25	2.16	9533
20	2.24	12010
15	2.33	15920
12	2.40	19610
10	2.46	23020
7.5	2.57	29110
6	2.65	34730
5	2.72	39630
3	3.03	57630
1	3.57	115200
0.1	6.12	402300
0.012	12.67	913400

Table 6.3 Raw data (continued)

laponite RD	13 mm disc silver paste	1.32 mm thick
frequency/kHz	capacitance/nF	resistance/Ω
100	0.9681	4922
66	1.0821	7489
50	1.1246	9851
40	1.1582	12070
33	1.1863	14180
25	1.2373	17870
20	1.2781	21260
15	1.3350	26210
12	1.3818	30620
10	1.4226	34520
7.5	1.4936	41260
5	1.6099	51790
3	1.7662	73530
1	2.2870	130800
0.1	5.4318	294000
0.012	13.711	593400

laponite RD + Ph_3SnCl	13 mm disc silver paste	1.22 mm thick
frequency/kHz	capacitance/nF	resistance/Ω
100	1.1481	733
66	1.4200	916
50	1.7272	1019
40	2.0190	1109
33	2.3006	1190
25	2.8432	1330
20	3.3622	1449
15	4.1580	1638
12	4.8764	1810
10	5.5490	1963
7.5	6.7717	2236
5	8.8492	2704
3	12.124	3455
1	22.521	5756
0.1	75.820	13020
0.012	269.72	19540

Figure 6.3 Raw data

laponite RD + Ph_2SnCl_2	13 mm disc silver paste	1.26 mm thick
frequency/kHz	capacitance/nF	resistance/Ω
100	1.0470	353
66	1.4032	413
50	1.8209	441
40	2.2445	459
33	2.6326	484
25	3.4505	512
20	4.2464	536
15	5.5385	570
12	6.8061	599
10	8.0210	623
7.5	10.336	665
5	14.609	730
3	22.426	814
1	54.802	1012
0.1	368.15	1524
0.012	2016.8	3155

laponite RD + $(Ph_3Sn)_2O$	13 mm disc silver paste	1.07 mm thick
frequency/kHz	capacitance/nF	resistance/Ω
100	2.4307	1164
66	2.683	1613
50	2.9008	1978
33	3.2345	2572
25	3.4983	3060
20	3.7171	3475
15	4.0259	4061
12	4.2891	4556
10	4.5264	4981
7.5	4.9460	5703
6	5.3207	6300
5	5.6596	6829
3	6.8644	8452
1	11.463	13330
0.1	38.218	41830
0.012	97.246	104300

Table 6.3 Raw data (continued)

laponite RD	13 mm disc	1.14 mm thick
+ 1g Ph_3SnCl	silver paste	
frequency/kHz	capacitance/nF	resistance/Ω
100	1.3370	1956
66	1.5568	2855
50	1.6819	3645
40	1.7780	4386
33	1.8433	5153
25	1.9810	6374
20	2.0940	7463
15	2.5205	9009
12	2.3820	10340
10	2.4940	11560
7.5	2.6881	13630
6	2.8505	15460
5	3.0040	16930
3	3.5081	21670
1	5.0924	36630
0.1	14.490	96250
0.012	39.640	190000

laponite RD	13 mm disc	0.92 mm thick
+ 4 g Ph_3SnCl	silver paste	
frequency/kHz	capacitance/nF	resistance/Ω
100	1.6131	992
66	1.7880	1469
50	1.9795	1762
40	2.1355	2012
33	2.2741	2227
25	2.5227	2574
20	2.7381	2868
15	3.0396	3259
12	3.3370	3562
10	3.6167	3820
7.5	4.1285	4237
6	4.6068	4588
5	5.0399	4919
3	6.7061	5859
1	13.418	8831
0.1	50.963	23250
0.012	138.6664	53190

Figure 6.4 Raw data

laponite RD + 5 g Ph_3SnCl	13 mm disc silver paste	1.00 mm thick
frequency/kHz	capacitance/nF	resistance/Ω
100	0.8187	836
66	1.0803	991
50	1.2895	1103
40	1.4814	1188
33	1.6688	1244
25	2.0102	1341
20	2.3523	1428
15	2.9174	1525
12	3.4845	1602
10	4.0415	1712
7.5	5.1513	1854
6	7.3316	2091
5	11.312	2497
3	26.065	3834
1	102.07	8579
0.1	151.57	9900
0.012	373.59	12500

laponite RD only	13 mm disc silver paste	1.20 mm thick
frequency/kHz	capacitance/nF	resistance/Ω
100	0.5154	5388
66	0.5869	7996
50	0.6318	10270
40	0.6664	12380
33	0.6947	14360
25	0.7419	17700
20	0.7809	20580
15	0.8349	24770
12	0.8894	27860
10	0.9229	30950
7.5	0.9877	30950
6	1.0467	40350
5	1.0910	45950
3	1.2674	57720
1	1.8629	86940
0.1	5.5978	201200
0.012	16.555	357900

Figure 6.4 Raw data (continued)

Ph_2SnCl_2 + laponite	17 mm disc	1.94 mm thick
stainless steel	minimum pressure	22°C
frequency/kHz	capacitance/nF	resistance/Ω
100	0.63	147
66	0.93	149
50	1.25	150
40	1.60	151
33	1.97	151
25	2.77	153
20	3.62	153
15	5.20	155
12	6.99	156
10	8.95	157
7.5	13.30	159
6	18.05	160
5	23.27	162
3	47.71	168
1	213.10	191
0.1	2781.0	357
0.012	14477.0	1087

Ph_2SnCl_2 + laponite	17 mm disc	1.94 mm thick
stainless steel	minimum pressure	26°C
frequency/kHz	capacitance/nF	resistance/Ω
100	0.648	126
66	0.968	127
50	1.316	128
40	1.670	125
33	2.051	126
25	2.888	126
20	3.813	126
15	5.534	127
12	7.464	128
10	9.585	130
7.5	14.33	131
6	19.69	132
5	25.57	133
3	49.52	136
1	237.9	153
0.1	3532.2	284
0.012	17256.0	992

Table 6.6 Raw data

Ph_2SnCl_2 + laponite	17 mm disc	1.94 mm thick
stainless steel	minimum pressure	29°C
frequency/kHz	capacitance/nF	resistance/Ω
100	0.697	107
66	1.044	108
50	1.420	109
40	1.819	109
33	2.246	109
25	3.178	110
20	4.216	111
15	6.150	112
12	8.330	112
10	10.74	113
7.5	16.14	114
6	22.26	115
5	29.00	116
3	60.92	120
1	286.8	136
0.1	4014.9	264
0.012	18319.0	986

Ph_2SnCl_2 + laponite	17 mm disc	1.94 mm thick
stainless steel	minimum pressure	35°C
frequency/kHz	capacitance/nF	resistance/Ω
100	0.77	86.9
66	1.18	86.0
50	1.62	86.5
40	2.10	86.8
33	2.61	87.1
25	3.74	87.6
20	5.00	88.0
15	7.35	88.7
12	10.00	89.1
10	12.94	89.6
7.5	19.52	90.5
6	26.94	91.2
5	35.11	91.9
3	73.65	94.7
1	360.4	107
0.1	5132.3	215
0.012	22458.0	842

Table 6.6 Raw data (continued)

Ph_2SnCl_2 + laponite	17 mm disc	1.94 mm thick
stainless steel	minimum pressure	40°C
frequency/kHz	capacitance/nF	resistance/Ω
100	0.82	72.7
66	1.29	73.2
50	1.78	73.6
40	2.32	73.8
33	2.90	74.0
25	4.18	74.4
20	5.61	74.7
15	8.31	75.2
12	11.37	75.6
10	14.76	75.9
7.5	22.42	76.6
6	31.10	77.2
5	40.72	77.8
3	86.36	80.0
1	412.7	88.7
0.1	6271.3	187
0.012	26122.0	746

Ph_2SnCl_2 + laponite	17 mm disc	1.94 mm thick
stainless steel	minimum pressure	47°C
frequency/kHz	capacitance/nF	resistance/Ω
100	0.95	58.6
66	1.49	58.9
50	2.09	59.1
40	2.75	59.3
33	3.47	59.5
25	5.07	59.8
20	6.87	60.0
15	10.27	60.4
12	14.15	60.7
10	18.47	61.0
7.5	28.21	61.5
6	39.29	62.0
5	51.56	62.5
3	109.94	64.3
1	527.78	71.5
0.1	7822.9	152
0.012	31717.0	613

Table 6.6 Raw data (continued)

Ph_2SnCl_2 + laponite	17 mm disc	1.94 mm thick
stainless steel	minimum pressure	57°C
frequency/kHz	capacitance/nF	resistance/Ω
100	1.11	44.4
66	1.77	44.6
50	2.53	44.8
40	3.36	44.9
33	4.26	45.0
25	6.29	45.2
20	8.57	45.4
15	12.91	45.6
12	17.88	45.8
10	23.41	46.0
7.5	35.94	46.4
6	50.23	46.8
5	66.10	47.1
3	142.2	48.4
1	695.2	53.8
0.1	10781.0	96.5
0.012	45298.0	419

Ph_2SnCl_2 + laponite	17 mm disc	1.94 mm thick
stainless steel	minimum pressure	63°C
frequency/kHz	capacitance/nF	resistance/Ω
100	1.55	37.8
66	2.53	38.1
50	3.61	38.3
40	4.78	38.5
33	6.04	38.6
25	8.80	38.6
20	11.85	39.1
15	17.54	39.4
12	23.93	39.6
10	30.95	39.9
7.5	46.66	40.3
6	64.35	40.7
5	83.87	41.1
3	175.7	42.3
1	818.6	47.4
0.1	11751.0	83.5
0.012	51485.0	332

Table 6.6 Raw data (continued)

Ph_2SnCl_2 + laponite	17 mm disc	1.94 mm thick
stainless steel	minimum pressure	70°C
frequency/kHz	capacitance/nF	resistance/Ω
100	1.69	31.8
66	2.81	32.0
50	4.06	32.2
40	5.45	32.3
33	6.95	32.4
25	10.28	32.6
20	14.02	32.8
15	21.06	33.0
12	29.00	33.2
10	37.77	33.4
7.5	57.42	33.8
6	79.58	34.2
5	104.0	34.5
3	218.8	35.6
1	10209.0	40.3
0.1	14341.0	73.3
0.012	63657.0	276

Table 6.6 Raw data (continued)

Ph_2SnCl_2 + laponite	13 mm disc	1.52 mm thick
silver paste	20°C	32% RH
frequency/kHz	capacitance/nF	resistance/Ω
100	1.834	516
66	2.236	631
50	2.571	714
40	2.863	801
33	3.174	856
25	3.794	938
20	4.374	1007
15	5.292	1112
12	6.144	1209
10	6.904	1308
7.5	8.440	1452
6	9.895	1573
5	11.28	1699
3	15.98	2088
1	31.38	3216
0.1	104.1	6044
0.012	372.6	8402

Ph_2SnCl_2 + laponite	13 mm disc	1.74 mm thick
silver paste	20°C	52% RH
frequency/kHz	capacitance/nF	resistance/Ω
100	1.235	371
66	1.712	402
50	2.182	423
40	2.653	443
33	3.121	461
25	4.059	494
20	5.005	518
15	6.566	553
12	8.082	587
10	9.579	615
7.5	12.48	664
6	15.19	708
5	17.62	750
3	26.45	873
1	56.02	1171
0.1	244.26	1984
0.012	1095.7	2704

Table 6.7 Raw data

Ph_2SnCl_2 + laponite	13 mm disc	1.89 mm thick
silver paste	20°C	79% RH
frequency/kHz	capacitance/nF	resistance/Ω
100	1.640	156
66	2.412	176
50	3.198	187
40	3.959	195
33	4.710	203
25	6.156	214
20	7.530	224
15	9.707	236
12	11.69	248
10	13.52	261
7.5	16.95	279
6	20.40	289
5	23.31	398
3	36.04	309
1	89.11	354
0.1	694.6	467
0.012	4204.0	585

Table 6.7 Raw data (continued)